Investigations on Flow Characteristics and Particulate Distributions in Gyro casting of Metal Matrix Composites

Thesis submitted to

UNIVERSITY OF CALICUT

in fulfillment for the award of the degree of

DOCTOR OF PHILOSOPHY

By

ABDUL SAMAD P A

Department of Mechanical Engineering

Government Engineering College, Thrissur-9

University of Calicut

June 2019

Investigations on flow characteristics and particulate distributions in Gyro casting of Metal Matrix Composites

Thesis submitted to

UNIVERSITY OF CALICUT

in fulfillment for the award of the degree of

DOCTOR OF PHILOSOPHY

By

ABDUL SAMAD P A

Under the Guidance of

Dr. SHALIJ P R
Associate Professor
Department of Production Engineering
Government Engineering College, Thrissur-9
University of Calicut

June 2019

DEPARTMENT OF MECHANICAL ENGINEERING
GOVERNMENT ENGINEERING COLLEGE, THRISSUR
Engineering College P.O, Ramavarmapuram,
Thrissur, Kerala, India, PINCODE - 680009
Phone No. 0487-2334144 Fax : 0487-2336124
Website : www.gectcr.ac.in

C E R T I F I C A T E

This is to certify that the thesis entitled "**Investigations on flow characteristics and particulate distributions in Gyro casting of Metal Matrix Composites**" is the record of bonafide research work done by **Mr. ABDUL SAMAD P A** under my supervision and guidance at Department of Mechanical Engineering, Govt. Engineering College, Thrissur in fulfillment of the requirements for the Degree of Doctor of Philosophy under the Faculty of Engineering, University of Calicut.

Thrissur-9
01.07.2019

Dr. Shalij P R
(Supervising Guide)
Associate Professor
Production Engineering
Government Engineering College Thrissur

Certified that the suggestions / corrections from the adjudicators as per Ref. No. 133904/RESEARCH-C-ASST-1/2019/Admn Dated 16.11.2019 from the Director of Research, University of Calicut, have been incorporated in this thesis.

Thrissur-9
20.11.2019

Dr. Shalij P R
(Supervising Guide)
Associate Professor
Production Engineering
Government Engineering College Thrissur

DECLARATION

I **Abdul Samad P A,** hereby declare that the thesis entitled "**Investigations on flow characteristics and particulate distributions in Gyro casting of Metal Matrix Composites"** is based on the original work done by me under the guidance of **Dr. Shalij P. R**, Associate Professor, Department of Production Engineering, Govt. Engineering College, Thrissur for the award of Ph.D under University of Calicut. I further declare that this work has not been included in any other thesis submitted previously for the award of any Degree, Diploma, Associateship or Fellowship or any other title for recognition.

Thrissur **ABDUL SAMAD P A**

01.07.2019

The suggestions / corrections from the adjudicators as per Ref. No. 133904/RESEARCH-C-ASST-1/2019/Admn Dated 16.11.2019 from the Director of Research, University of Calicut, have been incorporated in this thesis.

Thrissur **ABDUL SAMAD P A**

20.11.2019

ACKNOWLEDGEMENT

First and above all, I bow my head before the Almighty Lord whose grace has been with me always throughout the research work.

*I am thankful to **Dr. K.P. Indiradevi**, Director of Technical Education, Kerala and former Principal of Government Engineering College, Thrissur and **Dr.K.Vijayakumar**, former Director of Technical Education, Kerala for their wholehearted support during the conduct of this research. I am grateful to the Director and all the staff members of Directorate of Research, Calicut University for the timely support to complete the work and final submission of thesis.*

*I am also thankful to **Dr.Sheeba V S**, Principal, Government Engineering College, Thrissur and **Dr.Jayanand.B**, former Principal, Government Engineering College, Thrissur, and **Dr. Mohandas V P**, Head of the Mechanical Engineering Department, Government Engineering College, Thrissur, for providing the facilities to successfully carry out this research work.*

*Creative guidance makes a scientific research qualitative, and this has been imparted to me by **Dr. Shalij P R**, Associate Professor, Department of Production Engineering, Govt. Engineering College, Thrissur, as a helpful guide. I would like to express my sincere thanks to him for the trust, the insightful discussion, offering valuable advice and for the support during the whole period of the research which made this work possible. I also acknowledge for his patience and guidance during the preparation of thesis report.*

*I am highly indebted to external doctoral committee member **Dr.Pramod V R**, Professor, Department of Mechanical Engineering, NSS College of Engineering, Palakkad, for the valuable suggestions and help extended for the fulfillment of this research work. I express my sincere gratitude to the faculty and supporting staff members of Mechanical Engineering for giving an opportunity to carry out my research work in the Department of Mechanical Engineering, Government Engineering College Thrissur.*

*I extend my thanks to **Dr.A. Ramesh**, **Prof.E.C.Ramakrishnan, Dr. C.P. Sunilkumar**, former heads, Department of Mechanical Engineering, **Dr.Manesh K K**, Doctoral committee member, **Dr.K.R.Jayadevan**, Former Chairman of Doctoral Committee and my friend **Dr. Mubarak A K**, Associate Professor, Department Mechanical Engineering for the suggestions and encouragements extended to me during the course of the research work.*

*I record my sincere and utmost gratitude to my parents,**Abu Bucker** and**Nabeesa**for showering love and showing faith in me. Special thanks to my mother-in-law **Fathima Jamal** and beloved wife **Fazeela** for the untiring support provided to me during the entire period of research work. I also thank my son **Muhammad Rizwan,** my daughter **RizaMariyam,** my brother **Muhammad Rafi**, my sisters **Jasmin** and **Jesiya**for patiently cooperating with me to complete the work successfully.*

I have been enormously benefited from the advice, support, co-operation and encouragement given by my colleagues, friends, students during the course of this research work. I would like to offer my sincere thanks to all of them.

Thrissur-9 **ABDUL SAMAD P A**

01.07.2019

ABSTRACT

The enhanced specific strength of SiC Particulate Metal Matrix Composites (PMMC) has been the major contributing factor for finding applications in the aerospace and automotive industries. Uniform distribution of the particulates in PMMC controls the attainment of better mechanical properties. The most accepted method for producing such a composite is stir casting in which the homogeneity of particulate reinforcement is a significant challenge.

This research work proposes a new method for mixing the particulate reinforcement with the liquid and semi-solid aluminium matrix to ensure a uniform mix of the particulates using a Gyro Shaker. Gyro shaker is a dual axes rotation mixer commonly used for mixing high viscous fluids. It rotates about two mutually perpendicular axes which help in thoroughly mixing of the ingredients. Computational Fluid Dynamics (CFD) simulation model of the mixing device was developed for assessing the mixing performance and flow characteristics while mixing SiC particulates with Glycerol. The results of the simulation were also validated by experimentation. CFD simulation for liquid-solid mixing was conducted by using sand particles and glycerine/water mixture. Analogue fluid simulation of gyro casting was also carried out using water and glycerol/water mixture which are having closer value of viscosity as that of liquid aluminium and semi-solid aluminium. The distribution of the SiC particulates obtained from simulation was compared with stir casting simulations.

The proposed gyro casting method can be adopted for obtaining a homogeneous suspension of particulates as compared to the existing stir casting method for the production of PMMC. Advantage of this mixing is that it can be continued while solidification occurs, resulting in avoiding the formation of dendritic growth of microstructure, which helps in improving mechanical properties of the cast composite.

CONTENTS

LIST OF FIGURES

LIST OF TABLES

LIST OF ABBREVIATIONS AND NOMENCLATURES

C_D	drag coefficient
CFD	Computational Fluid Dynamics
CMC	Ceramic Matrix Composites
D	diameter of the mixing vessel
D_s	diameter of horizontal part of planetary mixer
d_S	diameter of particles of secondary phase
D_G	diameter of the turbine part
F	body force
FVM	Finite Volume Method
GCI	Grid Convergence Index
I	power meter reading for current
L	height of the mixing vessel
$\dot{m}$	mass transfer due to cavitation or user-defined mass sources
MI	Mixing Index
$\dot{m}_{qp}$	mass transfer from phase q to phase p
N	rotational speed of the impeller
n	number of phases
N_G	gyration speed
N_p	power number
N_{pG}	power number based on gyration speed
N_{pM}	power number based on characteristic velocity
N_s	spin speed
P	power for mixing
P/V	specific power
P_{md}	power consumed by mixing machine
PMMC	Particulate Metal Matrix Composite
P_w	power meter reading for power
R	field resistance of the electric motor
R_e	Reynolds Number
R_{eG}	Reynolds Number based on gyration speed
R_{eM}	Reynolds Number based on characteristic velocity
Re_s	relative Reynolds Number
RNG	Renormalized Group
S	modulus of the mean rate-of-strain tensor
$S\alpha_k$	source term
SIMPLE	Semi-implicit Method for Pressure Linked Equations
T_y	torque on the walls about y-axis
T_z	torque on the walls about z- axis
U_{ch}	characteristic velocity
$V_{dr,k}$	drift velocity of secondary phase k
V_m	mass-averaged velocity
VOF	Volume of Fluid
V_p	volume fraction of the secondary phase

Greek letters

α_k	volume fraction of phase k.
α_l	Volume fraction of liquid phase
α_2	volume fraction of the secondary phase
α_s	Volume fraction of solid phase
μ	viscosity of the primary liquid phase
μ_m	viscosity of the mixture
μ_s	viscosity of the secondary phase
μ_t	effective viscosity
μ_1	apparent fluid viscosity
Φv	viscous dissipation energy
ρ	density of liquid phase
ρ_m	density of mixture
ρ_1	Density of primary phase
ρ_2	Density of secondary phase
θ_{99}	Dispersion time

CHAPTER 1

INTRODUCTION

1.1 Introduction

Composites have a material configuration in which the reinforcement particulates are dispersed in continuous phase resulting in a combination of both the properties of the constituents. The composites are classified into three, according to the reinforcement forms. They are laminar composites, fibre reinforced composites and particulate composites. The quasi-isotropic properties of the particulates composites make it suitable for a large number of applications in engineering. According to the matrix materials used in the particulate composites, it is again classified into polymer matrix composites, metal matrix composites and ceramic matrix composites. Among these, the metal matrix composite is widely used in the aerospace, sports and automotive due to its better mechanical properties. Common metals used as matrix are Al, Mg, Zn, Cu etc. having a low density and strength. High strength particulates of SiC, Al_2O_3, MgO, BeO, CuO, SiO_2, TiC etc. are used as reinforcement in combination with the above matrix metals.

The Particulate Metal Matrix Composite (PMMC) produced by the combination of aluminium as matrix and SiC as particulates finds more applications in engineering due to its high specific strength. The strength of the cast composite primarily depends on the particulate homogeneity in the cast composite. Proper mixing of particulates in the production of PMMCs plays key roles in determining the mechanical properties of the composite. Numerical simulations have also shown that the non-uniform distribution of particulates reduces the strength of cast composites.

Manufacturing methods have a vital role in the distribution of particulates in the cast composite. PMMC are manufactured by liquid processing, semi-solid processing and solid processing. In liquid processing, molten metal is vigorously stirred using mechanical impeller at the time of adding particulates for keeping the dispersed particulates in suspension. It is a common manufacturing method due to its easiness and low manufacturing cost. However cannot be assured the complete homogeneity of particulate distribution in this processing. The introduction of particulate powder into semi-solid matrix material during mechanical stirring can improve the distribution of particulates inside the cast composite. The powder

metallurgy method, which is solid processing, can assure better homogeneity of particulates in the composites. But the manufacturing cost is very high compared to the other two types. The compromise between the quality and cost leads to thinking about a liquid processing technique with better mixing mechanism.

The quality of mixing of the particulates with matrix improves the quality of the composites. Mechanical stirrers were used for mixing the particulates and matrix. Most of the researches on improving the quality of liquid and particulates mixing were concentrated on the modification of mechanical stirrer (Abhishek et al., 2012; Alliet-Gaubert et al., 2006; Bai et al., 2017; Bao et al., 2018). The geometry and position of stirrers and several stirrers were changed in such investigations. The homogeneity of particulates was not observed in all area of the mixing vessel were not obtained in such studies due to the fluid flow fluctuations inside the mixing vessel. An alternate method of rotating the mixing vessel might be a solution for getting uniform flow inside the stirred vessel. The gyro shaker mixer commonly used for mixing highly viscous fluids such as paints is a method, which employs such a technique. In Gyro shaker, the mixing vessel rotates about two mutually perpendicular axes which causes mixing.

Before suggesting the two axes rotating device for mixing molten aluminium with SiC particulates, it might be an advantage to predict the performance of mixing using numerical analysis of the fluid flow inside the mixing vessel. Also, the measurement of fluid flow characteristics is difficult in a melt-metal system.

Several numerical simulations have been carried out for analysing the mixing in the stir casting with the help of Computational Fluid Dynamics (CFD) tools. Room temperature analogue fluid simulation is one of the methods for studying the SiC particulate distribution in stir casting. In this, the molten metal is replaced by equivalent viscosity fluid. The flow pattern inside the mixing vessel, which influences the efficiency of mixing, was also observed using CFD simulation. The flow patterns can be studied using CFD simulation for arriving at the flow parameters for the better uniformity of particulates.

1.2 Problem definition

The homogeneity of particulates in PMMC plays a vital role in attaining better mechanical properties. The present conventional methods of stir casting for manufacturing PMMC was not able to reach a perfect homogeneity of particulates. This was due to the poor mixing of particulates with the molten matrix material. So, the development of a better mixing

system which ensures efficient mixing would be highly visible in this area of manufacturing. Gyro shaker is a dual-axis rotating mixing device commonly used for mixing highly viscous fluids. The possibility of such dual-axis mixing system is studied in this thesis work. The development of a simulation model for studying particulate mixing with dual axis rotation of the mixing cylinder can ensure the possibility of adequate mixing. The developed simulation model can be used for conducting the blending of liquid metal with particulates and comparing with the existing mixing methods in the area of PMMC casting.

1.3 Objectives of the study

The following objectives were identified for the research work:

1 To develop simulations and conduct experiments on the two-axis mixing device.

2 To develop a new mixing method with two axis rotation for obtaining a homogeneous particulate mixture.

3 To compare the performances of the existing stirred vessel device with the two-axis mixing device.

4 To simulate PMMC casting in the new two-axis mixing device.

5 To compare the PMMC casting simulation on two axes mixing with the existing method and derive conclusions.

1.4 Methodology

Methodology adopted for doing the research is as follows. The primary objective of the research work was to develop a new mixing system for homogeneous mixing of liquid and particulates for the production of PMMC. For this, CFD simulation of dual axis rotation mixing was developed to conduct simulation for gyro casting. The design parameters for the CFD simulation for dual axis rotating mixing device were identified from the existing literature. The various models of simulations available were also identified from the previous studies. Different simulation models suitable for the Gyro casting were selected from among these.

The CFD simulation developed was validated with experiment. The Gyro shaker machines that are used for mixing highly viscous fluids, was employed for conducting the experiment. The height to diameter ratio of the mixing cylinder was fixed to one in the mixing vessel. Glycerine and SiC powder were used as the liquid and particulates, respectively.

The grid independence study of the CFD simulation model was conducted by refining the grid size to arrive at the best solution for the flow variables. The mixing power obtained from the experimental was compared with the CFD simulation results and validated.

CFD simulation for the Gyro casting was then compared with stir casting for assessing the effectiveness. The domain in Gyro casting mixing vessel was taken as the same as that of stir casting. Mixing time required and particle distribution at various locations inside the mixing vessel were compared at different mixing speeds in both liquid and semi-solid systems and derived conclusions.

1.5 Thesis outline

Chapter 1 delivers an introduction to the importance of the particulate distribution for improving quality of cast PMMC. The research gap, problem, objective of the study and the methodology adopted are also explained in this chapter

Chapter 2. contains the literature review in the area of PMMC. The research works carried out by previous researchers in different casting methods are explained in this chapter. CFD simulations in the area of stir casting and stirred vessels are reported here. The experiments conducted in the area of dual axis rotation machine are also reported. The summary of findings from the literature review added in the last section.

Chapter 3. contains the design parameters for the dual axis mixing device, which is proposed in this research work. The relevant non-dimensional parameters for a dual axis mixing device are explained in the chapter. Numerical modelling for a dual axis mixing device is also described in this chapter. The multiphase CFD simulation models and the turbulence models selected for the Gyro shaker are also elaborated.

The experiment for determining the mixing power and validation of the CFD simulation model are explained in Chapter 4. The detailed procedure of grid independence study for arriving at the best simulation result, and the flow characteristics obtained are discussed in this chapter.

In Chapter 5, the traditional mixing of solid particles with liquid is compared with the mixing inside a Gyro shaker. The CFD simulation conducted by Wang et al. (2010) in a stirred vessel is compared with the Gyro shaker for analyzing the difference in flow parameters.

CFD simulation of Gyro casting for comparison of the mixing performance with the stir casting is explained in Chapter 6. The particle distribution at various locations inside the Gyro casting mixing device is compared with the results taken from the work done by Naher et al. (2007).

The overall conclusion of the research work, on simulation model development for dual axis mixing device, Gyro casting simulation and comparison with stir casting are elaborated in Chapter 7. The scope of future work is also added in this section.

1.6 Summary

This chapter gives an introduction to the PMMC, its production processes and difficulties faced in improving the quality of the cast PMMCs. The research problem, objectives and methodology of the research work are also pointed in this chapter.

CHAPTER 2

LITERATURE REVIEW

The primary focus of the literature survey conducted was on the distribution of the particulates in the Particulate Metal Matrix composites (PMMC). The common materials for the matrix phase and particulate phase were identified along with the manufacturing methods which influence the strength and particulate distribution. Computational Fluid Dynamics (CFD) simulations for the particulate distribution were also considered. Mixing being the key factor, most of the referred journals were connected to chemical engineering process. The outcomes of the literature survey are presented in five subsections. The first one describes the materials used as reinforcement and matrix in the manufacturing of PMMC. The second one describes the methods of producing PMMC. The third gives information about the hydrodynamics of the fluid flow inside a stirred vessel. The fourth one observes the CFD works carried out in manufacturing of PMMC by the previous researchers. The last one describes the performance evaluation of mixing in a stirred vessel and the two axes rotation mixer.

2.1 Materials used in PMMC manufacturing

The old civilisation used composite made from mud and straw in which mud having a low tensile strength and straw having a high tensile strength. The example for composite made by nature is wood in which cellulose fibers act as reinforcement. The continuous phase in a composite is called matrix which has a low strength than the reinforcement. Based on the matrix material, the composites are classified as Polymer Matrix Composites (PMC), Ceramic Matrix Composites (CMC) and Metal Matrix Composites (MMC). Based on the reinforcement types, composites are classified as particulates composites, fibrous composites and laminated composites. Since the area under research is focused on PMMC, the following paragraphs explains the common materials used in PMMC.

The materials commonly used in PMMC as the matrix are Al, Mg, Ti, Zn, Cu etc. (Bodunrin et al., 2015). The different types of ceramic particles usually employed for reinforcement in the PMMC are SiC, Al_2O_3, MgO, BeO, CuO, SiO_2, TiC, TiO_2, Fe_2O_3, Fe_3O_4, ZnO, MnO_2, Gr etc. (Almadhoni and Khan., 2015). The combination of these materials also used as reinforcements for producing hybrid composites. Table 2.1 provides the details of

reinforcements and matrix materials in different PMMCs that are developed by different researchers in that decade.

Table 2.1 Properties of Aluminium Metal Matrix Composite (Yashpal et al. (2017))

Reference	Matrix material	Reinforcement	Particulate size	Hardness	Tensile strength (MPa)
Kalaiselvam et al. (2011)	A6061	12 wt.% B_4C	10 μm	80.8 HV	215
Kumar and Murugan (2012)	A6061	20 wt.% AlN	3-4 μm	79 BHN	241
Gopalakrishnan and Murugan (2012)	A6061	10 vol.% TiC	-	44 HV	115
Mazaheri at al. (2013)	Pure Al	10 vol.% B_4C	30 μm	51 HV	132
Niranjan et al. (2013)	A356	5.96 wt.% TiB_2	-	70.98 HV	261.84
Selvam et al. (2013)	A6061	10 wt.% SiC + 7.5 wt.% Fly ash	-	78.8 HV	213
Kumar et al. (2013)	A359	8 wt.% Al_2O_3	30 μm	72.8 HRC	148.7
Ezatpour et al. (2014)	A6061	1 wt.% Al_2O_3	40 nm	-	260
Dwivedi et al. (2014)	A356	15 wt.% SiC	25 μm	104.66 BHN	309.83
Sharma et al. (2015)	A6082	12 wt.% Si_3N_4	50 μm	93.5 VHN	201
Kohli et al. (2015)	A6061	3.5 wt.% Al_2O_3	40 nm	74.25 HRB	254.72

Youssef et al. (2005) conducted experiments for examining the behaviour of titanium diboride (TiB2) during solidification in metal matrix of pure aluminium and aluminium alloy. Kok. M. (2005) fabricated an aluminium alloy based PMMC with Al_2O_3 particulates as reinforcement using vortex method. El-Khair et al. (2007) fabricated a PMMC with Aluminium alloy as the matrix material and ZrO_2 as reinforcement for studying the erosion-corrosion behaviour of cast composite. Lashgari et al. (2010) produced an aluminium alloy matrix based composite using stir casting method. The reinforcement was used B_4C, along with a small amount of strontium added as a modifier for improving the wear properties of the cast composite. Zhang et al. (2010) fabricated ZrC particle reinforced metal matrix composite with tungsten as matrix material using hot-pressing method for studying the high-temperature electrical resistivity.

Khorshidi et al. (2011) made a Mg_2Si particulate reinforced composite with Al alloy having a small amount of lithium as matrix material for improving the mechanical properties. Alaneme et al. (2013) fabricated rice husk ash (HRA) – alumina reinforced PMMC with Al-Mg-Si alloy as matrix material using stir casting. The HRA was added for reducing the cost of the composite. He found that the addition of more quantity of HRA slightly reduces the strength of the cast composite. Ramnath et al. (2014) fabricated a hybrid composite by stir casting with aluminium alloy as the matrix material and two types of reinforcement particulates. The reinforcement particulates were $Al_2O_3$and B_4C. $Al_2O_3$and B_4C were powders added for increasing wear resistance and fracture toughness respectively. Prabhu, T.R. (2014) produced a hybrid composite using powder metallurgy with Fe, SiC, Gr and $BaSO_4$ powders for examining the dry sliding wear characteristics. Liu et al. (2015) made a composite with titanium as the matrix material and WC (Tungsten Carbide) particulates as reinforcement by laser beam processing.

2.2 PMMC manufacturing methods

The common manufacturing processes of PMMC are Liquid processing, Semi-solid processing and Solid processing. Strength and cost of the composite largely depends on its manufacturing process. The primary challenge in the manufacturing of composites is developing a cost effective method for obtaining the desired distribution of the reinforcement.

2.2.1 Liquid phase processing

In liquid processing, the matrix material is in liquid form while the reinforcement is in solid powdered form. The matrix material is heated to liquid state and powdered reinforcement is added to this matrix to get the desired composite. Researches on liquid phase processing that are reported are summarised in the subsequent sections.

2.2.1.1 Stir casting

The widely used manufacturing method for producing PMMC is the stir casting. In this method, the dispersed particulate reinforcement is stirred inside molten matrix metal using a mechanical stirrer. Hashim et al. (1999) had conducted a comparative study of the different manufacturing processes have found that stir casting is the best method for producing PMMC with high strength, least expensive and causing no damages to the particulate reinforcement.

The homogeneous distribution of the particulates is a major concern in stir casting. Prabu et al. (2006) conducted experiments for studying the particulate distribution to cast

composite by varying stirring speed and stirring time. He manufactured PMMC with aluminium alloy A384 as the matrix material and 10 vol% SiC of 16 μm size. At lower stirring speed and lower stir time, the clustering of particulates was noticed in the cast composite. Higher hardness of the composite was obtained for the cast composite produced at larger stirring speed and stirring time. Lina et al. (2011) conducted experiments for studying the effect of stirring temperature and stirring time on reinforcement distribution and tensile properties of the cast composite. The reinforcements selected wereAluminum Borate whisker and Silicon Carbide Particulates with the 6061Al matrix material. The study revealed that the homogeneity of reinforcement and tensile properties increased with decreasing the stirring temperature and increasing stirring time.

Behera et al. (2012) conducted experiments for studying the distribution of SiC particulates in metal matrix composites made by stir casting and its effect on mechanical properties. The study indicated that the distribution of SiC particles was not uniform throughout the casting.Yigezu et al. (2013) fabricated a hybrid composite using aluminium alloy as the matrix material and a mixture of SiC and Al_2O_3 powders as reinforcement using stir casting method. The microstructure study showed a fair distribution of $Al_2O_3$and clustering of SiC particulates. Ghauri et al. (2013) tested mechanical properties and conducted a microscopic study to evaluate the clustering of particulates in the stir cast PMMC. The agglomeration of SiC particles resulted in lowering of properties regarding toughness and hardness. They concluded that the centrifugal force of the larger particles causes the non-uniformity of the distribution of particulates.

Ezatpour et al. (2014) fabricated PMMC by stir casting with Al 6061 aluminium alloy as the matrix material and SiC of 40nm size as particulate. The amount of SiCnano particulates varied from 0.5 to 1.5wt %. The stir casting process followed by an extrusion process for producing the composite. He observed an agglomeration of nanoparticles at higher wt% loading. Aigbodion (2014) manufactured particulate composite with ash powder and Al-Cu-Mg alloy by stir casting method. Thewt % of SiC is varied from 2 to 10. The microstructure analysis shows the agglomeration of ash particulates in the matrix. Sharma et al. (2015) made Aluminium matrix composites with graphite particulates by stir casting process. The wt % of graphite is varied from 3 to 12. The microstructure of the cast PMMC shows a non-uniform distribution of graphite particulates. He manufactured PMMC with Silicon Nitride (Si_3N_4) particulate and Aluminium also. The wt % of Silicon Nitride is varied from 3 to 12. A non-uniform distribution of particulates was reported by conducting microstructure analysis.

Balaji et al. (2015) manufactured two types of aluminium alloy matrix based PMMC with SiC and Al_2O_3 as reinforcements. The mechanical properties of SiC reinforcement composite showed better mechanical properties than that of Al_2O_3 reinforcement composite. Kandpal et al. (2017) found clustering of Al_2O_3 particulates in the cast composite prepared by stir casting, where aluminium alloy Al 6061 was the matrix material. Kumar et al. (2018) prepared a magnesium alloy based metal matrix composite with SiC of 40 μm size. The volume fraction of SiC particulates varied from 3% to 12%. Fairly uniform distribution of particulates was observed in the cast composites.

2.2.1.2 Infiltration

In this process, liquid metal is infiltrated into a reinforcement material preform. Sahin and Acilar (2003) manufactured PMMC with aluminium alloy as the matrix material and SiC particulates as reinforcement. The particulate loading was up to 55 vol.%. This method was expensive as compared to stir casting method. The distribution of particulates was more uniform and the hardness and wear resistance were found more in high particulate loading. Hu et al. (2014) manufactured PMMC by infiltration method with aluminium as the matrix material and TiNifibers and SiC particulates as reinforcement. The amount of TiNifibers was 20 vol.% and SiC varied up to 20 vol.%. The cast composite showed high yield strength and elastic modulus.

2.2.1.3 Squeeze casting

In this method, the molten metal is squeezed into the reinforcement preform. Reihani (2006) prepared a PMMC using this method in which Al6061 molten alloy was squeezed into a SiC preform. The SiC loading was 30 vol.% with two different sizes of 16 and 22 μm. The microstructure of the cast composite showed a uniform distribution of particulates. The composite with decreasing particulate size showed better mechanical properties. Zhang et al. (2006) fabricated aluminium based hybrid composite using whiskers and nanoparticles of SiC. The whiskers loading was 20 vol.% and SiC nanoparticles with 35 nm size was varied up to 7 vol.%. The obtained composite showed a better distribution of reinforcements. The strength of the cast composite was found high with a high reinforcement loading. Beffort et al. (2007) manufactured an aluminium based PMMC with SiC of size 12.5 μm as reinforcement. The matrix material was superheated to 10^0 C above liquidus temperature and squeezed into SiC preform at a pressure of 1400 bar. The distribution of SiC particulates was homogeneous.

Table 2.2 Manufacturing processes of the PMMCs and their reinforcement distributions

Reference	Manufacturing process	Matrix material	Reinforcement material	Reinforcement distribution
Sahin and Acilar (2003)	Infiltration	Al-Si alloy	SiC - 149μm & 80μm size. up to 55 vol.%	Uniform
Prabu et al. (2006)	Stir casting	A384	SiC - 16μm size 10 vol.%	Clustering of particulates
Reihani et al. (2006)	Squeeze casting	Al6061	SiC preform - 16μm & 22μm size, 30 vol.%	Uniform
Zhang et al. (2006)	Squeeze casting	Al32024	SiC whiskers 20 vol.% and SiCnano particle 7 vol.%	Uniform
Beffort et al. (2007)	Squeeze casting	Al99.99% AlMg4 AlZn6 AlCu3 AlZn6Mg1	SiC – 12.5μm size 60 vol.%	Uniform
Lina et al. (2011)	Stir casting	Al6061	Aluminum borate whisker – 5 vol.%, SiC – 8-14μm size, 15 vol.%	Uniform
Amirkhanlou et al. (2011)	Compo-casting	Al6061	SiC - 3μm size 10 vol.%	Uniform after cold rolling
Sajjadi et al. (2012)	Compo-casting	A356	Al_2O_3up to 7.5 wt.% of 20μmsize and up to 4 wt.% of 50 nm	Uniform
Behera et al. (2012)	Stir casting	LM6	SiC – 37 μm size 5-12.5 wt.%	Segregation of particles
Kumar et al. (2013)	Electromagnetic stir casting	A359	Al_2O_3– 30 μm size 2-8 wt%	Uniform
Yigezu et al. (2013)	Stir casting	Mg foundry alloy with Al-4% and Cu-2.5%	SiC&Al_2O_3 – 37 μm size, 5 wt%	Fairly distribution of Al2O3 and clustering of SiC
Ghauri et al. (2013)	Stir casting	Al	SiC – 10 μm size, up to 30 vol.%	Agglomeration of SiC
Hu et al. (2014)	Infiltration	Al	Ti-50 at.%Nifibers – 20 vol.%, Sic - 5μm size & 35 vol.%	Uniform
Ezatpour et al. (2014)	Stir casting	Al6061	Al_2O_3 – 40 nm size up to 1.5 wt.%	Agglomeration of Al_2O_3
Aigbodion (2014)	Stir casting	A2009	Bagasse ash (sugarcane ash) – 10 wt%	Agglomeration of ash particulates
Wang et al. (2014)	Stir casting assisted ultrasonic vibration	AZ31B magnesium alloy	SiC – 10 μm& up to 13.5 vol.%, SiC – 60 nm & up to 1.5 vol.%	Non-uniform
Sharma et al. (2015)	Stir casting	A6082	Gr - 50μm size up to 12 wt.%	Non-uniform

2.2.2 Semi-solid phase processing

In semi-solid processing, the matrix material is in semi-solid form while the reinforcement is in solid powdered form. The research works reported on the three different methods of producing PMMCs in semi-solid phase processing are explained in the following subsections. Table 2.2 gives a consolidation of the research work reported on the different methods of semi-solid phase processing.

2.2.2.1 Compo-casting

Compo-casting is a vortex method in which semi-solid metal is mechanically stirred while introducing the reinforcement particulates. Amirkhanlou et al. (2011) prepared aluminium alloy based PMMC with 10 vol.% SiC particulates by compo-casting followed by a cold rolling process. The uniformity of particle distribution was more after the cold working process. He suggested that, Introducing particulates in semi-solid metal while mechanical stirring would reduce the formation of dendritic growth producing a fine-grained composite. Sajjadi et al. (2012) manufactured a PMMC with aluminium A356 as the matrix material and Al_2O_3 as reinforcement by both stir casting and compo-casting process.

The micrograph of the cast composite showed improved homogeneity of particulates was more in compo-casting than stir casting. He observed a better wettability of particulates was better in compo-casting. The mechanical properties were also found better in compo-casting. Khosravi et al. (2015) conducted experiments for studying the SiC particulate distribution in compo-casting. SiC particulates were mixed with semi-solid aluminium using stirrer and the mould vibrated during solidification. The cast composite showed better homogeneity of particulates and tribological properties.

2.2.2.2 Electromagnetic stir casting

In electromagnetic stir casting, the molten metal is stirred using an electromagnetic field. The stirring is maintained during the solidification to prevent the formation of dendritic growth for obtaining globular/spheroidal microstructure. The strength of such materials produced by this method is more than produced to stir casting method. Barman et al. (2009) conducted experiment and CFD simulation for Electromagnetic stir casting and found that the generation of non-dendritic microstructure during the solidification produced improved mechanical properties of the cast composite. Tennyson et al. (2010) and Meng-ou et al. (2010) produced aluminium alloys using this process. Kumar et al. (2013)

produced Al_2O_3 reinforced PMMC by this method. The matrix material was A359 aluminium alloy. The cast composite showed better mechanical properties with smaller grain size.

2.2.2.3 Ultrasonic processing

In ultrasonic processing, the particulate reinforcement is mixed with the molten matrix metal using ultrasonic vibrations. Murty et al. (2012) tested the mechanical properties of aluminium-fly ash nanocomposite prepared by the ultrasonic method. The microstructure reveals a homogeneous distribution of particulates. Wang et al. (2014) manufactured a composite using this process in which matrix material was magnesium alloy and reinforcement was SiC particulates. In his study, the magnesium alloy was heated to the semi-solid state, and SiC particulates were added while stirring. It was followed by ultrasonic treatment and again stirred the molten metal in the liquid state. Too long and short time for stirring during the ultrasonic treatment showed a non-uniform distribution of particulates.

2.2.3 Solid phase processing

In solid processing, both the matrix material and the reinforcement are in solid powdered form. Powder metallurgy is used in solid processing for producing PMMC.

In this method both the matrix and particulates materials in the powder form are thoroughly mixed and pressed at high pressure inside a steel die. Canakci and Varol (2014) fabricated a PMMC with AA7075 aluminium alloy as the matrix material and SiC particulates of size 16 μm and 2.5 to 10 wt.%. The microstructure study shows the non-homogeneous distribution of SiC particulates. The agglomeration of SiC particulates was found more for higher SiC particulate loading.

2.3 Computational Fluid Dynamics simulations of stirred vessels

Computational fluid dynamics (CFD) is widely used for simulating the liquid-liquid and liquid-solid mixing processes in stirred vessels (Oumer and Mamat, 2014). The hydrodynamics of the multiphase mixing system makes CFD simulation is more complicated due to the existence of various levels of interaction between the phases. CFD simulation models can be designed for the mixing process which can avoid empirical scaling as used in the experiments of the mixing system (Srilatha et al., 2010). Hydrodynamics of the mixing process can be predicted using CFD simulation for different geometries and operating conditions of the mixing container (Ramesha et al., 2012; Rao and Sivashanmugam, 2010;

Takahashi and Motoda,2009). Alfaro-Ayala et al. (2015) conducted CFD simulation in a stirred vessel for arriving the best position of the stirrer.

CFD analysis on multi-stage stirred vessels was also investigated by the researchers (Alliet-Gaubert et al., 2006). Alternate combinations of rotors and stators mounted on the mixing tank were also studied (Wu et al., 2014). Studies conducted on the CFD simulation of large-scale mixing vessels stirred with multiple radial impellers, and radial and axial up-pumping impellers were reported by Vrabel et al. (2000). Abhishek et al. (2012) proposed an improved geometry of stirrer like an anchor for improving the mixing efficiency. The deficiencies in stirred mixing such as formation of Isolated Mixing Regions (IMRs) which refer to mixed zones separated by fluid boundary, and non-uniformity of distribution of particles especially for highly viscous fluids are reported by Li et al. (2016), Wu et al. (2015) and Prabhu et al. (2006). The mixing time will be more for highly viscous fluids to get a homogenous mixture in a stirred tank (Naher et al., 2007).

Numerous CFD simulations of baffled mixing systems that improve the mixing performance were proposed by researchers (Nouri and Whitelaw, 1992; Takahashi and Motoda, 2009; Zhu et al., 2009; Singh et al., 2011). Many modifications including the different types of baffles and alteration of stirrer geometry were carried out for improving the mixing performance. Without baffles fitted on the sides of the mixing tank, a solid-body rotation is formed corresponding to the central whirlpool of the flow for low viscosity liquids. By introducing baffles, the mixing can be improved by getting the desired flow condition (Busciglio et al., 2017). However in some mixing processes like biological operations, the baffles may cause cell damage (Yang et al., 2013). Lassaigne et al. (2016) experimented on the effect of geometrical parameters of the stirred vessel on the improvement of particle distribution and found that the homogenization was improved with higher diameters and clearances of the impeller.

Gu et al. (2017) experimented with stirred vessel with a double punched rigid-flexible impeller and obtained a better solid particle suspension. Mishra and Ein-Mozaffari (2017) introduced a Maxblend impeller with a baffled mixing vessel for improving the homogeneity of the suspended particles. Significantly, Vikash et al. (2017) also conducted an experiment and CFD simulation in a stirred vessel with a rotor-stator high shear mixing impeller for improving the mixing performance. Again, Bao et al. (2018) carried out the Discrete Element Method (DEM) simulation for finding the best type of impellers working in a stirred vessel.

Related to this, the five types of impellers used were double helical ribbon, pitched blade ribbon, inner and outer helical ribbon, bottom helical ribbon and pfaudler. It is noteworthy that a combination of bottom helical ribbon, also with inner and outer helical ribbon was found more efficient for particle mixing. Interestingly, the strength of chaotic mixing can also be improved by placing the stirrer eccentrically (Yavuz and Sandeep, 2018).

CFD simulation is an effective method for identifying the unsteadiness and pulsating flow features (Zamiri and Chung, 2018). Meng et al. (2018) have performed CFD simulation for mixing in a new type of particle mixer by Eulerian-Eulerian approach. The VOF (volume of fluids) method which is a Euler-Euler multiphase approach was used for obtaining the flow features from the CFD simulation. Many researchers (Xie and Luo, 2018; Montante and Magelli, 2005) have conducted numerical simulation of solid-liquid suspensions attained by mechanical stirrer inside a stirred vessel using Eulerian-Eulerian method. In connection with this, Varela et al. (2018) conducted a numerical simulation of mixing inside a stirred vessel using RNG k-Ɛ turbulence model which is known by the name Eulerian-Eulerian approach for solving the flow fields of highly swirling flows. Zhao et al. (2014) conducted a CFD simulation of slurry mixing in a stirred vesselwith an improved intermig impeller, in which, the flow field was predicted using RNG k-Ɛ turbulence model. Significantly, Wu. (2010) also conducted a similar CFD simulation for a mixing study in aerated lagoons using RNG k-Ɛ turbulence model. A large number of CFD simulations were reported using the RNG k-Ɛ turbulence model as the multiphase simulation methodology for solving the solid-liquid mixing flow fields.

2.4 Computational Fluid Dynamics simulations of PMMC manufacturing

Measurement of fluid flow characteristics is difficult in a melt-metal system. Primarily due to this reason, several numerical simulations have been carried out by researchers for studying the mixing processes of the stir casting with the help of CFD tools. Table 2.3 shows a tabulation of the different multiphase and turbulence models used for simulation of flows in different equipments, as carried out by different authors.

Aldas and Mat (2005) investigated the particulate distribution of SiC particulates in PMMC with Pb and 20% Sn as matrix material by experimentally and theoretically. The theoretical analysis of stir casting was done by CFD analysis. He found that the particulate distribution near the wall was found more than the axis of the mixing vessel. Neher et al.,

(2007) conducted room temperature analogue fluid simulations for PMMC casting for studying the SiC particulate distribution in stir casting.

The flow pattern inside the mixing vessel which influences the efficiency of mixing was also observed by CFD simulation (Hashim et al., 2002). The developed FEA model for mixing molten aluminium contains SiC particulates was compared with the experiments done by replacing aluminium liquid with glycerol. They arrived at the optimum stirring speed and stirrer position for obtaining a more uniform distribution of SiC particulates. Montante and Magelli, (2005) had investigated the distribution of solid particles in liquid inside a stirred vessel using the CFD techniques. Su et al. (2010) conducted CFD simulation for optimization of process parameters such as stirrer geometry, blade angle, stirrer speed in stir casting process for producing aluminium metal matrix composite. Kumar et al. (2015) conducted CFD simulation of stir casting process for studying the effect of stirrer speed on the distribution of particulates inside the mixing vessel. The particulate phase and the continuous matrix phase were modelled using the multiphase modelling approach.

2.4.1 Numerical models for mixing

The Multiphase CFD simulations are carried out generally in Eulerian Granular or Mixture models. The Eulerian Granular model is a complex model for solving multiphase flow. It solves continuity and momentum equations for each phase. Most of the CFD simulation work reported for the stirred vessels is carried out in the Eulerian Granular model (Taghavi et al., 2011; Sing et al., 2011; Naher et al., 2007). For low particulate loading, the Mixture model can predict the flow field using a single momentum equation of the mixture fluid. The CFD simulation using Mixture model for stirred vessels and cyclone separator were conducted by many researchers (Moghari et al.,2011; Haavisto et al., 2009; Cokljat et al., 2006). Roudsari et al. (2012) conducted CFD simulation in the Eulerian model for understanding the droplet size distribution in a water and oil emulsion mixture while mixing.

2.4.2 Turbulence modelling

Deglon and Meyer(2006) and conducted CFD simulations for studying hydrodynamics inside a stirred vessel using standard k-Ɛ turbulence model. Panneerselvam et al. (2008) modelled CFD simulation of a mixing vessel used for mixing gas, fluid and solid particles in which the standard k-Ɛ turbulence model was used. Wang et al. (2010) conducted experiments and CFD simulation for examining the mixing performance of liquids with solid

particles. The results compared with the experiments shows better agreement while using the RNG k-Ɛ turbulence model.

Table 2.3 The multiphase models and turbulence models used in mixing equipments

Reference (Authors)	***Equipment used***	***Multiphase model***	***Turbulence model***
Micale et al. (2004)	Stirred vessel	Eulerian-Granular	Standard k-Ɛ
Montante and Magelli (2005)	Stirred vessel	Eulerian-Granular	Standard k-Ɛ
Khopkar et. al. (2005)	Stirred vessel	Eulerian-Granular	Standard k-Ɛ
Khopkar et al. (2006)	Tall gas-liquid Stirred vessel	Mixture	Standard k-Ɛ
Cokljat et al. (2006)	Cyclone separator	Mixture	RNG k-Ɛ
Torre et al. (2007)	Partially filled stirred vessel	(Volume of Fluid) VOF	Standard k-Ɛ
Neher et al. (2007)	Stir casting	Eulerian-Granular	Standard k-Ɛ
Panneerselvam et al. (2008)	Stirred vessel	Eulerian-Granular	Standard k-Ɛ
Jahoda et al. (2009)	Stirred vessel	Mixture	Standard k-Ɛ
Fletcher and Brown (2009)	Stirred vessel	Eulerian-Granular	Standard k-Ɛ
Haavisto et al. (2009)	Stirred vessel	Mixture	Standard k-Ɛ
Yu et a. (2010)	Anaerobic digester with bio-waste particle flow	Eulerian-Granular	Realizable k-Ɛ
Wang et al. (2010)	Stirred vessel	Eulerian-Granular	RNG k-Ɛ
Hreiz et al. (2011)	Cyclone separator	Eulerian-Granular	Standard k-Ɛ Realizable k-Ɛ RNG k-Ɛ
Taghavi et al. (2011)	Stirred vessel with dual Rushton turbine	Eulerian-Granular	RNG k-Ɛ
Tamburini et al. (2012)	Baffled stirred vessel	Eulerian-Granular	Standard k-Ɛ
Zhao et al. (2014)	Stirred vessel with intermig impeller	Eulerian-Granular	Standard k-Ɛ
Kumar et al. (2015)	Stir casting	Mixture	Realizable k-Ɛ

Taghavi et al. (2011) investigated the power consumption for mixing inside a Rushton turbine stirred vessel by conducting CFD simulation and compared the results. The RNG k-Ɛ turbulence model used in this simulation which is suitable for highly swirling flow could predict the mixing power more accurately. Hreiz et al. (2011) investigated the flow parameters inside a cyclone separator using CFD simulation. The simulations were carried

out in three different turbulence model namely standard k-Ɛ, RNG k-Ɛ and realizable k-Ɛ. They suggested that both the RNG k-Ɛ and realizable k-Ɛ turbulence model were better than the standard k-Ɛ turbulence model.

2.4.3 Validation of CFD simulation in mixing vessels

The validation with experiment is an essential step for developing a CFD simulation model. Shekhar and Jayanti(2002) developed a CFD simulation model for mechanically stirred mixing vessel which was validated with experiment. The study was conducted for laminar, transition and turbulent conditions of the fluid flow. The simulation model was validated by computing the mixing power and mixing time obtained from the correlation and from the literature. Deglon and Meyer (2006) developed a CFD simulation model for stirred tanks by validating with Power number, mean velocity components and turbulent kinetic energy from published experimental results. Zadghaffari et al. (2010) conducted CFD simulation of a stirred vessel and validated using power number, mean velocity components, mixing time, turbulent kinetic energy and turbulent dissipation rate from published experimental data.

The power consumed for the mixing process was obtained by subtracting the power obtained at no-load condition from loaded condition (Rao and Sivashanmugam, 2010; Andre at al., 2012). The mixing power by CFD simulation can be obtained by both Viscous dissipation method and Torque method. In Viscous dissipation method, the viscous dissipation energy was integrated over the entire domain of mixing to get the mixing power (Alliet-Gaubert et al., 2006). In Torque method, the torque acting on the walls of the impeller was used to determine the mixing power (Zhu et al., 2009; Coroneo et al., 2011).

2.4.4 Grid independence study

In CFD simulations, the domain under consideration is divided into small control volumes. Partial differential equations related to the flow fields are solved for each control volumes for obtaining results at discrete points. Here, the results obtained largely depend on the size of small control volumes. The results of a CFD simulation model should be grid independent. A quantified entity is more appropriate for checking whether the results are grid independent or not. Roache (1994) suggested the Richardson extrapolation method is the best mrthod for quantifying the grid independence using Grid Convergence Index (GCI). Ali et al. (2009) have conducted a Direct Numerical Simulation (DNS) of a flow around a square cylinder and took the results for flow variables having a GCI value less than 5%. Coughtrie et

al. (2013) have investigated the flow through an anaerobic gas-lift digester using CFD simulation with different turbulent closure models. The CFD simulation was carried out in fine, medium and coarse grids for obtaining the GCI value of the flow variables. They ensured that the GCI values were less than 5%. Volk et al. (2017), Almohammadi et al. (2013) and Longest and Vinchurkar (2007) were also reported the use of Richardson extrapolation method in a grid refinement study to arrive at a grid independent flow variable solution.

2.5 Dual axis rotation

The mixing of fluids with particulates is usually performed with mechanically agitated stirred vessels having an impeller arrangement which rotates about a single axis. Delaplace et al.(2007) have conducted experimented in a planetary mixer for determining the mixing performance of glucose syrup-water mixture. The planetary mixer is a device used for mixing powders and fluids in which the agitator rotates about two axes. The results obtained had to be compared with the usual mixing stirred vessel device. For this purpose, he conducted a dimensional analysis to get an expression for Reynolds number. The Characteristic velocity for the planetary mixer was derived using the maximum velocity of fluid flow inside the mixing system (Auger et al., 2013; Guillaume et al., 2012). Andre et al. (2012) and Auger et al. (2013) have conducted dimension analysis for comparing the mixing performance of a planetary mixer to derive an expression for Power number.

2.6 Summary

PMMC with Aluminium alloy as matrix material is widely used in many engineering applications. The composite made using this alloy exhibits a high specific strength. The widely used particulate reinforcement in such composites is SiC.

Stir casting is the most widely used manufacturing method for producing PMMC. The mechanical mixing of this process is less expensive than other processes for producing PMMCs. The pressure inside the mixing vessel of a stir casting device being low, the chance for damaging of reinforcements in the cast product is very low. However, the non-uniform distribution of the particulates is the major drawback in stir casting. A mechanical mixing system under low pressure is a better option for obtaining uniform distribution for avoiding such difficulties.

The understanding of hydrodynamics inside a mixing vessel is absolutely necessary for examining the mixing performance. Numerous CFD simulations had been conducted for

such mixing system by many researchers. The mixing performance was studied by changing the stirrer speed and stirrer positions inside the mixing vessel. CFD simulation was also conducted by changing the geometry and number of impellers.

CFD simulation of stir casting was also done by many researchers. In stir casting process, the molten metal is vigorously stirred inside the mixing vessel by an impeller. Conducting experiments inside such a molten metal system while stirring is very difficult. Here, simulation is the best alternative to understand the fluid flow behaviour in such mixing systems. The simulation models built for mixing systems has to be validated with experiments. For such purpose, analogue fluid simulations and experiments were carried out in which the selected fluid has almost same viscosity as that of the molten metal.

The CFD simulation for mixing fluid with particulates is usually conducted in Multiphase model. The multiphase simulation models widely used for such purpose are Eulerian granular model and mixture model. Among the turbulence model, the RNG k-Ɛ turbulence model is the best for catching the highly swirling characteristics of the fluid flow inside the mixing system.

The validation of simulation model with experiment is an essential procedure for developing the CFD simulation model. The Power number calculated from mixing power obtained from experiment is used by many researchers for comparing the experimental and simulation results. The mixing power from experiment is determined from the power consumed by the mixing machine. The Viscous dissipation method and Torque method are used for finding the mixing power from CFD simulation.

It is necessary to conduct the grid independence study for a CFD simulation for obtaining flow variables which is steady after the refinement of grid size. Richardson extrapolation method is the best way to quantify the grid independence. The GCI value of less than 5% after the refinement of grid size is a measure of grid independence of the flow variable.

The proposal for a new mixing system of dual axes rotation of mixing vessel for obtaining uniform distribution of particulates has to compare with the existing systems. However, the existing system of mechanical mixing is the single axis rotation of the stirrer. The comparison of the systems can be carried out based on the non-dimensional numbers such as Reynolds number and Power number. The Characteristic velocity of the flow inside the mixing vessel is also to be derived for the dual axis rotation of mixing vessel. These

parameters are derived by previous researchers for a planetary mixer having dual axis rotation. The same procedure can be used for deriving such parameters for dual axis rotating mixing vessel.

CHAPTER 3

NUMERICAL MODELLING OF DUAL AXIS ROTATION MIXING DEVICE

Development of the numerical model for simulating the dual axis rotation of the mixing device is explained in this chapter. The parameters of the process, models of numerical simulations and their expressions are derived in this chapter.

The continuous phase is the liquid in which the particulates are to be mixed is the primary phase. The particulates to be mixed are the secondary phase. The mixing flow in a rotating cylinder is complex to model. The clustering of particulate and the phase interactions are more intricate. The flow behaviour and interaction between the phases has to be understood before selecting the multiphase simulation models.

3.1 Dual axis mixing

The schematics of the planetary mixer and dual axis mixing vessel systems are shown in Fig. 3.1 and Fig. 3.2 respectively. The impeller inside the mixing chamber of a planetary mixer is rotated about two axes with bevel gear arrangements. This will help the agitation everywhere inside the mixing chamber. The mixing vessel of the proposed dual axis mixing device is rotated about two mutually perpendicular axes. The N_S and N_G are the spin speed and gyration speed respectively.

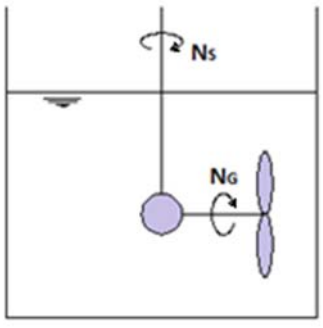

Fig. 3.1 Planetary mixer

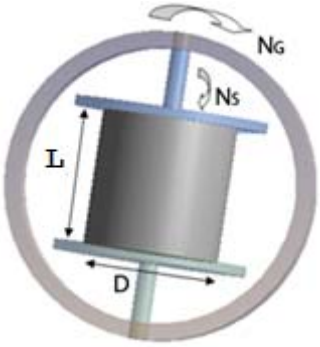

Fig. 3.2 Dual axis mixing device

The classical Reynolds Number and Power Number are not significant in gyro mixing due to the dual rotation of the mixing vessel. The maximum velocity inside the fluid system depends on spin speed and gyration speed of the mixing cylinder. Researchers have

proposed two parameters namely Characteristic velocity (U_{ch}) and Power number (N_p) to represent the properties of mixing. Planetary mixers having dual rotation of the mixing impeller uses the term Characteristic velocity for replacing the dual rotational speeds for the purpose of dimensional analysis. The most important and representative dimensionless parameter used extensively for a mixing systems is the Power Number. The Power Number is generally used to establish the validity of CFD simulations of flow in stirred tanks (Shekhar and Jayanti, 2002; Deglon and Meyer, 2006; Zadghaffari, 2010).

3.1.1 Mixing power

The term Mixing Power (P) is used to compare the quality of different types of mixers. Mixing power for a mixer depends on physical properties such as density and viscosity, operating parameters like stirrer speed and geometrical parameters like diameter of the mixing tank. It is the energy consumed for mixing in a period of time. It is a key factor for operating cost, scaling-up and design of mixing vessel. The mechanical agitator efficiency, mass transfer and circulation time also related to the mixing power. The mixing power can be calculated in two methods namely Viscous dissipation method and Torque method.

3.1.1.1 Viscous dissipation method

The power for mixing is arrived at using two methods as proposed by researchers. In the first method P is obtained by integrating the viscous dissipation energy, (Φv) over the entire mixing domain (Alliet-Gaubert et al., 2006). The power consumed for the mixing is dissipated in the liquid which is the work done against the viscous force.

$$P = \iiint_V \mu_1 \Phi v \, dV \tag{3.1}$$

where,

$$\Phi v = 2\left[\left(\frac{dV_x}{dx}\right)^2 + \left(\frac{dV_y}{dy}\right)^2 + \left(\frac{dV_z}{dz}\right)^2\right] + \left[\frac{dV_x}{dy} + \frac{dV_y}{dx}\right]^2 + \left[\frac{dV_x}{dz} + \frac{dV_z}{dx}\right]^2 + \left[\frac{dV_y}{dz} + \frac{dV_z}{dy}\right]^2 \tag{3.2}$$

and μ_1=Apparent fluid viscosity in PaS

3.1.1.2 Torque method

In the Torque method, the power for mixing is evaluated from overall torque on the walls due to the tangential stress distribution and pressure (Zhu et al., 2009 and Coroneo et al., 2011).

$$P = 2\pi N_S T_y + 2\pi N_G T_z \tag{3.3}$$

where T_y and T_z are the Torques on the walls in y-axis and z-axis respectively

The efficiency of mixing is expressed in term of Specific Power (P/V) which is the ratio of Mixing Power to the vessel volume.

3.1.2 Characteristic velocity

Characteristic velocity is the ratio of maximum velocity attained on the impeller tip and π. The characteristic velocity, $U_{ch}$for Planetary mixer is obtained using formula 3.4 and 3.5 (Delaplace et al., 2007 and Andre et al., 2012).

$$N_S D_G / N_G D_S < 1;\ U_{ch} = \left[(N_S^2 + N_G^2) \left(D_S^2 + D_G^2 \right) \right] \quad (3.4)$$

$$N_S D_G / N_G D_S > 1;\ U_{ch} = (N_R D_S + N_G D_G) \quad (3.5)$$

where, D_G and D_S are the gyration circle diameter and mixing impeller diameter respectively.

This formula can be used for calculating the Characteristic Velocity in a Gyro shaker also which is given in formula 3.6.

$$U_{ch} \text{ of Gyro Shaker } = (N_S D + N_G L) \quad (3.6)$$

where, D and L are the diameter and length of rotating vessel.

3.1.3 Reynold's number

The Reynolds Number $(R_e)$for stirred vessel is obtained using equation number 3.7 (Zhu et al.,2009) .

$$R_e = \frac{\rho N D^2}{\mu} \quad (3.7)$$

where, ρ is the density of fluid inside the mixing vessel, N is the stirrer speed, D is the diameter of the stirrer and μ is the viscosity of the fluid.

The Reynolds Number (R_{eM}) for the planetary mixing based on characteristic velocity is obtained by the equation 3.8 (Delaplace et al., 2007 and Andre et al., 2012).

$$R_{eM} = \frac{\rho \quad u_{ch} D}{\mu} \quad (3.8)$$

Similarly, Reynolds Number (R_{eG}) based on the Gyration speed are obtained using equation 3.9.

$$R_{eG} = \frac{\rho \quad N_G D^2}{\mu} \quad (3.9)$$

3.1.4 Power number

The energy supplied to the stirred vessel is consumed for shearing the fluid. This energy per unit time is known as Mixing power (P). The mixing efficiency is indicated by Power Number (N_p) which depends on the fluid properties and geometry of the mixing vessel. The Power Number for stirred vessel is obtained using equation number 3.10 (Zhu et al.,2009).

$$N_p = \frac{P}{\rho N^3 D^5} \tag{3.10}$$

The Power Number (N_{pM}) for the planetary mixing based on characteristic velocity are obtained by the equation 3.11 (Delaplace et al., 2007 and Andre et al., 2012).

$$N_{pM} = \frac{P}{\rho u_{ch}^3 \ L^2} \tag{3.11}$$

Similarly, Power Number (N_{pG}) based on the Gyration speed are obtained using equation 3.12.

$$N_{pG} = \frac{P}{\rho N_G^3 D^5} \tag{3.12}$$

3.2 Effect of particulate loading

The interaction between the primary liquid phase and secondary particulate phase is an important parameter for selecting the multiphase CFD simulation model. The particulate loading (β) which is the ratio of mass of the dispersed particulate phase to the mass of continuous liquid phase is used for the selection (Crow et al., 1998).

$$\beta = \frac{\alpha_d \rho_d}{\alpha_c \rho_c} \tag{3.13}$$

Where, $\alpha_d$and α_c are the volume fractions of the secondary dispersed phase and primary continuous phase respectively. ρ_d and ρ_c are the densities of the secondary dispersed phase and primary continuous phase respectively. If particulate loading is very low (β << 1.0), then the fluid flow influences the particulates through turbulence and drag and the influence of the particulates on fluid flow is negligible (ANSYS Fluent Theory Guide, 2013). The multiphase CFD simulation models such as Eulerian, Discrete phase and Mixture are well suitable in such situations to predict the flow features. If the particulate loading is intermediate the influence of the secondary phase is considerable. If the particulate loading is high (β>>1.0), particle pressure and viscous stress should be considered. In the CFD

simulation of Al-SiC PMMC, the particulate loading is intermediate and is equal to 0.296. In such case, Stokes number (St) which is defined as the ratio of particle response time (τ_d) to the system response time (τ_s) should be considered.

$$St = \frac{\tau_d}{\tau_s} \tag{3.14}$$

$$\tau_d = \frac{\rho_d d_d^2}{18\mu_c} \tag{3.15}$$

$$\tau_s = \frac{L_s}{V_s} \tag{3.16}$$

Where, d_d is the particle diameter, μ_c is the viscosity of fluid, Ls is the characteristic length and Vs is the characteristic velocity. The characteristic velocity is taken as the maximum velocity of flow inside the stirred vessel and the characteristic length is taken as the diameter of the stirred vessel (Mattei and Vozzi., 2016).

In this CFD simulation, the Stokes number is very much less than unity and is equal to $1x10^{-5}$. In such situation, the secondary phase particles will follow the flow closely. The Mixture model and Eulerian granular model are more appropriate in this situation (ANSYS Fluent Theory Guide, 2013). The above two multiphase modes are mathematically formulated by Eulerian-Eulerian approach.

3.3 Multiphase models

CFD solvers uses the Finite Volume Method (FVM) in which the fluid domain under consideration is divided into a finite set of control volumes. The conservation equations of fluid flow such as mass, momentum and energy, species etc are to be formulated and solved for each finite control volumes for simulating the flow field. In this work, numerical simulation of the Gyro shaker flow was modelled by three types of multiphase models namely Eulerian kƐ dispersed turbulence model, Mixture model and Volume of fluids (VOF) model. These models and the corresponding governing equations are described in the following sections.

3.3.1 Eulerian Granular Model

The set of momentum and continuity equations for both primary and secondary phases are considered in Eulerian Granular model. Kinetic theory is applied for the secondary granular phase. The coupling between the primary phase and secondary phase is achieved through the pressure and inter phase exchange coefficients. The Eulerian granular dispersed turbulence model is suitable for a dilute secondary phase where the turbulence of the continuous primary phase is dominant. However, particle collisions are not considered in

this model. Transport equations are solved for predicting the turbulence field of the continuous primary phase. In this model, the pressure is same for all the phases. Most of the CFD simulation works reported for the stirred vessels are carried out in Eulerian Granular model (Taghvi et al., 2011; Sing et al., 2011; Naher et al., 2007; Deglon and Meyer, 2006). The following governing equations are solved for the primary liquid phase and secondary granular phase (Zhao et al.,2014).

The continuity equation is:

$$\frac{\partial}{\partial t}(\propto_l \rho_l) + \nabla.(\alpha_l \rho_l v_l) = 0 \tag{3.17}$$

and

$$\frac{\partial}{\partial t}(\propto_s \rho_s) + \nabla.(\alpha_s \rho_s v_s) = 0 \tag{3.18}$$

The momentum equation is:

$$\frac{\partial}{\partial t}(\propto_l \rho_l v_l) + \nabla.(\alpha_l \rho_l v_l v_l) = -\alpha_l \nabla p + \nabla.\bar{\bar{\tau}}_l + \alpha_l \rho_l g + F_l + K_{sl}(v_s - v_l) \tag{3.19}$$

$$\frac{\partial}{\partial t}(\propto_s \rho_s v_s) + \nabla.(\alpha_s \rho_s v_s v_s) = -\alpha_s \nabla p + \nabla.\bar{\bar{\tau}}_s + \alpha_s \rho_s g + F_s + K_{ls}(v_l - v_s) \tag{3.20}$$

Where, the subscripts 'l' and 's' stands for liquid and solid respectively which are the primary and secondary phases in mixing,

and $\bar{\bar{\tau}}_{l,s}$ is the phase stress-strain tensor which is:

$$\bar{\bar{\tau}}_{l,s} = \alpha_{l,s}\mu_{l,s}\left[\left(\nabla v_{l,s} + \nabla v_{l,s}^{T}\right) - \frac{2}{3} I \nabla . v_{l,s}\right] \tag{3.21}$$

The cell volume fractions of primary liquid phase and secondary solid phase are constrained by the equation:

$$\alpha_l + \alpha_s = 1 \tag{3.22}$$

The momentum exchange coefficient is calculated using equations 3.23, 3.24 and 3.25. It is obtained using Gidaspow model -which is used when viscous forces dominate the flow behaviour - and combination of the WEN and YU model and the Ergun equation (ANSYS Fluent Theory Guide, 2013).

$$K_{ls} = K_{sl} = \frac{3}{4} C_D \frac{\alpha_s \alpha_l \rho_l |v_s - v_l|}{d_s} \alpha_l^{-2.65} \tag{3.23}$$

$$C_D = \frac{24}{\alpha_l Re_s}[1 + 0.15(\alpha_l Re_s)^{0.687}] \tag{3.24}$$

$$Re_s = \frac{\rho_l d_s |v_s - v_l|}{\mu_l} \quad (3.25)$$

3.3.2 Mixture Model

In this model, the turbulence field is same for both primary and secondary phases. Both the phases are assumed to be inter penetrating continuum and moves at different velocities. The relative velocity between phases are determined by assuming that the Stokes number of the flow is considerably lower than unity. It solves continuity and momentum equations for the mixture. The effect of interaction of the inter-phase mass, momentum and energy is included in this model. The CFD simulation using Mixture model for stirred vessels and cyclone separator were conducted by several researchers (Moghari et al.,2011; Haavisto et al., 2009; Cokljat et al., 2006).

The continuity equation is given as under:

$$\frac{\partial}{\partial t}(\rho_m) + \nabla.(\rho_m V_m) = 0 \quad (3.26)$$

$$\text{where, } V_m = \frac{\sum_{k=1}^{n} \alpha_k \rho_k V_k}{\rho_m} \quad (3.27)$$

$$\text{and } \rho_m = \sum_{k=1}^{n} \alpha_k \rho_k \quad (3.28)$$

Momentum equation is obtained by summing up the individual momentum equations for all phases.

$$\frac{\partial}{\partial t}(\rho_m V_m) + \nabla.(\rho_m V_m V_m) = -\nabla p + \nabla.[\mu_m(\nabla V_m + \nabla V_m^T)] + \rho_m g + F + \nabla.\left(\sum_{k=1}^{n} \alpha_k \rho_k V_{dr,k} V_{dr,k}\right) \quad (3.29)$$

$$\mu_m = \sum_{k=1}^{n} \alpha_k \mu_k \quad (3.30)$$

$$V_{dr,k} = V_k - V_m \quad (3.31)$$

The volume fraction equation for secondary phase p:

$$\frac{\partial}{\partial t}(\alpha_p \rho_p) + \nabla.(\alpha_p \rho_p V_m) = -\nabla.(\alpha_p \rho_p V_{dr,p}) + \sum_{q=1}^{n}(\dot{m}_{qp} - \dot{m}_{pq}) \quad (3.32)$$

3.3.3 Volume of Fluid Model

The surface-tracking method is used in VOF model for the primary and secondary phases. Each phases shares a single set of momentum equations by tracking the volume fraction of each phase. Governing equations are solved using the volume fraction in each cell. Turbulence and energy equations are solved for the mixture and no empirical

correlations are used for predicting the interaction between phases (ANSYS Fluent Theory Guide, 2013). The model does not support for void region where no phases are existing. Even though this model is designed for immiscible liquids for a sharp interphase between phases, the validity of this model is also evaluated in this paper.

The density is calculated using;

$$\rho = \alpha_2\rho_2 + (1-\alpha_2)\rho_1 \tag{3.33}$$

The Continuity Equation for the volume fraction of the k^{th} phase is given in equation 3.34 which is solved only for the primary phase.

$$\frac{\partial \alpha_k}{\partial t} + V.\nabla\alpha_k = \frac{S\alpha_k}{\rho_k} \tag{3.34}$$

The secondary phase volume fraction is obtained using the equation 3.35.

$$\sum_{k=1}^{n} \alpha_k = 1 \tag{3.35}$$

The single momentum equation for the entire domain is solved using the equation 3.36.

$$\frac{\partial}{\partial t}(\rho V) + \nabla.(\rho VV) = -\nabla p + \nabla.[\mu(\nabla V + \nabla V^T)] + \rho g + F \tag{3.36}$$

where velocity V is taken as the mass averaged variable:

$$V = \frac{\alpha_1\rho_1V_1+\alpha_2\rho_2V_2}{\rho} \tag{3.37}$$

The secondary phase in the simulation of Gyro Shaker is a granular phase, for which knowledge of viscosity is necessary for simulation modelling. The viscosity of secondary granular phase is applied using the formula proposed by Raju and Mehrotta (2000) for studying the casting of particulate metal matrix composites. The proposed equation is as given in equation 3.38.

$\mu_s = \mu\left(1 + 2.5V_p + 10.05V_p^2\right)$ (3.38) where V_p is volume fraction of the secondary particulate phase.

3.4 Turbulence modelling

For all Models, the RNG k-Ɛ turbulence flow model which produces better results for highly swirling and rapidly strained flow was reasonably chosen (Kaushal et al., 2012; Hreiz et al., 2011; Taghvi et al., 2011;Wang et al., 2010; Deglon et al., 2006). A statistical method called 'Renormalization group (RNG)' is used for deriving the RNG k-ε turbulence model

from the instantaneous Navier-Stokes equation. Effect of swirl on turbulence and additional term in turbulent kinetic energy dissipation rate equation for improving accuracy of flow behaviour is also included in this model. The governing equations for modelling turbulent kinetic energy (k) and turbulent energy dissipation rate (Ɛ) are given in equation 3.39 and 3.40 (Wang et al., 2010).

$$\frac{\partial}{\partial t}(\rho k) + \frac{\partial}{\partial x_i}(\rho k u_i) = \frac{\partial}{\partial x_j}\left(\alpha_k \mu_t \frac{\partial k}{\partial x_j}\right) - \rho\overline{u_i' u_j'}\frac{\partial u_j}{\partial x_i} - \rho\varepsilon \tag{3.39}$$

$$\frac{\partial}{\partial t}(\rho \varepsilon) + \frac{\partial}{\partial x_i}(\rho \varepsilon u_i) = \frac{\partial}{\partial x_j}\left(\alpha_\varepsilon \mu_t \frac{\partial \varepsilon}{\partial x_j}\right) - C_{1\varepsilon}\frac{\varepsilon}{k}\rho\overline{u_i' u_j'}\frac{\partial u_j}{\partial x_i} - C_{2\varepsilon}\rho\frac{\varepsilon^2}{k} - R_\varepsilon \tag{3.40}$$

The effective viscosity (μ_t) by considering the effect of swirl is:

$$\mu_t = \rho C_\mu \frac{k^2}{\varepsilon} f\left(\alpha_s, \Omega, \frac{k}{\varepsilon}\right) \tag{3.41}$$

$$R_\varepsilon = \frac{C_\mu \rho \eta^3 (1-\eta/\eta_0)}{1+\beta\eta^3}\frac{\varepsilon^2}{k} \tag{3.42}$$

The closure coefficients are, α_k=1.393, α_ε=1.393, C_μ=0.0845, α_s=0.07, η_0=4.38 and β=0.012.

$\eta = Sk/\varepsilon$, where,S is the modulus of the mean rate-of-strain tensor and is given by

$$S = \left(2S_{ij}S_{ij}\right)^{\frac{1}{2}} \text{ where, } S_{ij} \text{ is the rate-of-strain tensor} \tag{3.43}$$

$$S_{ij} = \frac{1}{2}\left(\frac{\partial \bar{u}_i}{\partial x_j} + \frac{\partial \bar{u}_j}{\partial x_i}\right) \tag{3.44}$$

Ω is the characteristic swirl number and the model constants are, $C_{1\varepsilon}$=1.42 and $C_{2\varepsilon}$=1.68.

For all the simulation models, the effect of mass transfer due to cavitation, evaporation-condensation and boiling are not considered. Lift force, which is significant only if the size of the particles is very large and virtual mass force, which is significant only if the secondary phase density is much smaller than primary phase were also not considered (Wang et al., 2010).

3.5 Governing equations for Rotating Reference Frame

Since the mixing domain was continuously rotating about two axes, the governing equations of the fluid flow was formulated in Rotating Reference Frame (RRF)

approach. In RRF formulation for the fluid flow, two additional terms for the acceleration of the fluid is added in momentum equations. The additional acceleration terms are Coriolis acceleration and centripetal acceleration. So, the additional terms in the momentum equations for primary liquid phase and secondary particulate phase are (Nino-Lopez and Gelves-Zambrano, 2015):

$$F_l = -2 \propto_l \rho_l(\omega \times V_l) - \alpha_l \rho_l \omega \times (\omega \times r) \tag{3.45}$$

$$F_s = -2 \propto_s \rho_s(\omega \times V_s) - \alpha_s \rho_s \omega \times (\omega \times r) \tag{3.46}$$

where, $2 \propto_l \rho_l(\omega \times v_l)$ is the Coriolis force, $\alpha_s \rho_s \omega \times (\omega \times r)$ is the centripetal force, ω is the angular velocity and r is the position vector.

3.6 Computational domain and mesh

The Computational domain of the CFD simulation was a cylinder having both diameter and height of 140 mm. It was assumed that the entire domain was filled with liquid as primary phase and particulates as secondary phase. The flow inside the mixing vessel was highly swirling due to the dual axis rotation of the mixing cylinder. In that situation, the hexahedral and tetrahedral meshes showed convergence difficulties. The gradient calculations of the flow properties in such highly swirling flows would be better, if the number of neighbouring were more.So, the domain obtained in tetrahedral mesh is converted to polyhedral mesh with more neighbouring cells which showed a monotonic convergence. The computational domain with polyhedral mesh is shown in Fig. 3.3.

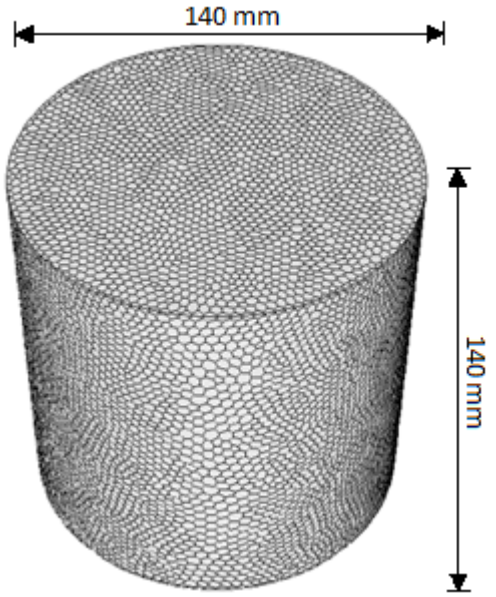

Fig. 3.3 Computational domain with mesh

3.7 Boundary conditions

No-slip boundary condition was applied to the closed rotating walls so that the velocity of the fluid stuck on the walls was the same as that of the velocity of the walls. This is due to the adhesive force between the molecules of the fluid and wall which is considerably higher than the cohesive force between the fluid molecules.

3.8 Numerical scheme

The governing equations for the fluid flow are solved using a finite volume based fluid dynamics CFD code in Fluent version 14 software. The simulation was carried out for the mixing of SiC of 30 microns in glycerine. The centre of the mixing tank was kept as the origin of the coordinate system such that the y- axis is along the centre line of the mixing tank. For all the simulation models, first order upwind implicit formulation for unsteady integration and a second order upwind scheme discretization for spatial derivatives were adopted. The pressure-velocity coupling used in Eulerian model, Mixture model and VOF model were Phase Coupled SIMPLE, SIMPLE and PISO respectively. For all the models, Gradient formulation was Least squares cell based and volume fraction parameter was QUICK. For the VOF model, the User Defined Function (UDF) for the viscosity of the secondary phase was compiled and hooked for the simulation. The time step of the transient simulation was set to 0.001 sec for all the simulation models so that the mixing cylinder was rotated through 2^0 about the spin axis and 1^0 about gyration axis in each time step for the maximum gyration speed of 176.8 rpm. The spin was given to the walls by wall motion option and gyration was given by the frame motion option of the software. The simulation was run till the mixing power shows no variation with respect to flow time.

3.9 Grid independence study

Richardson extrapolation method was used for grid independence study to check whether the flow variable under consideration is grid independent or not. Three significantly different set of grids have to be selected for this study. The representative cell sizes h_1, h_2 and h_3 has to be find out using the formula given in equation 3.47.

Grid size Size; $$h = \left[\frac{\sum_{i=1}^{N}(\Delta V_i)}{N}\right]^{\frac{1}{3}} \qquad (3.47)$$

Where, N = total Number of cells in the Domain

ΔV_i is the volume of the i^{th} cell

It is desirable that the grid refinement factor, $r=h_{coarse}/h_{fine}$, be greater than 1.3 (Celik, 2008), and simulations are run to determine the values of key variables (Φ) important to the objective of the simulation study.

Let $h_1<h_2<h_3$, then the grid refinement ratio, $r_{21}=h_2/h_1$ and $r_{32}=h_3/h_2$.

The apparent order, p, of the method was calculated using the expression:

$$p = \frac{1}{\ln(r_{21})}\left|\ln\left|\frac{\varepsilon_{32}}{\varepsilon_{21}}\right| + q(p)\right| \tag{3.48}$$

$$q(p) = \ln\left(\frac{r_{21}^{p}-s}{r_{32}^{p}-s}\right) \tag{3.49}$$

$$S=1.Sign(\varepsilon_{32}/\varepsilon_{21}) \tag{3.50}$$

where, $\varepsilon_{32}=\Phi_3-\Phi_2$, $\varepsilon_{21}=\Phi_2-\Phi_1$

The extrapolated value of the variable Φ was calculated using the formula 3.51:

$$e_{ext}^{21} = \frac{(r_{21}^{p}\emptyset_1-\emptyset_2)}{(r_{21}^{p}-1)} \tag{3.51}$$

The approximate relative error was found out using the formula3.52:

$$e_{a}^{21} = \left|\frac{\emptyset_1-\emptyset_2}{\emptyset_1}\right| \tag{3.52}$$

The approximate relative error (e_a^{21}) and extrapolated relative error (e_{ext}^{21})were calculated by:

$$e_{a}^{21} = \left|\frac{\emptyset_1-\emptyset_2}{\emptyset_1}\right| \tag{3.53}$$

$$e_{ext}^{21} = \left|\frac{\emptyset_{ext}^{12}-\emptyset_1}{\emptyset_{ext}^{12}}\right| \tag{3.54}$$

The Grid Convergence Index (GCI) for the fine grid was estimated using the following formula.

$$GCI_{fine}^{21} = \frac{1.25e_a^{21}}{r_{21}^{p}-1} \tag{3.55}$$

The convergence conditions of the system were checked before evaluating the extrapolated value. The convergence conditions are;

1. Monotonic convergence; 0<R<1

2.Oscillatory convergence; R<0

3.Divergence; R>1

where R is the convergence ratio and is determined by the equation; $R=\varepsilon_{21}/\varepsilon_{32}$.

The Grid Convergence Index (GCI) is a measure of convergence for grid refinement studies. It determines how much the solution approaches the asymptotic value. The GCI value less than 5% is an acceptable measure of grid independent converged solution.

3.10 Summary

In this chapter the models of simulations, and the parameters of comparing the different models are described. The properties of mixing were assessed using the flow Characteristic velocity and Power Number. Characteristic velocity is a measure of maximum velocity of fluid inside the mixing chamber and Power Number is a measure of power consumed for mixing. The mixing in stir casting and gyro casting has to be compared for the quality of mix. So, Characteristic velocity of gyro shaker was derived for comparing the results obtained from same characteristic velocity conditions of the stirred vessel.

The Power Number was calculated using the mixing power obtained from viscous dissipation method and torque method. The selection of multiphase model is a key factor for getting consistent results. From the particulate loading and Stoke's number, it is advantages to use Mixture and Eulerian granular models for CFD simulation of flow inside the mixing vessel. Most of the simulation works in mixing of fluids with solid particulates were reported in Eulerian granular k-Ɛ model. Since the fluid flow was highly swirling, the RNG k-Ɛ turbulence model was selected. The grid independence study is also an important factor for getting a reliable result.

CHAPTER 4

EXPERIMENTAL VALIDATION OF CFD MIXING MODEL

4.1 Experiment

The experimental setup for finding the mixing power at various gyration speeds of the mixing cylinder was arranged at Heat Engines Laboratory of Government Engineering College, Thrissur. The different aspects of the experiment are described in subsequent sections.

4.1.1 Materials selection

The glycerine was taken as the liquid in which the particulates to be mixed. The glycerine is highly viscous and can be treated as Newtonian fluid. A measurable quantity of mixing power can be obtained by using this fluid due to its high viscosity. The particulate to be mixed was selected as SiC powder with 30μm size. The vol.% of SiC particulates was taken as 20.

Viscosity of the Glycerine measured at various temperature using Brookfield DV 2T Extra Viscometer was found to be 0.4659 PaS at 34^0C which was the room temperature where the experiments were conducted. Density of glycerine measured using Density Meter DMA 35 Anton Paar instrument and was found to be 1259 kg/m^3 at a temperature of 22.4^0C. The same value of viscosity was used for simulation by neglecting the very small deviation for the room temperature of 34^0C. An amount of 1.3786 kg of SiC with 30μm size was weighed using Shimadzu ATY224, electronic weighing balance of accuracy 10^{-4} grams and added to the glycerine to the mixing vessel for getting volume fraction of 20% for the secondary phase. The mixing tank was cylindrical in shape and made of transparent acrylic material, so that the mixing could be observed visually. Both the diameter and height of the mixing tank was kept as 140 mm.

4.1.2 Specifications of measuring instruments

The specification of Viscometer, Density meter, Electronic weighing balance, Power meter and Tachometer are listed below.

Brookfield DV 2T Extra Viscometer:

- Speeds: 0.1 – 200 rpm
- Temperature sensing range: -100^{0}C to 300^{0}C
- Viscosity accuracy: ± 1.0% of full scale range
- Viscosity repeatability: ± 1^{0}C for -100^{0}C to +149^{0}C, ±2^{0}C for +150^{0}C to +300^{0}C
- Operating environment: 0^{0}C to 40^{0}C temperature range and 20% - 80% Relative humidity

Density Meter DMA 35 Anton Paar:

- Measuring range:Density: 0 to 3 g/cc, Temperature: 0 to 40^{0}C, Viscosity: 0 to approx. 1000 mPa.s
- Accuracy: - Density: 0.001 g/cc, Temperature: 0.2^{0}C
- Repeatability: - Density: 0.0005 g/cc, Temperature: 0.1^{0}C
- Resolution: - Density: 0.0001 g/cc, Temperature: 0.1^{0}C

Shimadzu ATY224, electronic weighing balance:

- Capacity: 220g, Minimum display: 0.1 mg
- Repeatability: ≤ 0.1 mg, Linearity: ± 0.2 mg
- Stabilisation time: Approx. 3.0 seconds
- Operating temperature and humidity limits: 5 – 40^{0}C, 20- 85% RH

PX110 Power meter – Metrix:

- Network type: Single-phase and three-phase
- Bandwidth: DC to 1 kHz, Power range: 10 W to 1 kW
- Resolution: 0.1 W, Power factor range: 1.0
- Voltage range: 0.5 to 600 V RMS, Resolution: 100 mV
- Current range: 10 mA to 2 A – 2 A to 10 A
- Resolution 1 mA – 10 mA, Operating temperature: 0 to 50^{0}C

Digital photo type tachometer:

- Range: 60 to 100000 rpm, Resolution: 0.1 up to 999.9 rpm, 1 above 1000 rpm
- Accuracy: ± (0.05% ± 1 digit), Sampling rate: 1 second
- Measuring distance: 100 to 300 mm, Operating temperature: 0 to 60^{0}C

4.1.3 Experimental setup

Experiment was conducted on the Gyro Shaker mixer for mixing of SiC in glycerine. The equipments used for conducting experiment is shown in Fig.4.1.The mixing cylinder was rotated in both spin and gyration axis using a 1 hp induction motor. The single phase ac power supply was connected to an auto transformer which acts as the speed regulator for varying the voltage of power supply to the induction motor. Power and current were measured using PX110 Power meter – Metrix which was connected in between the induction motor and speed regulator. A non-contact RPM sensor was employed for measuring the spin and gyration speeds of the mixing vessel. The photograph of the experimental setup is shown in Fig. 4.2. The maximum speed of Gyro Shaker was 180 rpm and the machine was unsteady below the speed of 135 rpm. So, the measurements of power were taken at 5 different speeds between 135 and 180 rpm.

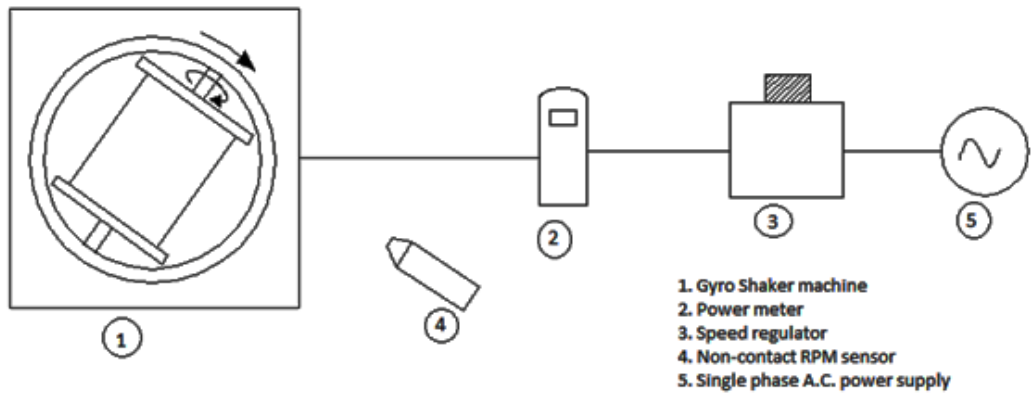

Fig. 4.1 Schematic of experimental setup

4.1.4 Experiment procedure

The empty mixing tank was loaded in the gyro shaker machine and clamped. The electrical connection to the speed regulator and power meter were connected as shown in Fig. 4.1. The field resistance of the motor(R)was measured using a multi meter and found to be 2Ω. The single phase A.C. power supply to the speed regulator was connected and the speed regulator was adjusted to get a gyration speedof 138.2 rpm. The gyration speed was measured using the non-contact rpm sensor. The current (I) and power (P_W) drawn by the electric motor was noted from the power meter readings. The experiment was repeated for gyration speed of 143.5 rpm, 151.8 rpm, 165.4 rpm and 176.8 rpm.

The lid of the empty mixing tank was opened and 1.3786 kg of SiCwas added into the mixing cylinder. The tank was then filled with the glycerine liquid and closed

with the lid. The mixing tank was loaded in the gyro shaker machine and clamped. The speed regulator was adjusted to get a gyration speed of 138.2 rpm. The current and power drawn by the electric motor was noted from the power meter readings. The experiment was repeated for gyration speeds of 143.5 rpm, 151.8 rpm, 165.4 rpm and 176.8 rpm. Equation 4.1 is used to determine the power consumed by the machine. It was assumed that the frictional power of the machine depends only on the rotation speed of tank. The power for mixing the fluid for a particular speed of rotation was calculated by subtracting the power at no load condition from the loaded condition (Andre et al., 2012; Rao and Sivashanmugam, 2010).

$$P_{md} = P_w - I^2R \tag{4.1}$$

Fig. 4.2 Experimental setup

4.2 Validation for CFD mixing model

The CFD simulation model for the Gyro shaker mixing has to be validated with the experiments. The results obtained from the simulation must be grid independent. For this, the Grid Convergence Index (GCI) value for each simulation for different gyration speeds has to be determined. The variation of mixing power and flow characteristics are studied from the results obtained from CFD simulations.

4.2.1 Grid Independence study

The grid independence study was carried out before arriving at the grid resolution for the simulation. The Mixing Power was calculated from the extrapolated value evaluated from the Grid Independence study. Two methods namely Viscous Dissipation method and Torque method are used for predicting the mixing power. The different mesh sizes used for grid independence study was selected for a grid refinement factor of 1.37. The mesh sizes considered are 108859, 42657 and 16707 numbers of polyhedral cells with average cell sizes of 1.93 mm, 2.64 mm and 3.61 mm respectively. These cells are obtained by converting 619899, 223734 and 91436 tetrahedral cells to polyhedral cells. The quality of the polyhedral mesh is listed in Table 4.1. The minimum orthogonal quality, Maximum skewness and maximum aspect ratio are found good for CFD simulation.

Table 4.1 Quality of mesh

No. of polyhedral cells	108,859	42,657	167,07
Minimum orthogonal quality	0.52	0.51	0.50
Maximum Skewness	0.48	0.49	0.50
Maximum aspect ratio	8.3	8.5	7.8

Table 4.2$Grid\ Convergence\ Index\ \ GCI_{fine}^{21}$ (%)for Mixing power

Gyration speed (rpm)	Viscous dissipation method			Torque method		
	Eulerian granular model	Mixture model	VOF model	Eulerian granular model	Mixture model	VOF model
138.2	0.85	4.31	2.87	1.66	1.37	1.24
143.5	0.89	4.02	4.15	1.33	1.51	1.86
151.8	0.86	3.27	4.77	0.36	1.41	2.91
165.4	0.97	3.77	4.93	0.50	1.73	2.71
176.8	1.37	3.56	2.92	0.50	1.22	1.32

The grid independence study was carried out for mixing power, volume weighted average velocity and pressure. The GCI value for the above parameters are listed in Table. 4.2 and Table. 4.3. All the simulation model showed Grid Convergence Index (GCI) value less than 5%. The convergence ratio obtained for all the models are between 0 and 1 which indicates monotonic convergence. The effect of Grid resolution for mixing at 176.8 rpm gyration speed on the mixing power for Viscous Dissipation method and Torque method is

shown in Fig.4.3 (a) and (b) respectively. A monotonic convergence was observed for the solution of mixing power in both Viscous Dissipation method and Torque method. There were no significant variations in mixing power obtained by using the 619899, 223734 polyhedral cells. So, further refinement of the cells was not considered.

Table 4.3Grid Convergence Index GCI_{fine}^{21} (%)for volume weighted average pressure and velocity

Gyration speed (rpm)	GCI_{fine}^{21} (%) for volume weighted average pressure			GCI_{fine}^{21} (%) for volume weighted average velocity		
	Eulerian granular model	Mixture model	VOF model	Eulerian granular model	Mixture model	VOF model
138.2	1.23	0.05	0.92	1.66	0.30	1.20
143.5	1.20	0.02	0.74	1.12	0.07	1.26
151.8	2.81	0.43	0.15	3.25	0.03	1.23
165.4	0.65	0.23	0.71	1.09	0.00	1.46
176.8	0.26	0.58	0.90	054	0.03	1.71

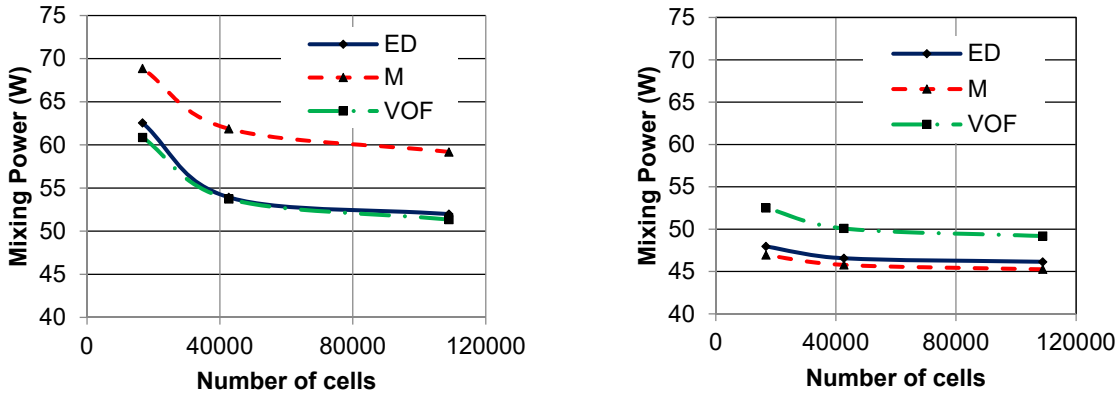

(a) Viscous Dissipation Method *(b) Torque Method*

Fig. 4.3. Effect of Grid resolution on Mixing Power. ED: Eulerian dispersed model, M: Mixture model, VOF: Volume of fluid model

4.2.2 Specific power for mixing

Specific Power characteristics of the Gyro Shaker based on characteristic velocity for the Viscous Dissipation method and Torque method are shown in Fig.4.4 (a) and (b). The specific power for mixing increases almost linear with respect to gyration speed for all the simulation models. Mixing power obtained by Viscous Dissipation method is greater than that of Torque method which is in concurrence with the results reported by Alliet-Gaubert et

al. (2006). Specific Power for the mixing derived from the Viscous Dissipation method for the Mixture model and Specific Power derived from Torque methods for VOF model show better agreement with the experimental results. Since the mixing power derived from velocity gradients for Viscous dissipation method shows better agreement with experiment results, it can be concluded that the velocity distribution obtained from mixture model is better than the other models.

Similarly, the pressure distribution also shows a better agreement in VOF model than the other models, the mixing power obtained from Torque method is more close to the experimental results. The Viscous Dissipation method for obtaining the mixing power predicts more accurate results than Torque method. The difference in torque obtained between simulation using Torque method and experimental results was due to the low accuracy for predicting the pressure acting on the faces of boundary cells. Since Stokes number of the flow is 1x10-5, the secondary phase particles will follow the flow closely, and hence the simulation results were in better agreement with experiment for Mixture model. The VOF model with modified viscosity for the secondary phase yields almost similar velocity, pressure and volume fraction distribution as that of the mixture model.

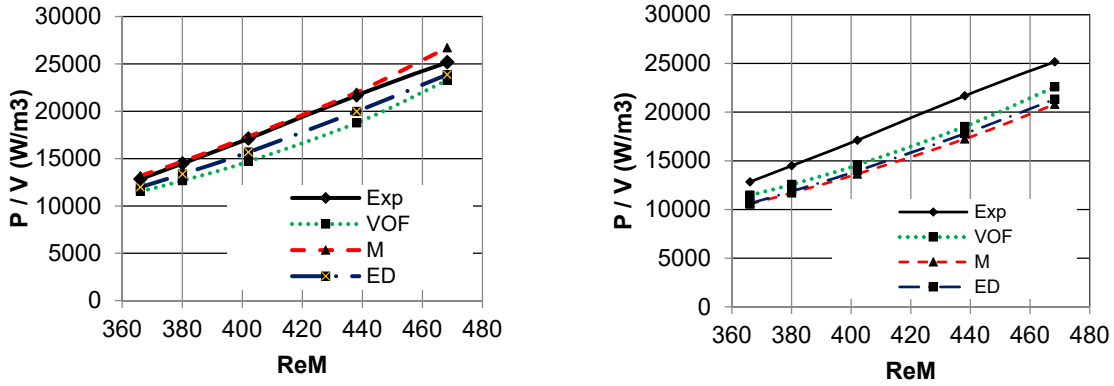

(a) Viscous Dissipation Method *(b) Torque Method*

Fig. 4.4. Specific Power characteristics of the Gyro Shaker based on characteristic velocity. Exp: Experiment, VOF: Volume of fluid model, M: Mixture model, ED: Eulerian dispersed model.

The maximum deviation of Mixing Power as predicted using Viscous Dissipation Method for Mixture Model, VOF Model and Eulerian kƐ dispersed turbulence Model by the experimental value as the basis was 6.1%, 17.4%and 8.4% respectively. The maximum deviation of Mixing Power predicted by Torque Method concerning the experimental value for Mixture Model, VOF Model and Eulerian kƐ dispersed turbulence Model and are 20.4%,

14.8% and 18.3% respectively. The best computational cell for CFD analysis for mixing was found to be polyhedral which took low CPU time and provided better convergence.

4.2.3 Power number

The variation of Power number with respect to Reynolds number based on Characteristic velocity is shown in Fig. 4.5 (a) and (b). Variations of Power number with respect to Reynolds number based on gyration speed is also same since the Characteristic velocity is directly proportional to the Gyration speed.

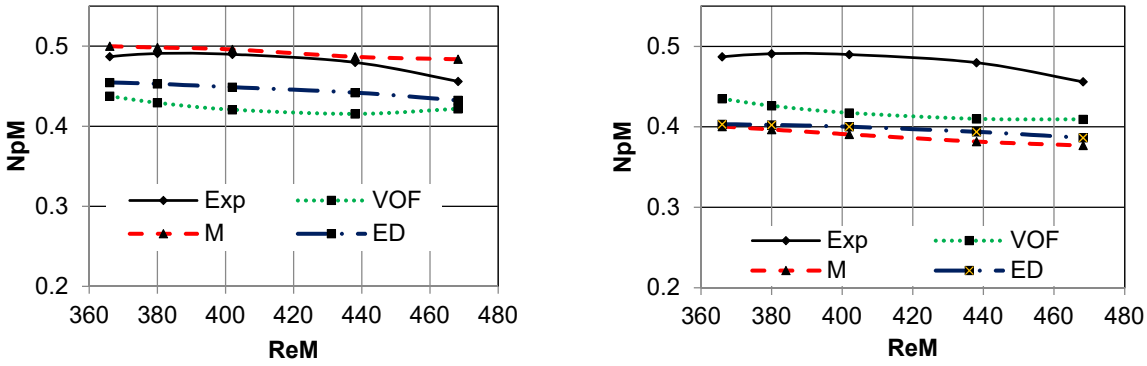

(a) Viscous Dissipation Method *(b) Torque Method*

Fig. 4.5. Power number as a function of Reynolds number based on characteristic velocity. Exp: Experiment, VOF: Volume of fluid model, M: Mixture model, ED: Eulerian dispersed model.

The flow regime can be assumed as transition region since the variation of power Number based on characteristic velocity and Gyration speed is not constant with respect to the Reynolds number based on characteristic velocity and Gyration speed.

4.2.4 Flow characteristics

The models are simulated and run until the mixing power reaches steady state. To analyse the mixing pattern in different models, the state of the mixture after 2 seconds of mixing time is studied. Various parameters of the mixture for the different models are examined and compared to each other. The simulation for all gyration speed conducted in the experiment is considered in the simulation. The results for the maximum gyration speed of 176.8 rpm are explained in this section.

4.2.4.1 Streamlines of particles

Streamline of the secondary phase for the Eulerian k-ε Dispersed model for 176.8 rpm gyration is shown in Fig.4.6. The secondary phase particles attained a maximum velocity of 2.589 m/s at the top and bottom corners of the mixing tank. The velocity of secondary phase

particles was low at the centre of the mixing tank. It was observed from the streamline that the particles were vigorously mixing at the centre of the tank even though their velocity was low.

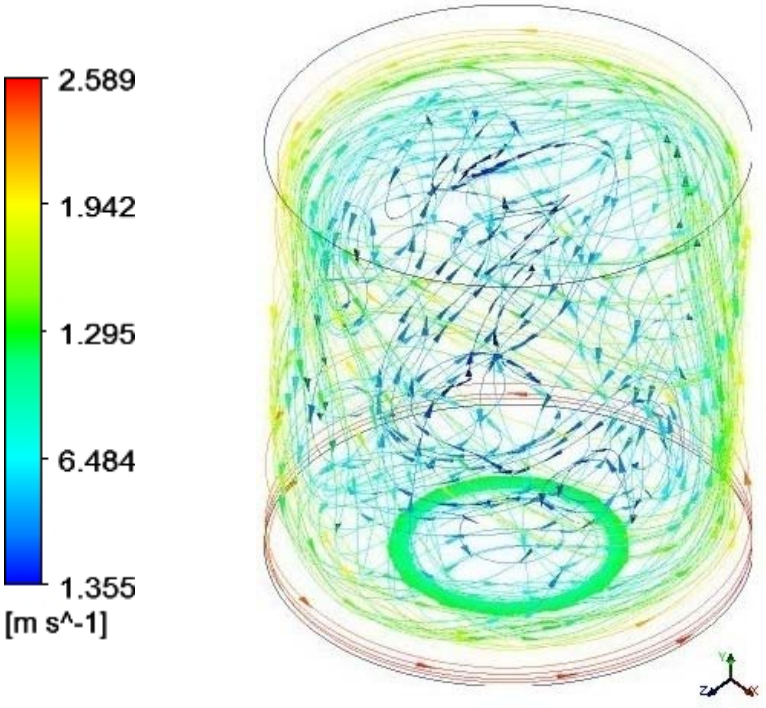

Fig.4.6. Streamline of Secondary Phase

4.2.4.2 Pressure contours

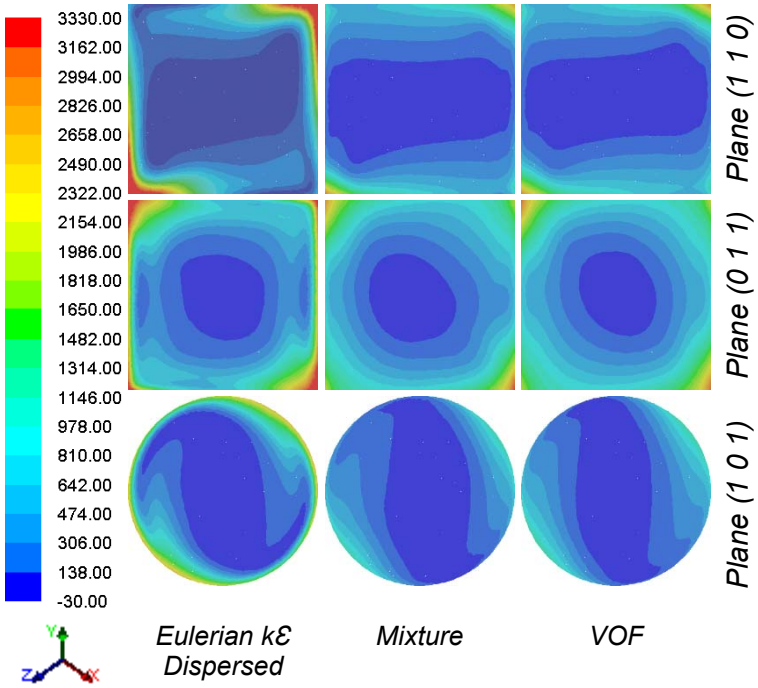

Fig. 4.7. Contours of static pressure (Pa) of mixture at 138.2 rpm gyration speed

The contours of the static pressure of the mixture at various gyration speeds are given in Fig. 4.7, Fig. 4.8, Fig. 4.9, Fig. 4.10 and Fig.4.11 The contours for static pressure and primary phase velocity were comparable for all the Multiphase simulation models. The mixture static pressure and primary phase velocity were minimum at the center of the mixing tank and maximum near to the edges of the mixing tank at top and bottom.

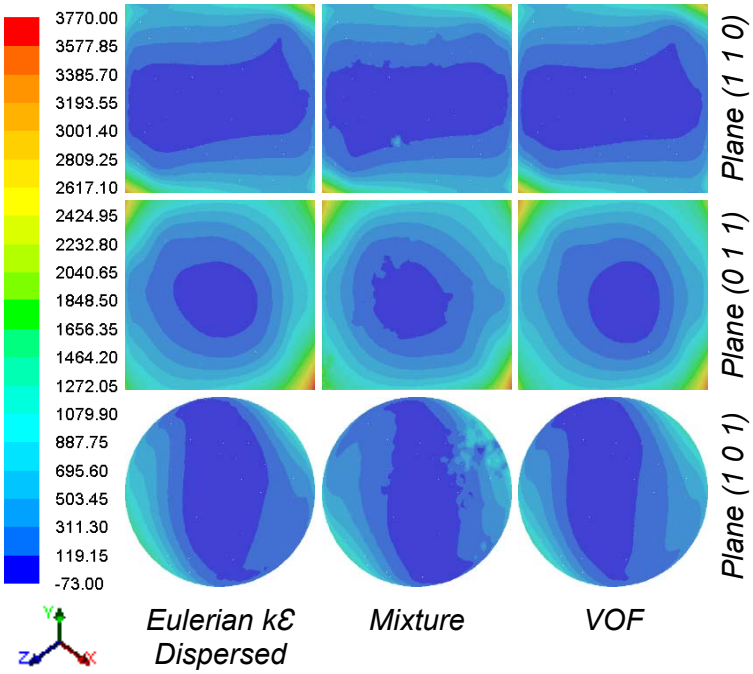

Fig. 4.8. Contours of static pressure (Pa) of mixture at 143.5 rpm gyration speed

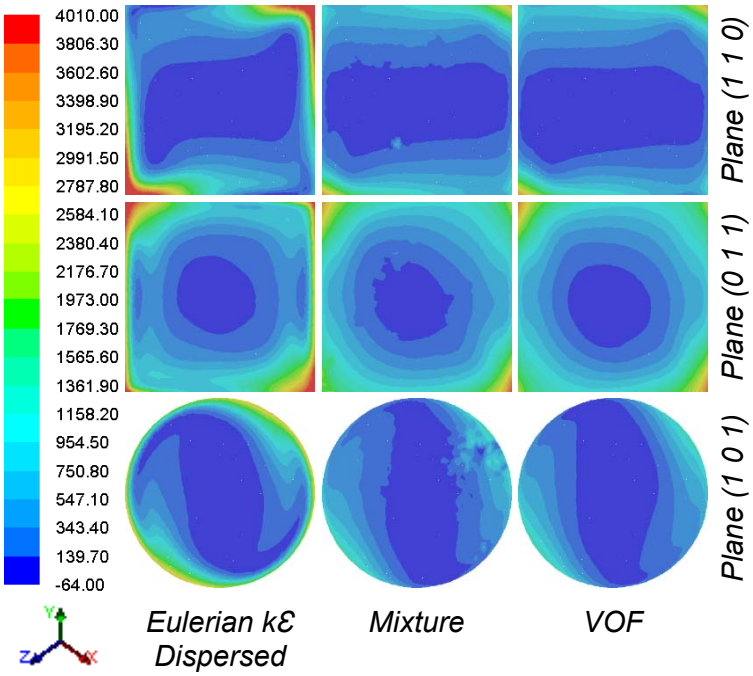

Fig. 4.9 Contours of static pressure (Pa) of mixture at 151.8 rpm gyration speed

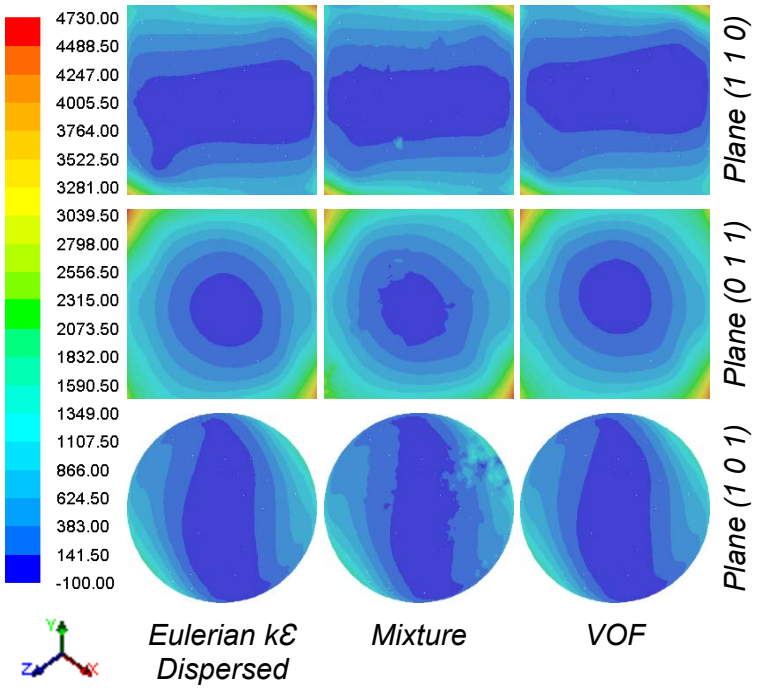

Fig. 4.10. Contours of static pressure (Pa) of mixture at 165.4 rpm gyration speed

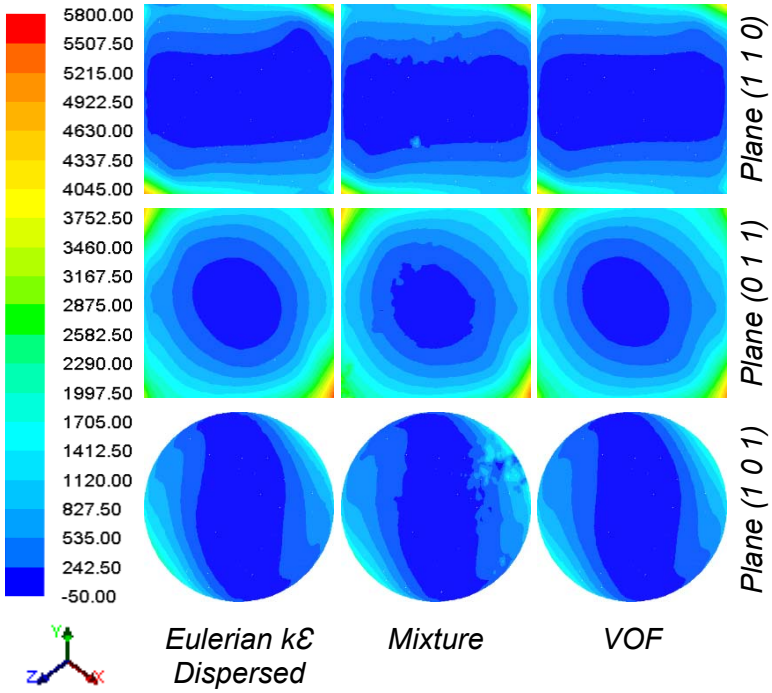

Fig. 4.11. Contours of static pressure (Pa) of mixture at 176.8 rpm gyration speed

4.2.4.3 Velocity contours

The contours of the velocity of primary phase at various gyration speeds are given in Fig. 4.12, Fig. 4.13, Fig. 4.14, Fig. 4.15 and Fig.4.16. Both the Primary and secondary phase velocities are almost the same for all the models.

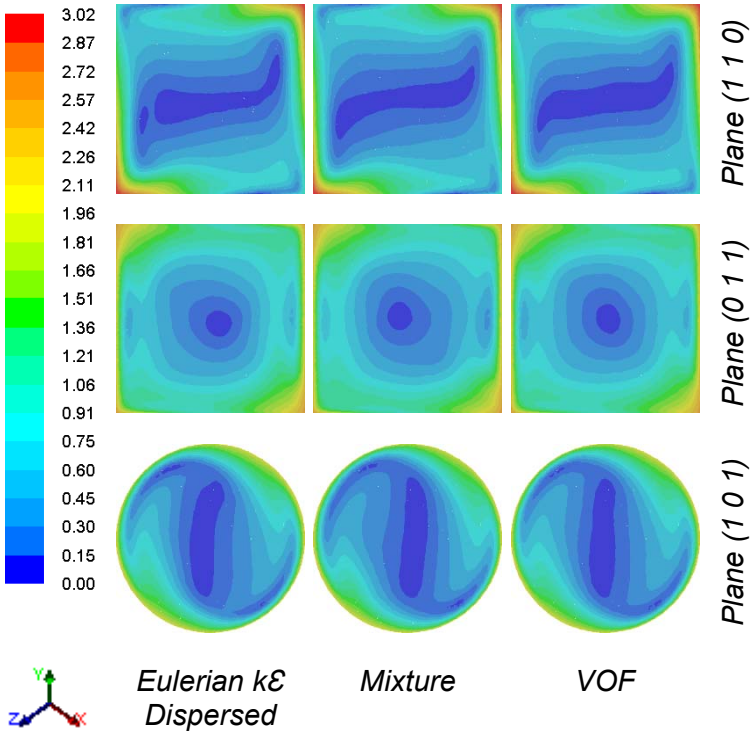

Fig. 4.12. Contours of velocity magnitude for phase-1 (m/s) at 138.2 rpm gyration speed

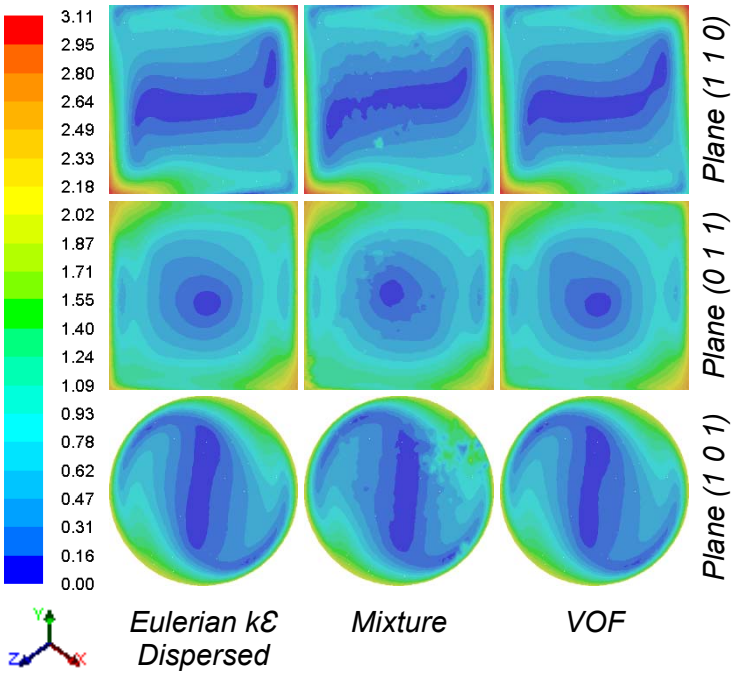

Fig. 4.13. Contours of velocity magnitude for phase-1 (m/s) at 143.5 rpm gyration speed

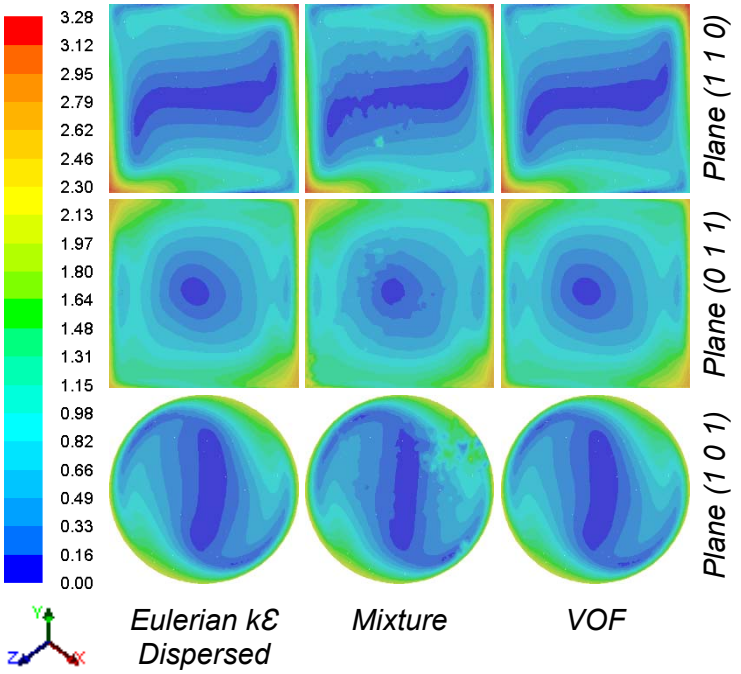

Fig. 4.14. Contours of velocity magnitude for phase-1 (m/s) at 151.8 rpm gyration speed

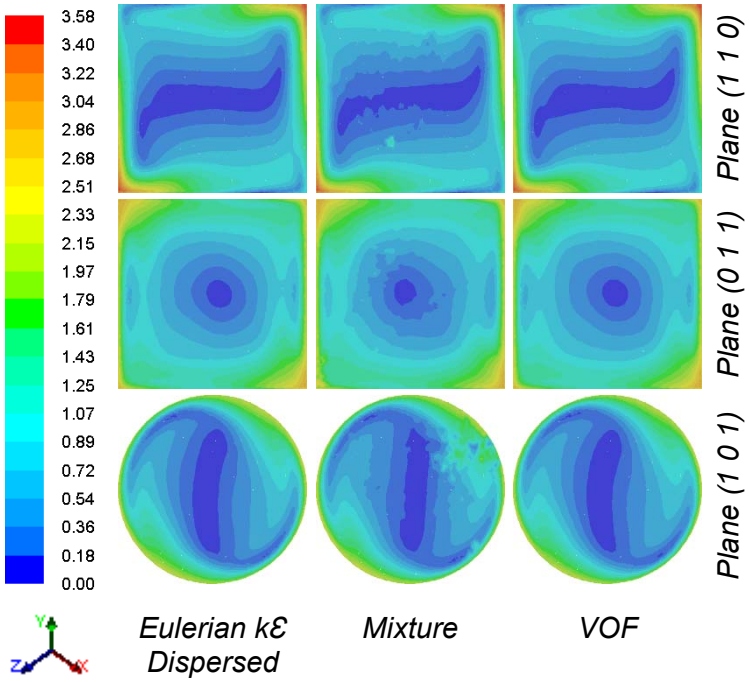

Fig. 4.15. Contours of velocity magnitude for phase-1 (m/s) at 165.4 rpm gyration speed

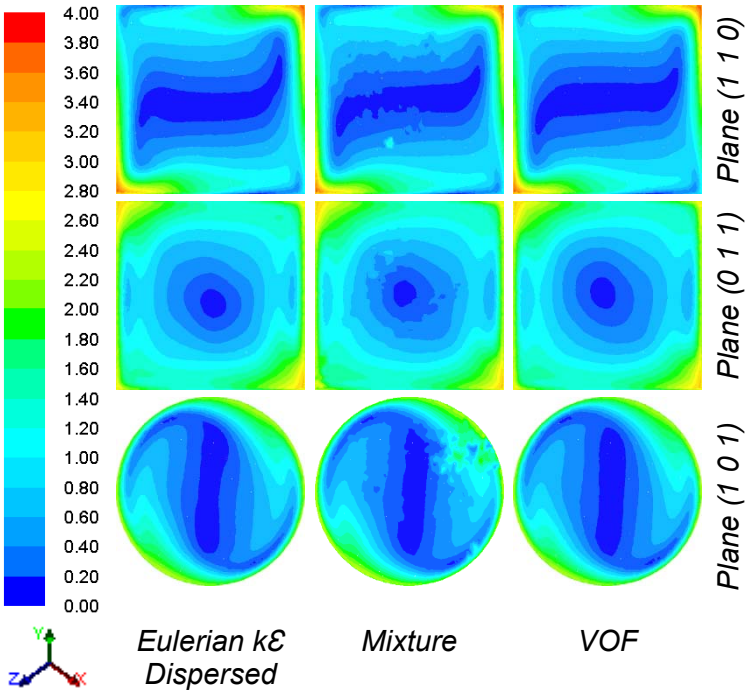

Fig. 4.16. Contours of velocity magnitude for phase-1 (m/s) at 176.8 rpm gyration speed

4.2.4.4 Volume fraction contours

The contours of the volume fraction of secondary phase at various gyration speeds are given in Fig. 4.17, Fig. 4.18, Fig. 4.19, Fig. 4.20 and Fig.4.21. . For a complete mixing, the volume fraction for the secondary phase should be 20% throughout the mixing vessel. Before the mixing, the standard deviation of the secondary phase volume fraction was 0.4.

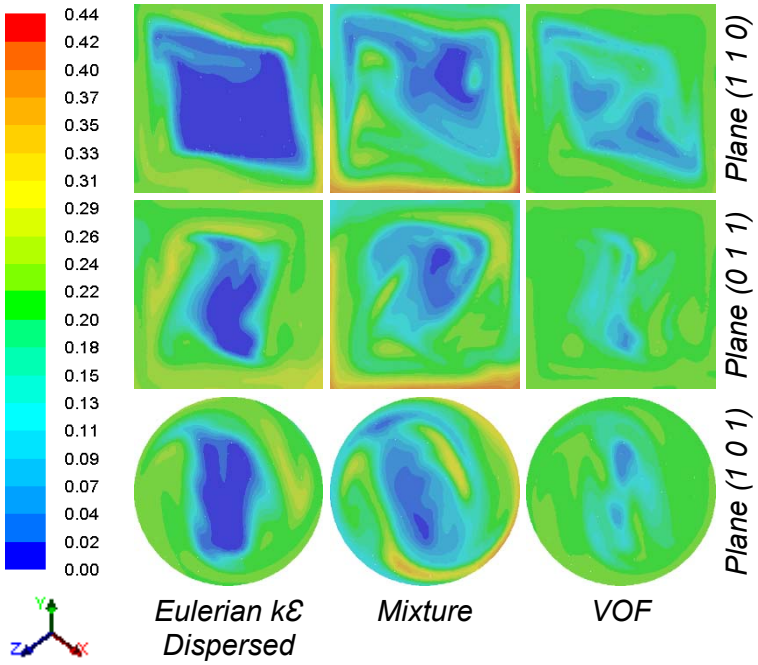

Fig. 4.17. Contours of volume fraction for phase-2at 138.2 rpm gyration speed

Volume fraction for the secondary phase is high near to the walls and low at the centre of the mixing vessel for all the models. This is due to the density difference between the phases.

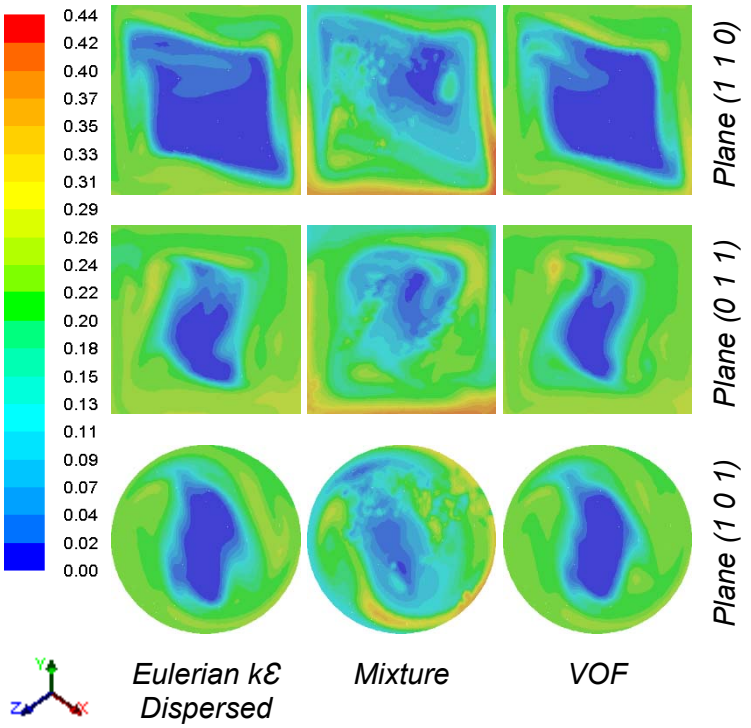

Fig. 4.18. Contours of volume fraction for phase-2 at 143.5 rpm gyration speed

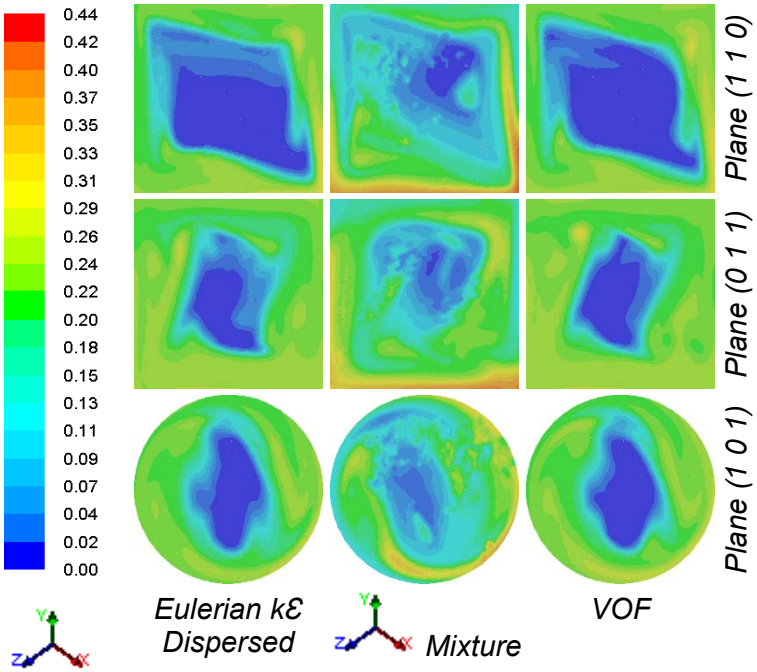

Fig. 4.19. Contours of volume fraction for phase-2at 151.8 rpm gyration speed

The standard deviation of secondary phase was found to be decreasing as the speed increases. This indicates the increasing rate of mixing with the increase in speed. The

maximum value of standard deviation was at 138.2 rpm gyration speed and values obtained as 0.0723, 0.0785 and 0.1124 for Eulerian k-ε Dispersed Model, Mixture Model and VOF Model respectively. The minimum value of standard deviation was at 176.8 rpm gyration speed and values obtained as 0.0705, 0.0731 and 0.0794 for Eulerian k-ε Dispersed Model, Mixture Model and VOF Model respectively.

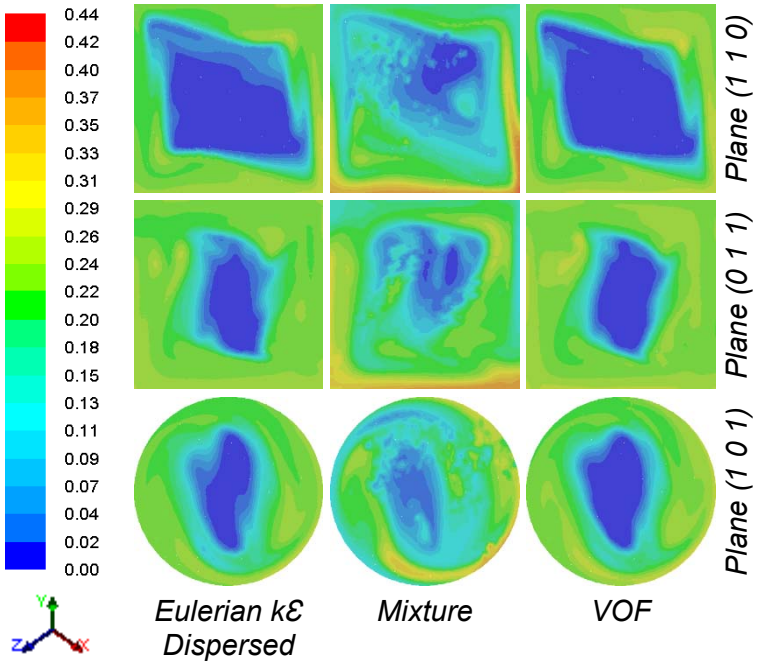

Fig. 4.20. Contours of volume fraction for phase-2 at 165.4 rpm gyration speed

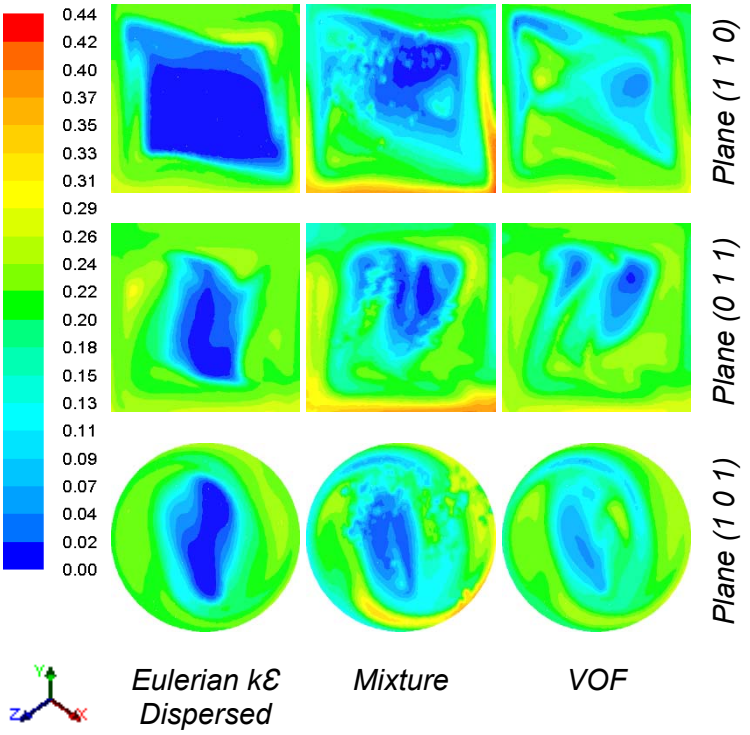

Fig. 4.21. Contours of volume fraction for phase-2 at 176.8 rpm gyration speed

4.2.4.5 Pressure and velocity profiles

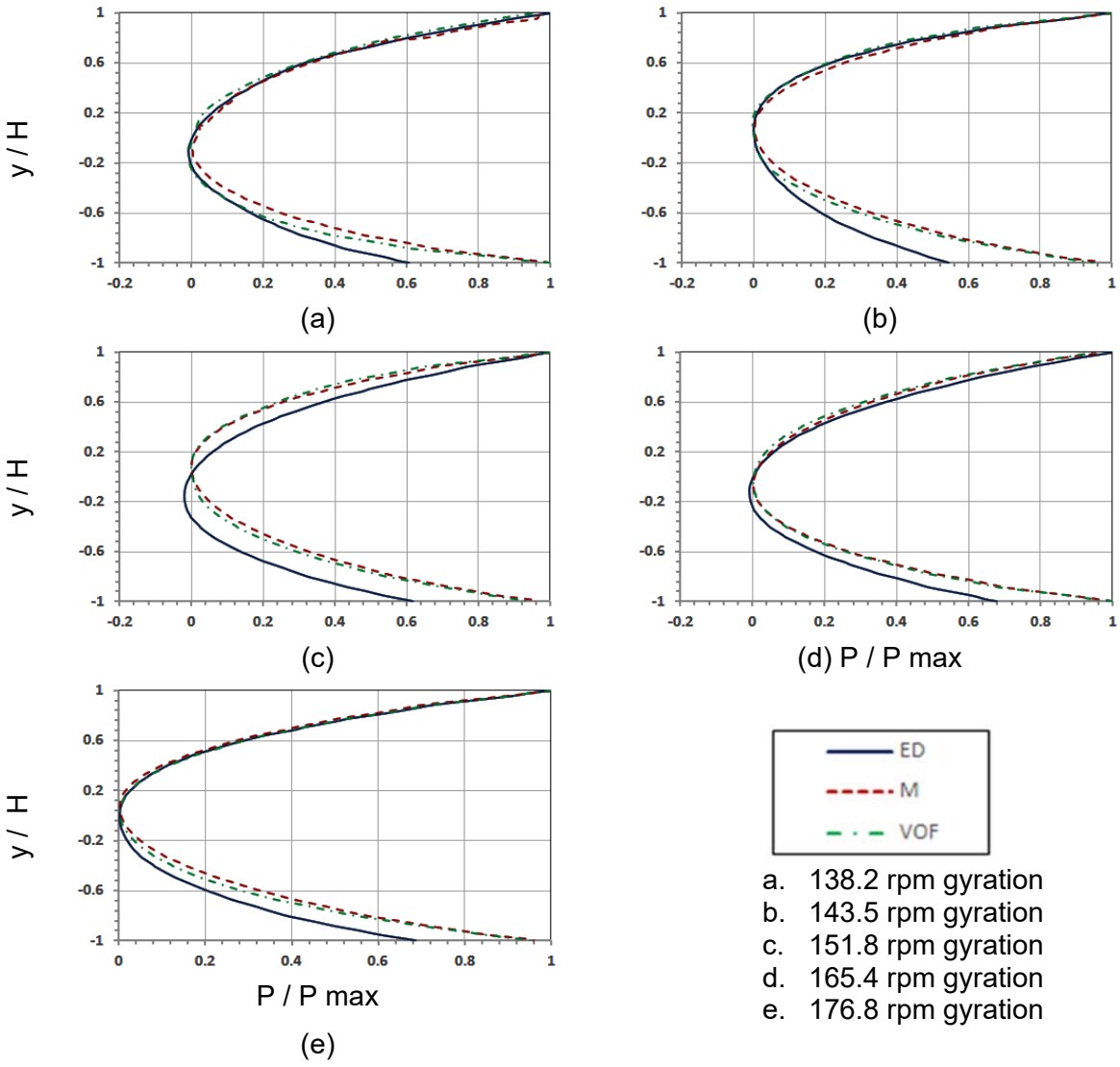

Fig. 4.22. Normalised profile of axial static Pressure for Mixture

The normalised static pressure of mixture for different gyration speeds observed at the different dimensionless height, and radial coordinates on x-y plane are shown in Fig. 4.22 and 4.23 respectively. The normalised static pressure obtained using the static pressure (P) and maximum pressure (Pmax) inside the mixing domain. The dimensionless height obtained using the y-coordinate (y) of the location and height (H) of the cylinder. At the minimum gyration speed of 138.2 rpm, as seen from the Fig. 4.22, the static pressure along the axis of the mixing tank was maximum at the bottom and top of the mixing vessel for all simulation models. The maximum static pressure observed was 1119 Pa for the Eulerian k-ε Dispersed model. For Mixture and VOF models, static pressure observed was 911 Pa and

881 Pa, respectively. The minimum static pressures observed were -9.9 Pa, 1.3 Pa and -8.4 Pa for the respective models. The static pressure was the lowest at the center of the tank. The variation of mixture static pressure along the axis was almost similar for Mixture and VOF simulation models.

At the minimum gyration speed of 138.2 rpm, the maximum static pressure along radius was observed on the walls of the mixing tank for all the simulation models. The maximum radial pressure is 835 Pa, 837 Pa and 838 Pa for Eulerian k-ε Dispersed, Mixture and VOF models respectively. For all the simulation models, static pressure along the radius was minimum near the center of the tank. These values were -27.5 Pa, -12.3 Pa and -8.2Pa for Eulerian k-ε Dispersed, Mixture and VOF models respectively.

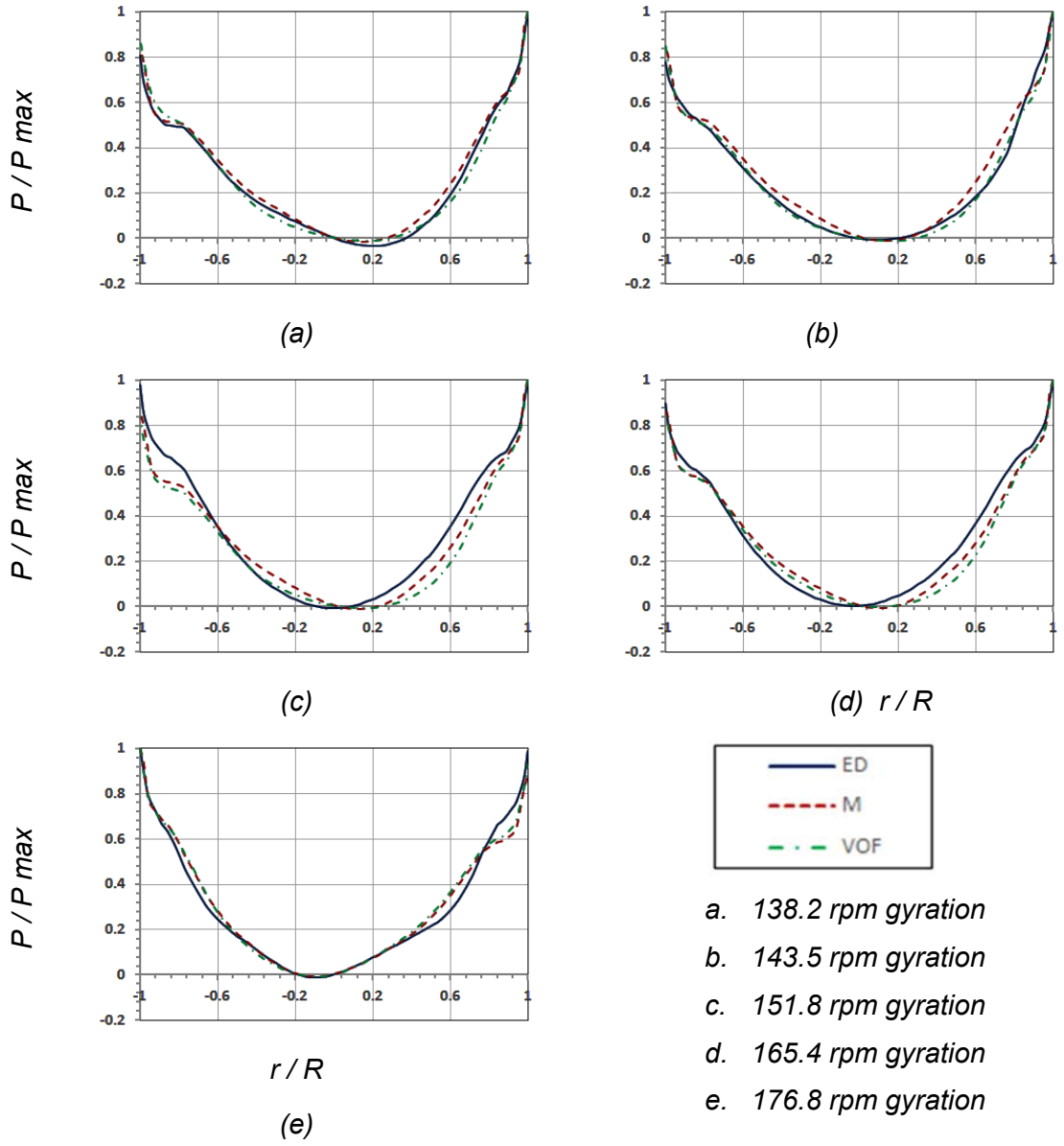

Fig. 4.23. Normalised profile of radial static Pressure for Mixture

The normalised static pressure of mixture for maximum speed of 176.8 rpm gyration speed observed at the different dimensionless height, and radial coordinates on x-y plane are shown in Fig. 4.22 and 4.23 respectively. As seen from the Fig. 4.22, the static pressure along the axis of the mixing tank was maximum at the bottom and top of the mixing vessel for all simulation models. The maximum static pressure observed was 1797 Pa for the Eulerian k-ε Dispersed model. For Mixture and VOF models, static pressure observed was 1549 Pa and 1502 Pa, respectively. The minimum static pressures observed were 3.7 Pa, 1.8 Pa and 4.4 Pa for the respective models. The static pressure was the lowest at the center of the tank. The variation of mixture static pressure along the axis was almost similar for Mixture and VOF simulation models.

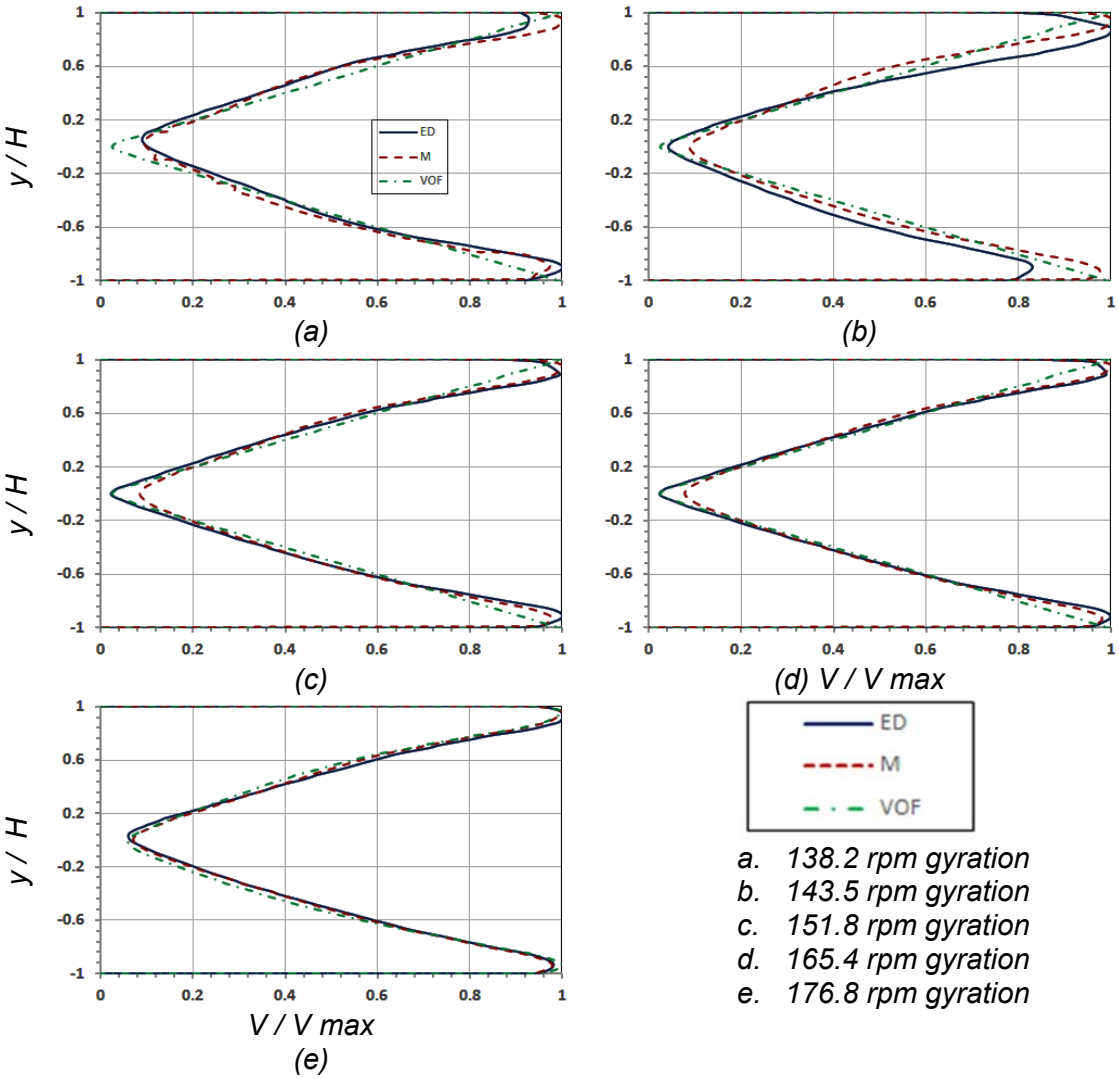

Fig. 4.24. Normalised Profiles of the phase-1 axial velocity

At maximum gyration speed of 176.8 rpm, the maximum static pressurealong radius was observed on the walls of the mixing tank for all the simulation models. The maximum

radial pressure was 1422 Pa, 1416 Pa and 1340Pa for Eulerian k-ε Dispersed, Mixture and VOF models respectively. For all the simulation models, static pressure along the radius was minimum near the centre of the tank. These values were -9.6 Pa, -8.7 Pa and -7.7 Pa for Eulerian k-ε Dispersed, Mixture and VOF models respectively.

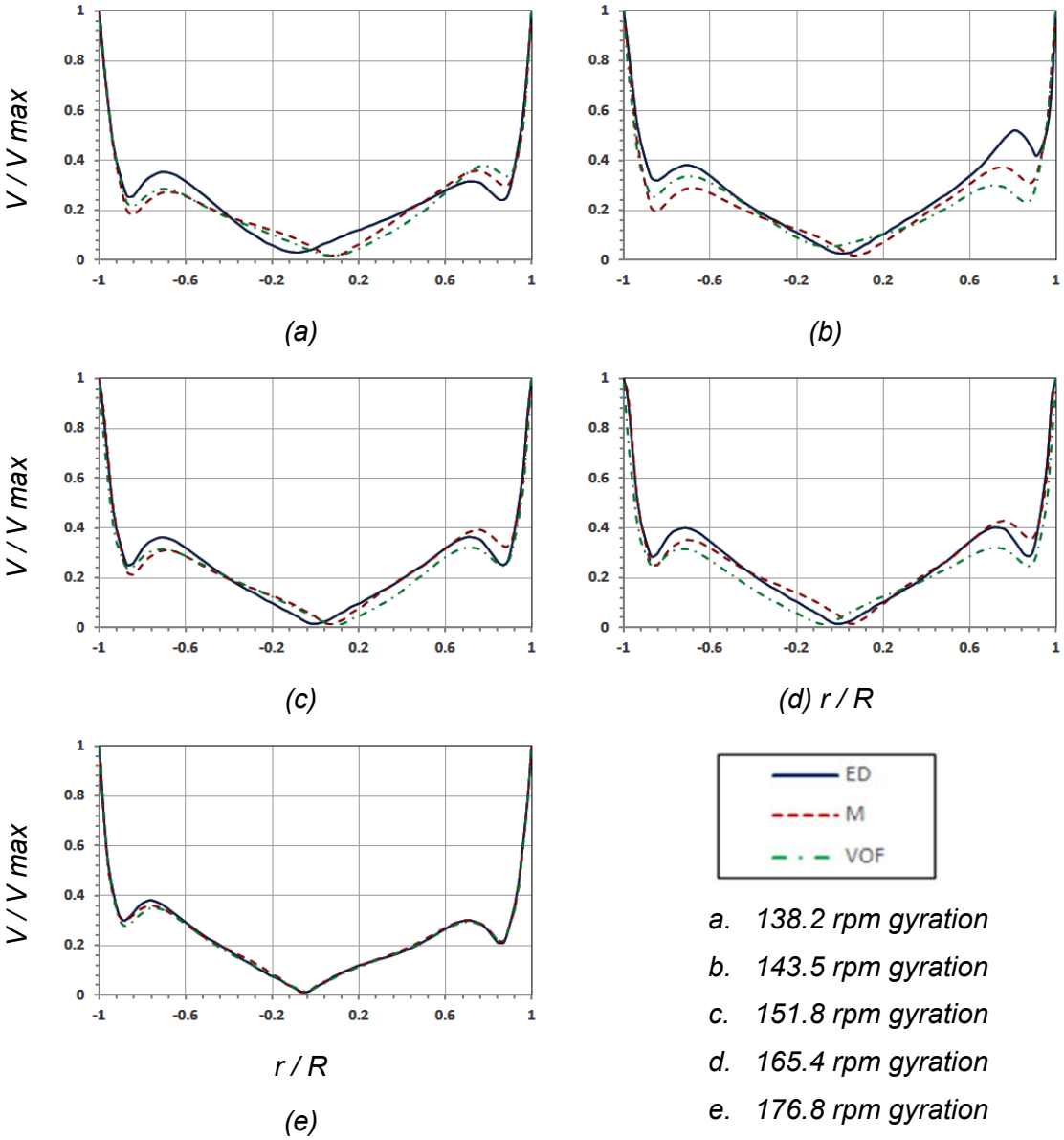

Fig. 4.25. Normalised Profiles of the phase-1 radial velocity

The velocity profiles of the primary phase for various simulation models at different gyration speeds are shown in Fig. 4.24 and Fig. 4.25. At lower gyration speed of 138.2 rpm, the velocity of phase-1 along the axis was maximum near to the walls which are 1.12 m/s, 1.09 m/s and 1.01 m/s for Eulerian k-ε Dispersed, Mixture and VOF models respectively. Minimum velocity was near to the center of the mixing tank which were 0.102 m/s, 0.101 m/s

and 0.026 m/s for Eulerian k-ε Dispersed, Mixture and VOF models respectively. The radial velocity was maximum near the wall which was 2.26 m/s for all the models. The minimum radial velocity were 0.071 m/s, 0.039 m/s and 0.044 m/s for Eulerian k-ε Dispersed, Mixture and VOF models respectively.

At maximum gyration speed of 176.8 rpm, the velocity of phase-1 along the axis was maximum near to the walls which were 1.37 m/s, 1.36 m/s and 1.33 m/s for Eulerian k-ε Dispersed, Mixture and VOF models respectively. Minimum velocity was near to the center of the mixing tank which were 0.08 m/s, 0.10 m/s and 0.08 m/s for Eulerian k-ε Dispersed, Mixture and VOF models respectively. The radial velocity was maximum near the wall which was 2.89 m/s for all the models. The minimum radial velocity were 0.036 m/s, 0.031 m/s and 0.046 m/s for Eulerian k-ε Dispersed, Mixture and VOF models respectively. The velocity and pressure were minimum near the center of the tank due to the centrifugal effect. The primary phase velocity for Eulerian k-ε Dispersed, Mixture and VOF models were almost similar. Both the primary and secondary phases are having the same maximum and minimum velocity magnitude for all the models. This was due to tendency of the secondary particulate phase to follow the highly viscous primary phase flow.

4.3 Summary

This chapter explained the experimental setup and the conformation of results with the CFD simulations. The experiment was conducted using the particulate solid phase as SiC and continuous liquid phase as glycerine. Sophisticated instruments were used for measuring the physical properties of the ingredients and readings from experiments. The mixing tank first loaded with 20% volume of SiC particulates and the rest of the tank was filled with glycerine. The readings were taken at no load and loaded conditions. The gyration speed of the mixing vessel was varied in between 138.2 rpm and 176.8 rpm. The mixing power was calculated by subtracting the power consumed at no load conditions from the loaded conditions.

The mixing of two-phase ingredients in a Gyro shaker is modelled using CFD software and experiments were conducted on a gyro shaker to validate the simulation. CFD simulation of the Gyro Shaker mixing was carried out in three multiphase models. A grid independence study was conducted to arrive at best mesh and type of cells. The Polyhedral element was found to be the best choice for the CFD simulation which shows better convergence with a minimum number of cells consuming low CPU time. The derived

characteristic velocity, Reynolds Number and Power Number can be used for further studies on Gyro Shaker mixer.

Out of the three simulation models, Mixture model shows better agreement with the experimental results. The Viscous Dissipation Method is better than Torque method for obtaining Mixing Power for the Gyro Shaker. The VOF model which is generally used for simulating immiscible liquids gave better results for simulating flows in Gyro Shaker also with the modified secondary phase viscosity.

The CFD simulation model can replace empirical correlations while scaling up of the system. Simulation can also be used for predicting the mixing behaviour in particulate mixing for the production of Metal Matrix Composites where the mixing process is at elevated temperature. A well-validated simulation model can be used to optimise the process parameters of the mixing systems.

CHAPTER 5

CFD SIMULATION OF LIQUID-SOLID DISPERSION IN A GYRO SHAKER

In this chapter, the development of CFD simulation of liquid-solid dispersion in the dual axis mixing for solid particulates is explained. Also, the solid particle distribution was compared for stirred vessel with gyro shaker mixer. Wang et al. (2010) have conducted a CFD simulation for analysing the solid particle distribution in a stirred vessel without baffles. The primary liquid phase of their work was glycerine/water mixture with density and viscosity of 1115.1 kg/m^3 and 0.006406 PaS respectively. The secondary particulate phase was sand with a density of 2779.2 kg/m^3. The diameter of the sand particle and loading was 137 μm and 4.62 vol. % respectively, so that 128.47 g/L of solid particle concentration for a perfectly homogeneous mixture. Both the diameter and liquid level of the cylindrical mixing vessel was 140 mm. The mixing was performed by mechanical agitation using an impeller with a diameter of 70 mm. The CFD simulation was conducted for a stirrer speed of 200 rpm, 250 rpm and 300 rpm.

5.1 Numerical scheme

For the glycerine/water and sand particle mixing simulation of Gyro shaker, the first-order upwind scheme was chosen for the spatial derivatives and volume fraction parameter as simulation conducted by Wang et al. (2010). The pressure-velocity coupling and the gradient formulation was SIMPLE and least squares cell-based respectively. The bottom of the mixing vessel was patched with 4.62 vol. % of sand particles. The gyration speed of the gyro shaker was calculated by equating the characteristic velocity of gyro shaker and stirred vessel taken by Wang et al. The stirrer speed in the stirred vessel was 200 rpm, 250 rpm and 300 rpm. Hence, the simulation of Gyro shaker mixing was conducted for a gyration speed of 33.33 rpm, 41.66 rpm and 50 rpm. The time step size for the transient simulation was taken as 0.001 sec. As in the case of gyro shaker machine, the spin speed of the mixing vessel was set as twice as that of gyration speed.

5.2 Results and discussion

The results of simulation of Gyro shaker and its comparison with the studies reported by Wang et al. (2010) is described in this section.

5.2.1 Grid independence study

The results extracted from the CFD simulation model should be independent of the size of the small control volumes. The Richardsons extrapolation method was used for finding the Grid Convergence Index (GCI). The three sets of fine, medium and coarse size cells were obtained by dividing the computational domain into 619899, 223734, 91436 number of tetrahedral cells. Since the CFD simulation showed difficulties in convergence due to the local fluctuation flow, the tetrahedral cells are converted to 108859, 42657, 16707 number of polyhedral cells. The grid refinement factor was 1.37, and the average cell sizes were 1.93mm, 2.64mm, 3.61mm. The percentage grid convergence index value for the mixing power, the volume weighted average of pressure and velocity for the simulation model are tabulated in Table. 5.1. Since all the GCI values for the above parameters were less than 5%, it was concluded that the CFD simulation was grid independent

Table 5.1 Grid convergence index (%)

Gyration speed (rpm)	33.33	41.66	50.00
Equivalent stirrer speed (rpm)	200	250	300
GCI: mixing power	1.30	1.88	3.47
GCI: Volume weighted average velocity	0.21	0.03	0.00
GCI: Volume weighted average pressure	3.52	4.44	3.50

5.2.2 Mixing effectiveness

The mixing quality is obtained using the standard deviation (σ) of solid particle concentrations at the sampling points inside the mixing region (Wang et al., 2010).

$$\sigma = \sqrt{\frac{1}{n}\sum_{i=1}^{n}\left(\frac{C}{C_{\propto}} - 1\right)^2} \tag{5.1}$$

where, n is the number of sampling locations,C is the solid particle concentration at the current time at the sampling points and $C_{\propto}$ is the solid concentration of the completely mixed fluid.

The x, y and z coordinates in the CFD simulation were taken in such a way that the axis of the mixing cylinder as y-axis and centre of the mixing cylinder coincides with the origin of the coordinate system. The eight sampling locations coordinates taken in the simulation conducted by Wang et al. (2010) are listed in Table. 2. For this, the coordinate system was chosen such a way that the mixing cylinder axis coincides with the z-axis and x-y plane with bottom plane of the mixing vessel. The same sampling points were taken in the simulation of gyro shaker mixing. The mixing is incomplete, if σ>0.8 and the mixing is in just suspension condition, if 0.2<σ<0.8. For a homogeneous suspension of solid particles, the σ should be less than 0.2. The time required for getting a specified degree of homogeneity from the commencement of mixing is called mixing time (Kasat et al., 2008). The time to reach the value of C/C_{∞}within ±5% of the perfect mix is taken as the mixing time.

Table 5.2 Representative points

Coordinate	X (m)	Y(m)	Z(m)
Point - 1	0.0354	0.0354	0.01
Point - 2	0.05	0	0.01
Point - 3	0.0283	0.0283	0.05
Point - 4	-0.0354	-0.0354	0.05
Point - 5	0.0247	0.0247	0.095
Point - 6	0.0424	0.0424	0.095
Point - 7	0.0354	0.0354	0.125
Point - 8	-0.05	0	0.125

5.2.2.1 Mixing time

The concentration of secondary phase sand particle in a perfectly homogeneous mixture is 4.62 % of the total mixing tank volume. The time taken by the simulation to run from the commencement of mixing to attaining a value of C/C_{∞}in between 0.95 and 1.05 was chosen as mixing time. The mixing time obtained from gyro shaker mixing for an equivalent stirrer speed of 200 rpm, 250 rpm and 300 rpm were 30.1 sec, 27.2 sec and 30.8 sec respectively. The variation of concentration of sand particles at the eight sampling locations for simulation conducted by Wang et al. and gyro shaker mixing concerning simulation run time are as shown in Fig. 5.1 (a) & (b) respectively. The gradual mixing was found in the stirred vessel. But in gyro shaker mixing, the sand particle concentration was found fluctuating due to the highly recirculation flow.

The mixing time for stirred vessel and gyro shaker mixer at various equivalent stirrer speeds are plotted in Fig. 5.2. The mixing time in stirred vessel was found decreasing as the stirrer speed increases. The mixing time in gyro shaker was found decreasing as the speed changed from 200 rpm to 250 rpm. However, it has increased as the speed increased from 250 rpm to 300 rpm. This was due to the increased local fluctuations of the particles concentration at sampling points 1 & 2. Increased mixing time was found for extremely low and high speeds of gyration of the mixing cylinder.

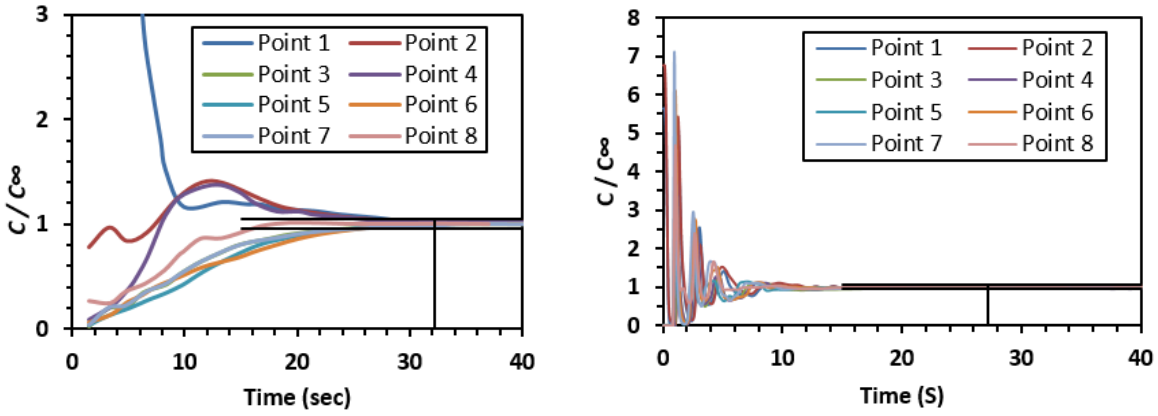

(a) *(b)*

Fig. 5.1. Mixing time in the glycerine/water-sand system at an equivalent stirrer speed of 250 rpm. (a) Stirred vessel simulation by Wang et al. (b) Gyro shaker Simulation.

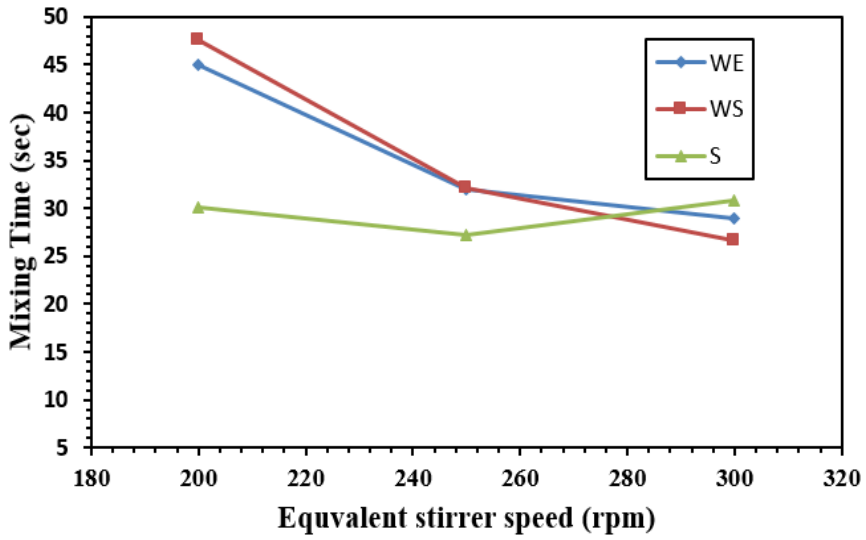

Fig. 5.2. Mixing time for different stirrer speeds. WE: Experimental results taken from Wang et al. WS: Simulation results taken from Wang et al. S: Simulation results from gyro shaker mixing.

5.2.2.2 Solid particle distribution

The standard deviation of the solid particle concentration after completing the mixing at various sampling points are shown in Fig. 5.3. It is obtained that the standard

deviation of the sand particle concentration at the different sampling locations was well below the value of 0.2. The standard deviation of the solid particle concentration at 200 rpm, 250 rpm and 300 rpm were found 0.02815, 0.02641 and 0.03519 respectively. The standard deviation inside the stirred vessel was found decreasing as the speed increases.

In gyro shaker, its value was minimum in between 200 rpm and 300 rpm.The mixing quality was found better at lower gyration speed of the mixing vesel. At higher speeds the the solid particles concetrated near the walls causes a higher value of standard deviation. The standard deviation of the solid particle concentration inside the stirred vessel was found decreasing as speed was increased.The standard deviation of the sand particle concentration in gyro shaker was lower than that of stirred vessel which indicated a more homogenous mixture in Gyro shaker mixing.

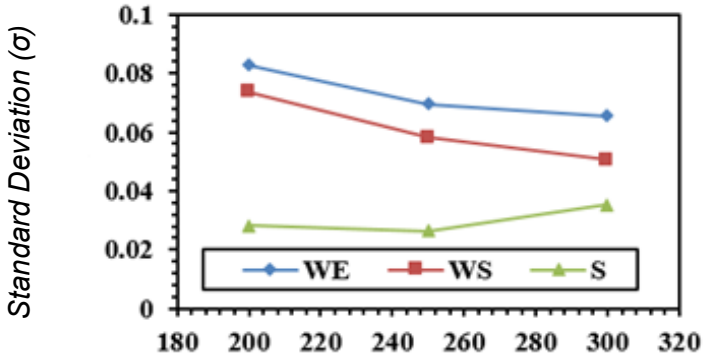

Fig. 5.3. The standard deviation of solid particle concentration. WE: Experimental results taken from Wang et al. WS: Simulation results taken from Wang et al. S: Gyro shaker simulation.

The variation of the ratio of the concentration of sand particle (C) after reaching the mixing time to the completely homogenised mixture (C_{avg}) at various locations inside the mixing region at an equivalent stirrer speed of 250 rpm is shown in Fig. 5.4.

The sand particle concentration along the axial direction at various dimensionless radial locations is plotted for stirred vessel and gyro shaker. The minimum and maximum value of $C/C_{avg}$was found as 0.930635 and 1.074424 at locations where r/R=0.357 and 0.857 respectively. In both cases, the homogeneity of the mix is weak at the bottom of the mixing vessel where the sand particles were patched at the beginning of mixing. The mixing in stirred vessel was found poor near the impeller region. In gyro shaker, a deviation of mixing quality was observed near the centre of the mixing tank. This was due to the effect of

centrifugal force which pushes the sand particles towards the walls of the container. The sand particle distribution was found more homogeneous in gyro shaker than a stirred vessel.

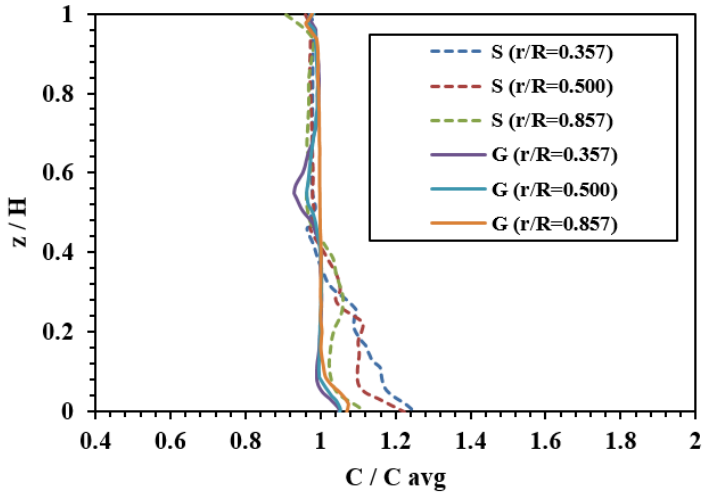

Fig. 5.4. Comparison of simulation models on the axial sand distribution. S: Stirred vessel G: Gyro shaker.

5.2.3 Flow characteristics

The flow characteristics of the simulation of Gyro shaker and Stirred vessel are compared in this section.

5.2.3.1 Velocity contours and stream lines

The velocity contours of the primary liquid phase at various equivalent stirrer speeds for gyro shaker on the x-y plane are as shown in Fig. 5.5.

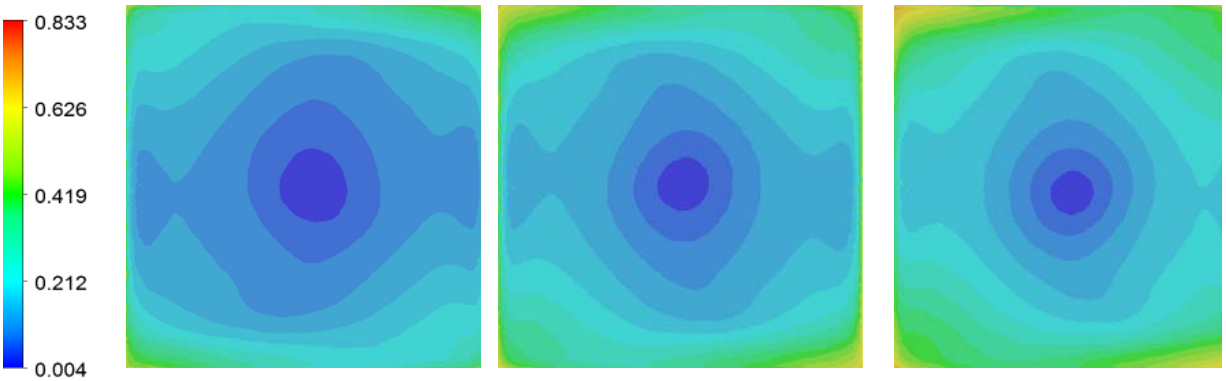

200 rpm *250 rpm* *300 rpm*

Fig. 5.5. Contours of fluid velocity (m/s) in the Gyro shaker mixer.

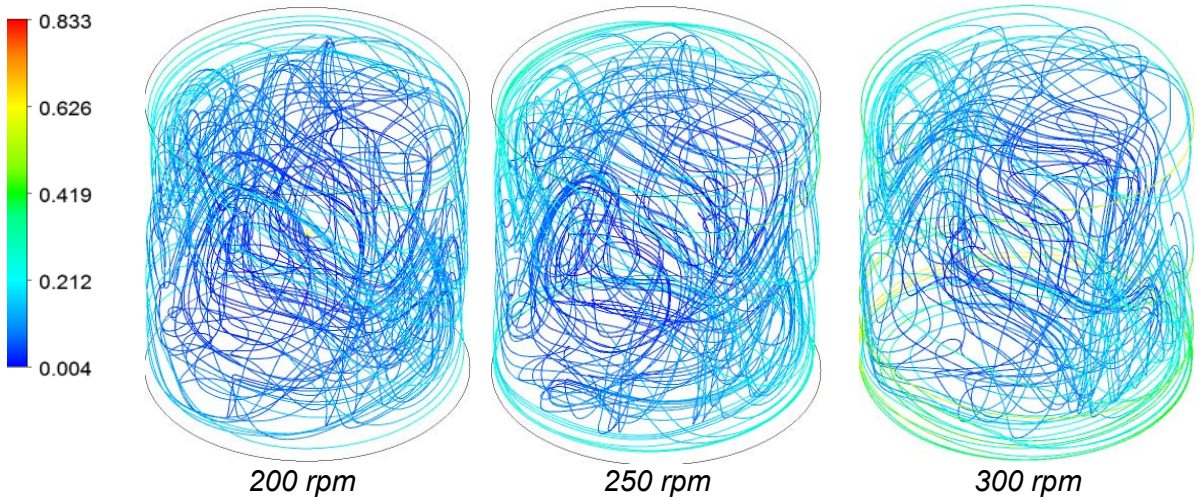

Fig. 5.6. Stream lines coloured by velocity (m/s) in the Gyro shaker mixer.

The velocity was found to be minimum near the centre of the tank and maximum near the corners of the container. The velocity of fluid flow was more at a higher rotation of the mixing tank. The stream lines of the fluid particles after 40 seconds from the commencement of stirring at various equivalent stirrer speeds for gyro shaker are shown in Fig. 5.6. The fluid moves at low velocity near the centre of the mixing vessel in an irregular mode. When the fluid flow reaches the walls of the container, the fluid velocity becomes tangential to the walls. The stream lines of the fluid flow indicated a vigorous mixing of the ingredients inside the mixing vessel.

5.2.3.2 Particle distribution contours

The contours of normalised sand distribution for the gyro shaker after reaching a flow time of 40 seconds is shown in Fig. 5.7. The maximum and minimum value observed for the particulate volume fraction at 200 rpm was 0.038533 and 0.0545371 respectively. At equivalent stirrer speed of 250 rpm, the corresponding values were 0.0379427 and 0.0557681.

Similarly, at equivalent stirrer speed of 300 rpm, the corresponding values were 0.0380725 and 0.05300738. The concentration was low near the centre and high near the corners of the mixing tank. This was due to the trapping of sand particles near the edges of the container. The volume fraction contours of sand for stirred vessel and gyro shaker are shown in Fig. 5.8. An accumulation of sand particles near the bottom of mixing tank is found in stirred vessel. However, a uniform distribution of sand particles is observed in gyro casting

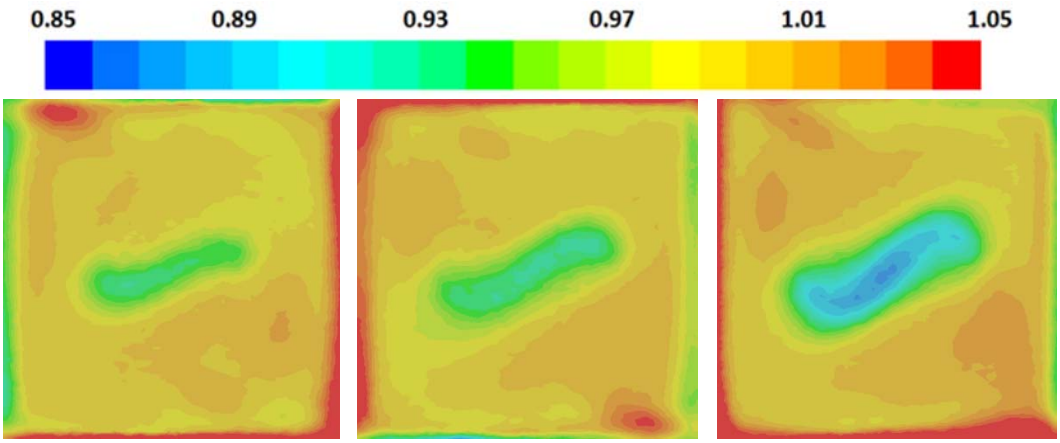

Fig. 5.7. Contours of C/C_{∞} of Sand after 40 sec in Gyro shaker mixing.

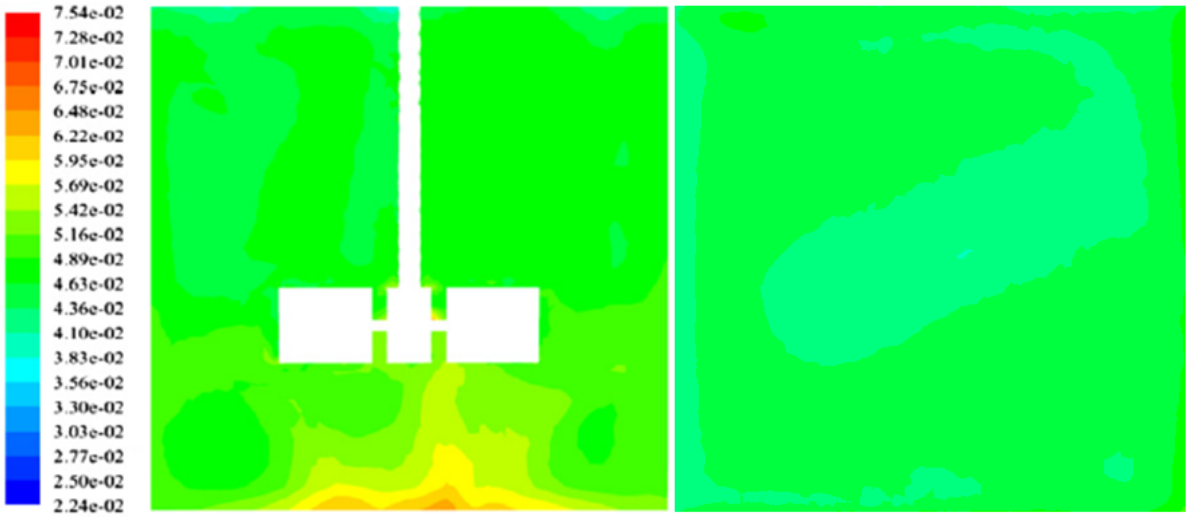

Fig. 5.8. Contours of volume fraction of sand at 250 rpm of stirrer speed (a) Stirred Vessel (Wang et al.) after 3600 Sec. (b) Gyro Shaker after 28 Sec.

5.2.3.3 Swirling strength

The swirling motion around local centres can be visualised by swirling strength. The imaginary part of complex eigenvalues of velocity gradient tensor is called swirling strength.

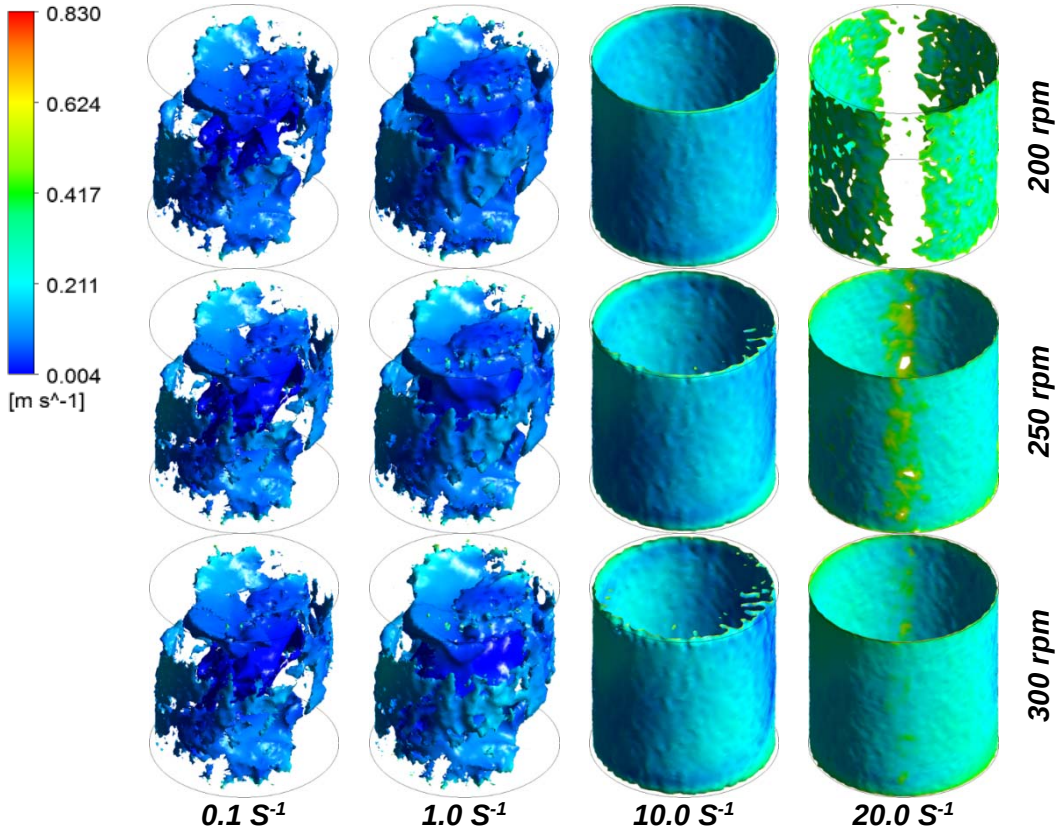

Fig. 5.9. Isosurface of vortices for swirling strength at different speeds coloured by velocity.

It provides information about the fluid flow for the local rate of rotation. The maximum value of swirling strength for the equivalent stirrer speed of 200 rpm, 250 rpm and 300 rpm is 29.66 S^{-1}, 36.66 S^{-1} and 43.48 S^{-1} respectively. The isosurface for constant swirling strength of 0.1 S^{-1}, 1 S^{-1}, 10 S^{-1} and 20 S^{-1} at different speeds are shown in Fig. 5.9. The local swirling strength is maximum near the side walls where the fluid velocity was maximum. It is found minimum at the centre of the mixing vessel where the velocity was minimum.

5.3 Summary

In this chapter, the CFD simulation conducted in a stirred vessel by Wang et al. (2010) for mixing glycerine/water solution with sand particles was compared with the gyro shaker mixing. The mixing time and concentration of the sand particles obtained from stirred vessel was compared with gyro shaker mixing. The homogeneity of mixture was found better in gyro shaker mixing. The flow parameters such as velocity, volume fraction of sand particles, streamlines and swirling strength were also observed to be better in the gyro shaker mixing as compared to the stirrer mixing.

CHAPTER 6

GYRO CASTING SIMULATION

The CFD simulation of producing Al-SiC PMMC by gyro casting method and comparison for particulate distribution and mixing time with stir casting is described in this chapter. The simulation is conducted for the same characteristic fluid velocity and same volume of domain as in the case of stir casting. Two simulations, analogues to liquid aluminium and mushy state aluminium as matrix materials were conducted. In the analogue simulations, the aluminium liquid and mushy state aluminium were replaced by water and glycerine/water mixtyre respectively.

6.1 Computational domain and mesh

The simulation of stir casting was carried out in laminar model for glycerine/water system and k-Ɛ turbulent model in water system similar to the simulations conducted by Neher et al., (2007). They were conducted an experimental study on mixing of SiC particulates in liquids with two different viscosity levels for examining the effect of viscosity of liquids in dispersion time. The particle size and speed of stirring are also varied during the experiment. CFD simulation was also conducted to determine the steady-state particulate distribution in the stir casting of liquid aluminium and mushy state aluminium with 10% SiC of 13 μm size. The experiment and simulation were conducted by replacing liquid aluminium with water having an almost same viscosity of 1 mPaS. Similarly, the mushy state aluminium was replaced by glycerine having almost the same viscosity of 300 mPaS. The computational domain of the stirred vessel was a crucible of 105 mm diameter and is filled with liquid at the height of 65 mm. The stirrer was made of steel having four blades with a diameter of 80 mm. In this work, the dispersion time and particulate distributions obtained from the CFD simulation model of gyro casting was compared with the values obtained from the works conducted by Neher et al., (2007).

The computational domain for gyro casting was a cylinder having both diameter and length of 90 mm for keeping the volume of domain same as the domain in the stir casting. The size of the SiC particulate was 13 microns and volume fraction was kept at 10%. The Spin speed was set to twice than that of Gyration speed. CFD simulation was carried out with values of spin speed and gyration speed selected such a way that the characteristic

velocity would be the same as that of the characteristic velocity in the experiment conducted by Neher et al., (2007). Mixing performance of the CFD simulation model of gyro casting was compared with the CFD simulation model developed for stir casting by Neher et al., (2007) to mix SiC particulates with water and glycerine/water solution. The computational domain for comparing the mixing performance was designed for the same quantity of liquid phase and particulate phase taken in the stir casting.

6.2 Boundary conditions and numerical schemes

No-slip boundary condition was applied to the closed rotating walls so that the velocity of the fluid stuck on the walls has the same as that of the velocity of the walls. The CFD simulation for the water system was conducted in Eulerian standard k-Ɛ dispersed multiphase model. Water was taken as primary phase and SiC particulates was taken as secondary phase. For all the gyration speeds, second order upwind implicit formulation for unsteady integration and a second order upwind scheme discretization for spatial derivatives were adopted. The pressure-velocity coupling used was Phase Coupled SIMPLE. The Gradient formulation was Least squares cell based and volume fraction parameter was QUICK. The time step of the transient simulation was set to 0.001 sec for all the gyration speeds. The spin was given to the walls by wall motion option and gyration is given by the frame motion option of the software. The simulation was run up to 60 seconds of flow time. The steady state simulation was also conducted for the same numerical scheme.

The CFD simulation for glycerine/water system was conducted in laminar model. The first order upwind implicit formulation for unsteady integration was taken. All other numerical schemes were taken as same as that of water system. The transient simulation was run up to 30 seconds of flow time. Steady state simulation was also conducted for comparing the effectiveness of mixing with stir casting.

6.3 Mixing index

The mixing time is the time taken for the segregated state of the liquid and particulate phase to attain a given degree of homogeneity. The Mixing Index (MI) proposed by Rose and Robinson (Bai et al., 2017: Huang and Kuo, 2014) as shown in equation 6.1 was used for assessing the mixing time. The symbols σ and σ_0 in the equation indicate standard deviations of the volume fraction of secondary particulate phase at sampling points inside the mixing domain at the current time and at the initial time. In the presented CFD simulation for comparing the mixing effectiveness, all the cell centre values of the volume fraction of

SiC particulates inside the domain are taken as sampling points. As usually taken in stirred vessels, the dispersion time (θ_{99}) is considered as the mixing time when Mixing Index (MI) reaches 0.99.

$$\text{Mixing index}=1-(\sigma/\sigma_0) \quad (6.1)$$

6.4 Grid independence study

The grid independence study was carried out for both the simulation models developed for water and glycerine/water systems for comparing with the stir casting results. The CFD simulation was carried out for three domains of polyhedral cells with a grid refinement factor of 1.39. Tetrahedral cells of 632495, 231057 and 84085 numbers were converted to polyhedral cells of 111055, 41336 and 15497 numbers for obtaining the monotonic convergence of the flow parameters. The Grid Convergence Index (GCI) for mixing power, volume weighted average pressure and volume weighted average velocity obtained for the above flow parameters were less than 5%. So, it is concluded that the CFD simulation is grid independent.

Table 6.1 Grid Convergence Index for various Gyration speed in the water system

Gyration speed (rpm)	29.09	58.18	72.73	87.27
Equivalent stirrer speed (rpm)	100	200	250	300
GCI (%) ; Mixing power	0.97	3.73	2.00	1.12
GCI (%) ; Volume weighted average pressure	0.00	0.28	0.35	0.09
GCI (%) ; Volume weighted average velocity	0.00	0.11	0.13	0.03

Table 6.2 Grid Convergence Index for various Gyration speed in glycerine/water system

Gyration speed (rpm)	58.18	87.27	116.36	145.45
Equivalent stirrer speed (rpm)	200	300	400	500
GCI (%) ; Mixing power	1.69	1.81	3.73	2.51
GCI (%) ; Volume weighted average pressure	0.08	0.29	0.37	0.63
GCI (%) ; Volume weighted average velocity	3.04	0.20	0.15	0.29

6.5 Mixing performance analysis in water system

The distributions of particulates distribution at various positions and after various mixing times inside the mixing vessel of the gyro casting were analysed and compared with stir casting. The major findings of the sane are explained in the following paragraphs.

6.5.1 Particle distribution

The distribution of SiC particulates in the water system at various locations for different equivalent stirrer speeds at 40 seconds, 50 seconds and 60 seconds after the commencement of mixing along with the steady-state simulation are shown in Fig. 6.1, 6.2, 6.3 and 6.4. The steady state distribution of SiC particulate obtained from the simulation conducted by Neher et al., (2007) was also plotted in these graphs for comparing with stir casting. The various radial distances along the central axis of the mixing vessel at cross sections P, Q, S and T were taken from the bottom of the tank at height ratio of 0, 0.108, 0.538 and 0.769 respectively (Neher et al., 2010). The positions of P, Q, S and T represented the bottom wall, bottom region, middle region and top regions of the mixing vessel respectively.

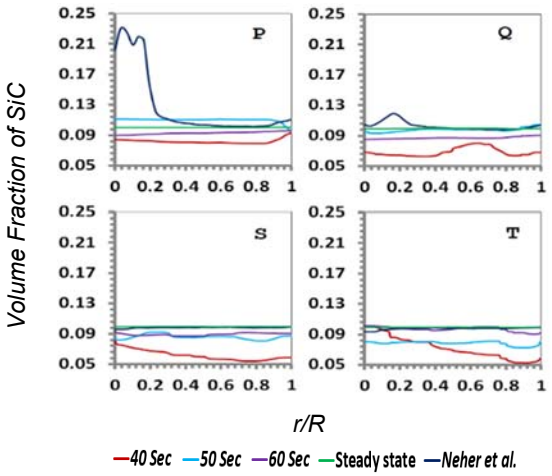

Fig. 6.1. Distribution of SiC in the water system at an equivalent stirrer speed of 100 rpm

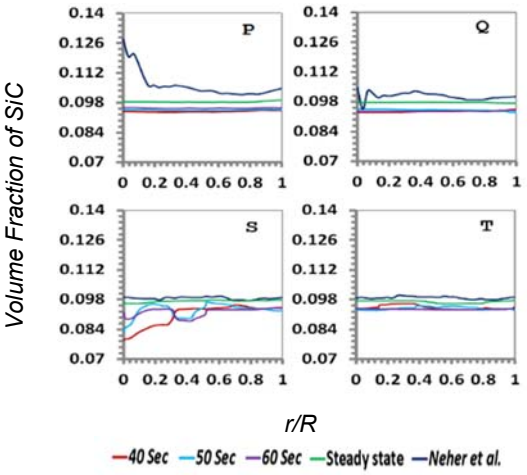

Fig. 6.2. Distribution of SiC in the water system at an equivalent stirrer speed of 200 rpm

For a perfect homogenous suspension of particulates, the volume fraction of SiC particulate should be 0.1 everywhere inside the fluid domain. At lower speeds, the time taken to reach a uniform distribution was found to be more in the water system for gyro casting. At lower speeds, there was an accumulation of SiC particulates near the centre of the bottom wall in the water system for stir casting. The SiC particulate distribution at the

lower region of the mixing vessel was found to be more uniform at higher speeds in gyro casting. Even though there was some degree of non-uniformity in the distribution of SiC particulates in the middle and upper regions of the mixing vessel, the particulate distribution was better in the water system which describes the mixing of SiC particulates in liquid aluminium.

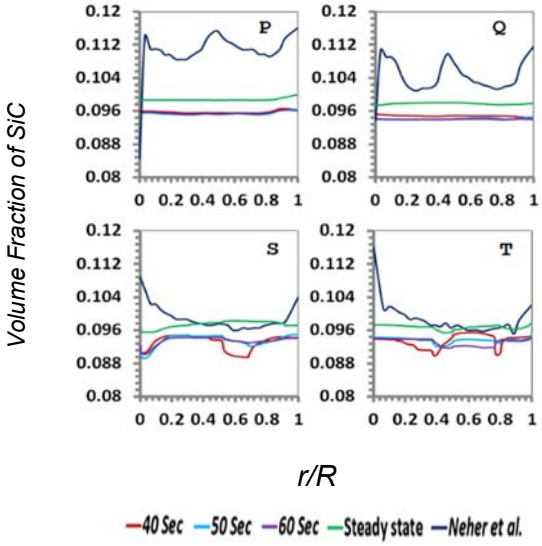

Fig. 6.3. Distribution of SiC in the water system at an equivalent stirrer speed of 250 rpm

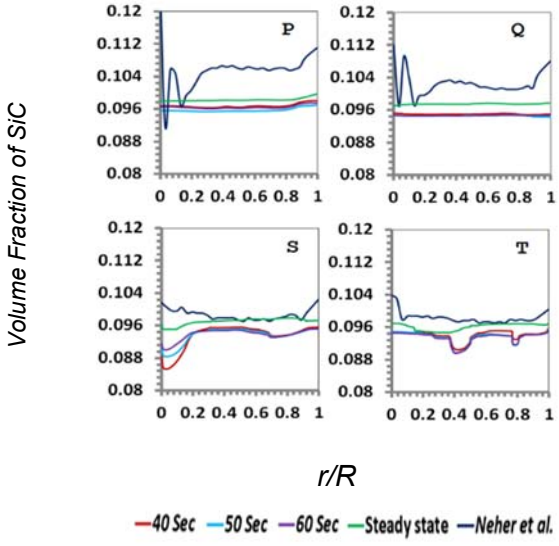

Fig. 6.4. Distribution of SiC in the water system at an equivalent stirrer speed of 300 rpm

The maximum volume fraction in Gyro casting simulation was seen near the bottom walls which were 0.1002, 0.0993, 0.0999 and 0.0997 respectively for equivalent stirrer speeds of 100 rpm, 200 rpm, 250 rpm and 300 rpm. The minimum volume fraction in Gyro casting simulation was seen near the top region of the mixing vessel which was 0.0994, 0.0962, 0.0954 and 0.0947 respectively for equivalent stirrer speeds of 100 rpm, 200 rpm, 250 rpm and 300 rpm.

6.5.2 Mixing time

Mixing time for the water system for both stir casting and gyro casting are tabulated in Table 6.3. The mixing time was high at 200 rpm in stir casting which indicates the stirrer speed was very much close to the just-suspension speed. The mixing time was almost same for 200 rpm, 250 rpm and 300 rpm for stir casting. In stir casting, the mixing was achieved by the rotation of the impeller. Far regions from the impeller get mixed slowly. When the speed was increased, the centrifugal action threw away the particulates at a higher rate against the viscous resistance offered by the fluid resulting a better mixing. Mixing time for gyro shaker

was found to be decreasing as the speed was increased but slightly increased at a gyration speed of 87.27 rpm which was due to the low recirculation of the particulates through the centre of the mixing tank.

Table 6.3 Time to achieve uniform distribution of SiC particulates in the water system

Neher et al. stirring speed (rpm)	Gyration speed (rpm)	Mixing time, θ_{99} (Sec)	Neher et al., (2007) dispersion time (Sec)
100	29.63	61.84	170
200	58.18	43.44	16
250	72.73	26.85	15
300	87.27	27.24	14

6.5.3 Volume fraction contours

The contours of volume fraction inside the mixing vessel before the commencement of mixing is shown in Fig. 6.5. The SiC particulates of 10 vol.% of the total domain were patched before the beginning of the transient simulation. The contours of the volume fraction of the SiC particulate at the middle of the vertical section for water system at 40 seconds, 50 seconds and 60 seconds after the commencement of mixing are shown in Fig. 6.6.

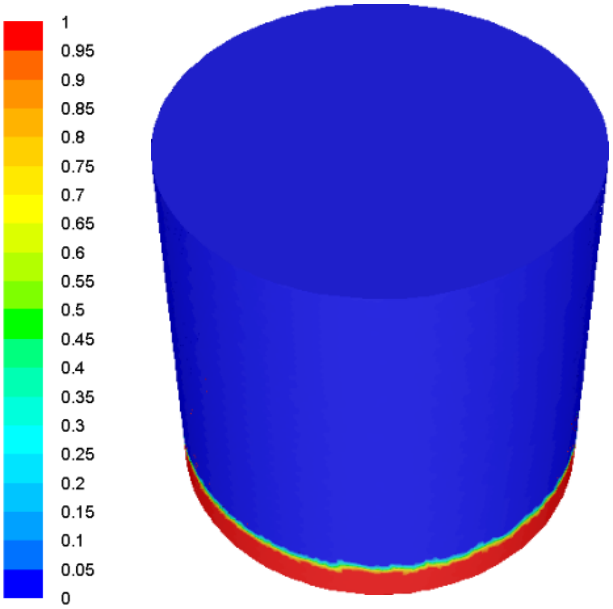

Fig. 6.5. Contours of volume fraction before the

commencement of mixing.

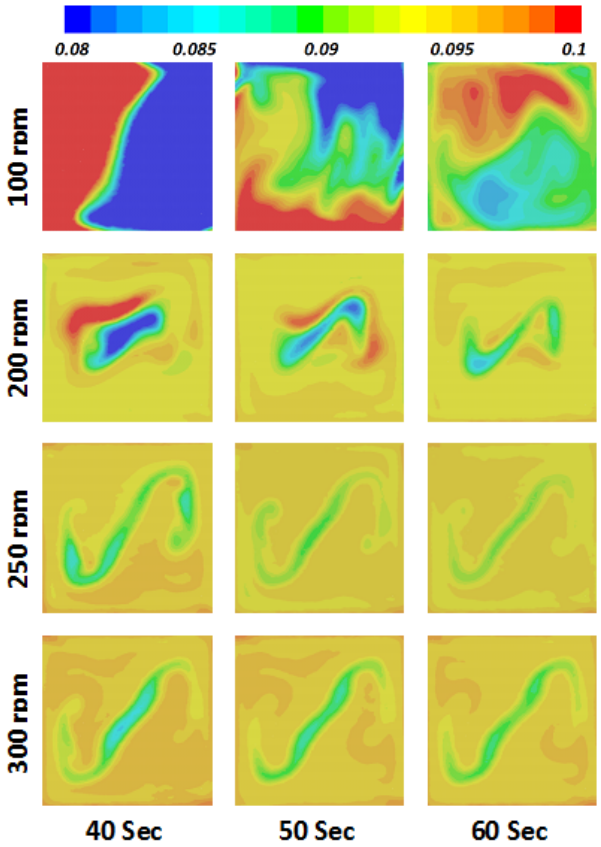

Fig. 6.6. Contours of the Volume fraction of SiC in the Water system

As the speed was increased, the rate of mixing also increased. A non-uniformity of particulate distribution was found near to the centre of the mixing tank at lower gyration speed in water system. It is clear from the volume fraction contours that the mixing near the centre of the tank is very slow compared to the area near the walls.

6.6 Mixing performance analysis in glycerine/water system

6.6.1 Particle distribution

The particulate distribution for glycerine/water system after 10 seconds, 20 seconds and 30 seconds and steady state are plotted in Fig. 6.7, 6.8, 6.9 &6.10. These figures show that the mixing rate was more in the glycerine/water system.

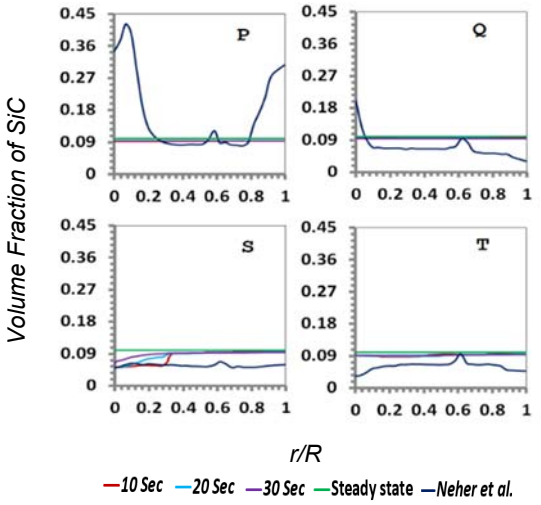

Fig. 6.7. Distribution of SiC in glycerine/water system at an equivalent stirrer speed of 200 rpm

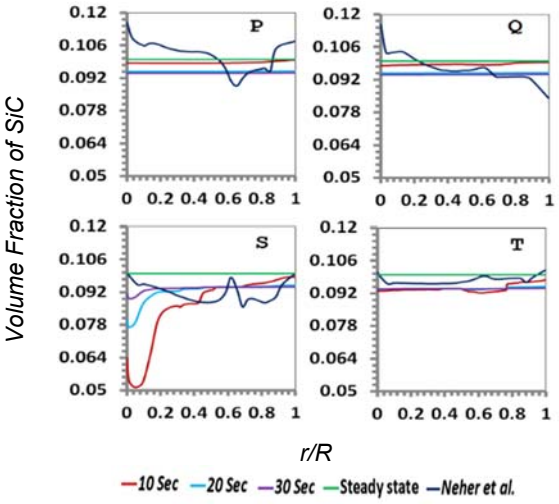

Fig. 6.8. Distribution of SiC in glycerine/water system at an equivalent stirrer speed of 300 rpm

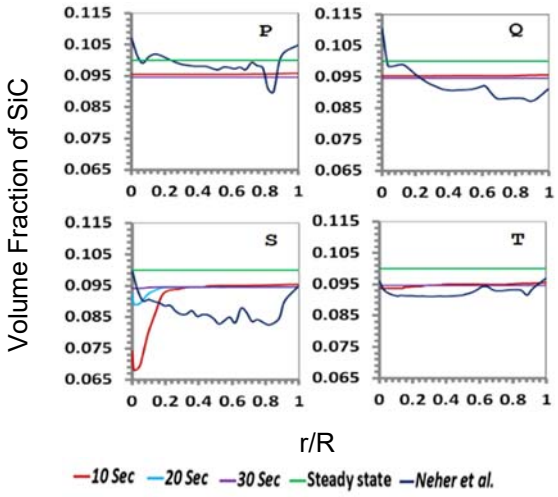

Fig. 6.9. Distribution of SiC in glycerine/water system at an equivalent stirrer speed of 400 rpm

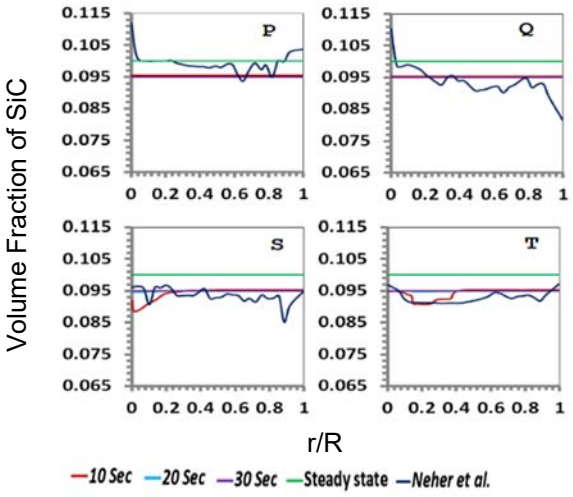

Fig. 6.10. Distribution of SiC in glycerine/water system at an equivalent stirrer speed of 500 rpm

The SiC particulate distribution was found to be more uniform in glycerine/water system for gyro casting. The higher viscosity of the glycerine/water system provided better mixing in case of gyro casting than stir casting. The accumulation of particulates near the centre of the tank was noticed at lower speeds in the stir casting. The maximum and minimum values of particulate concentration observed were 0.1000 and 0.0999 respectively. The fluctuation in concentration level of particulates inside the mixing domain was found to be more in stir casting than gyro casting for glycerine/water system.

6.6.2 Mixing time

Mixing time for both stir casting and gyro casting for the glycerine/water system are tabulated in Table 6.4. Mixing time in stir casting was found to be much higher than that of the gyro casting. The viscous resistance offered by the fluid was more in this glycerine/water system than the water system. Fluid near the stirrer will mix more and the movement of the particulates towards the far regions is constrained by the high viscous resistance offered by the fluid in stir casting. The contours of volume fraction for the SiC particulates are as shown in Fig. 6.11. The mixing time for glycerine/water system was found to be low in case of gyro casting as compared to that of stir casting. It was also lower than water system of gyro casting. Besides, the centrifugal action created by the high viscous fluid inside the rotating vessel of gyro casting device produces better recirculation of fluid.

Table 6.4. Time to achieve uniform distribution of SiC particulates in glycerine/water system

Neher et al. stirring speed (rpm)	Gyration speed (rpm)	Mixing time, θ_{99}(Sec)	Neheretal.,(2007). dispersion time (Sec)
200	58.18	26.34	2335
300	87.27	15.97	1030
400	116.36	9.80	720
500	145.45	6.26	540

6.6.3 Volume fraction contours

The contours of the volume fraction of the SiC particulate at the middle of the vertical section for water system at 10 seconds, 20 seconds and 30 seconds after the commencement of mixing are shown in Fig. 6.11. As the speed was increased, the rate of mixing also increased. A non-uniformity of particulate distribution was observed near the centre of the mixing tank at lower gyration speed in glycerine/water system. The mixing was found to be faster at higher gyration speed.

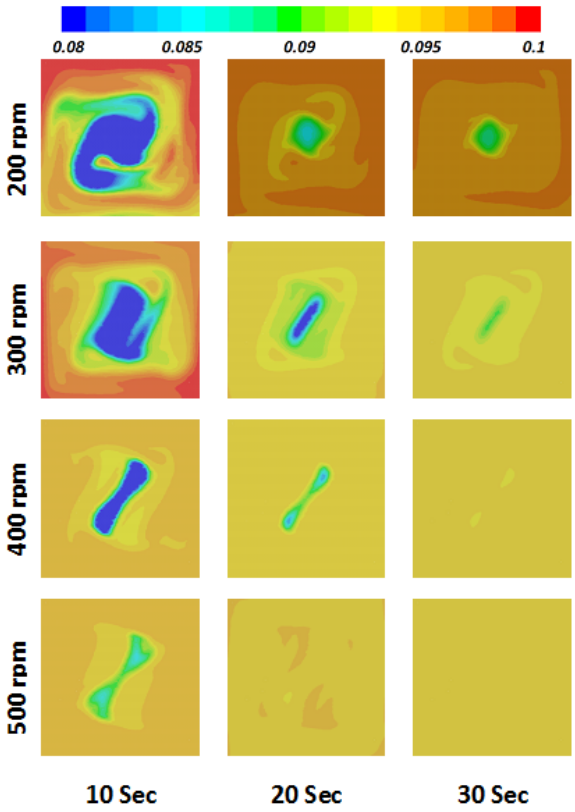

Fig. 6.11. Contours of the Volume fraction of SiC in glycerine/water system

6.7 Steady state simulation

The contours of the volume fraction of SiC particulates on a vertical mid plane obtained from the steady-state simulation for the water system and glycerine water system are shown in Fig. 6.12 and 6.13. The centrifugal force had resulted in transporting particulates as the speed was increased. This has resulted in a small amount of increased concentration near the walls of the mixing tank in the water system as it was having low viscosity. The difference in volume fraction of the SiC particulates in the glycerine/water system having increased viscosity was negligibly small. The minimum and maximum value of volume fraction of SiC particulates were 0.09379 and 0.10006 respectively in water system for equivalent stirrer speed ranging from 100 rpm to 300 rpm. The minimum and maximum value of volume fraction of SiC particulates were 0.09999 and 0.10001 respectively in glycerine/water system for equivalent stirrer speed ranging from 200 rpm to 500 rpm.

The isosurface of volume fraction of secondary particulate phase for water and glycerine/water systems are shown in Fig. 6.14, Fig. 6.15 and Fig. 6.16. The variation of volume fraction of the particulates was found to be low at 100 rpm in water system which showed a better mixing. As the speed increased, the particles concentration found to be

more near to the walls of the container. Hence, it was concluded that slow rotational speed provided better mixing in water system. There was not much of a difference in particle concentration inside the fluid domain of glycerine/water system. Only a slight increase of particle concentration towards the walls of the container was observed with the increase in speed. The speed of rotation of the mixing vessel has no considerable effect on the particle distribution, hence a lower speed may be preferred.

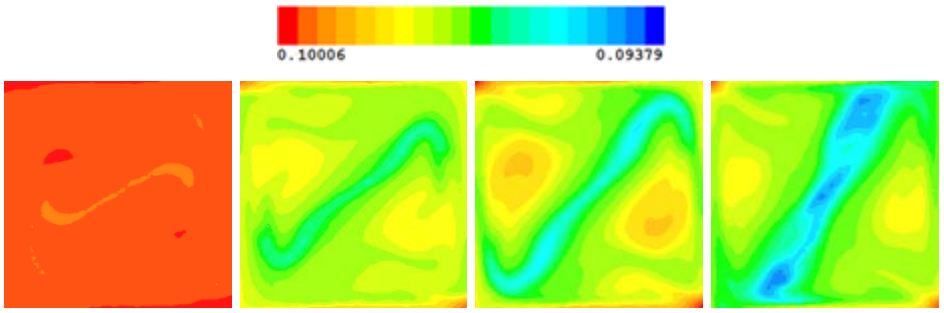

Fig. 6.12. Contours of the volume fraction of SiC in steady-state simulation for water system

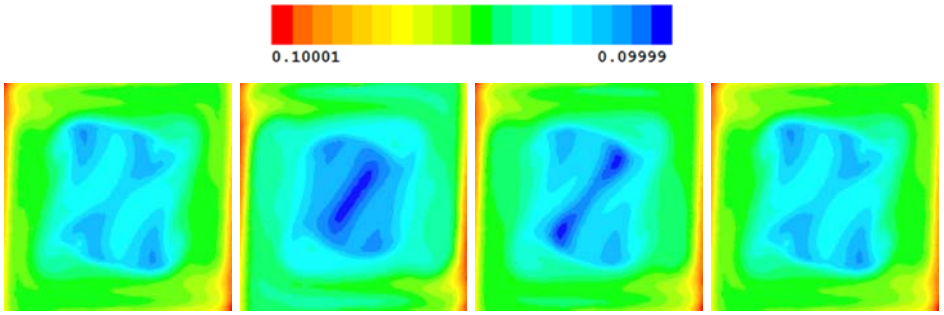

Fig. 6.13. Contours of the volume fraction of SiC in steady-state simulation for glycerine/water system

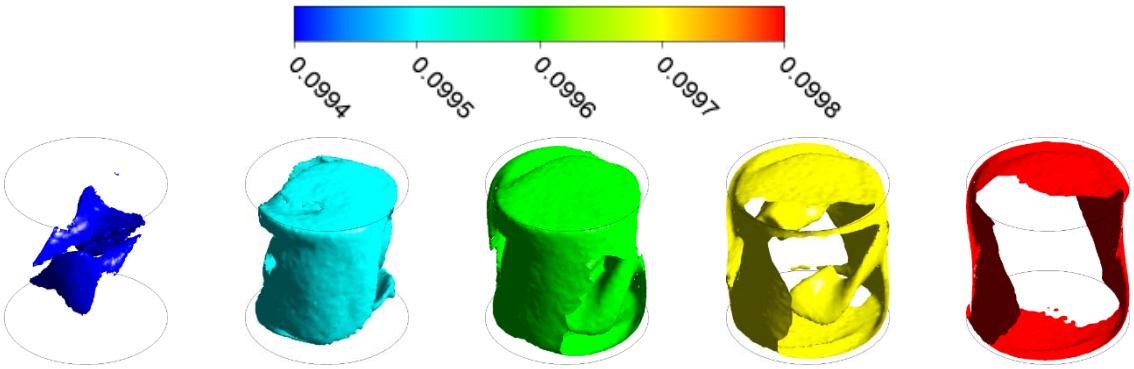

Fig. 6.14. Isosurfaces of volume fractions of SiC particulates at an equivalent stirrer speed of 100 rpm for water system.

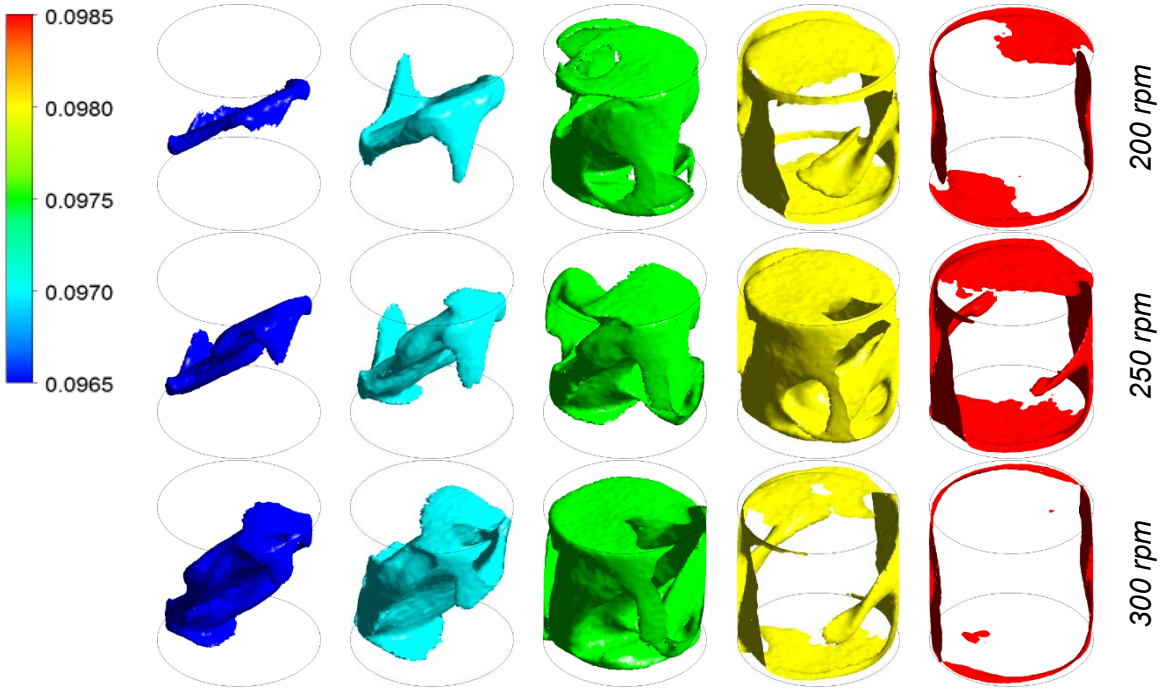

Fig. 6.15. Isosurface of volume fractions of SiC particulates at different equivalent stirrer speeds in water system.

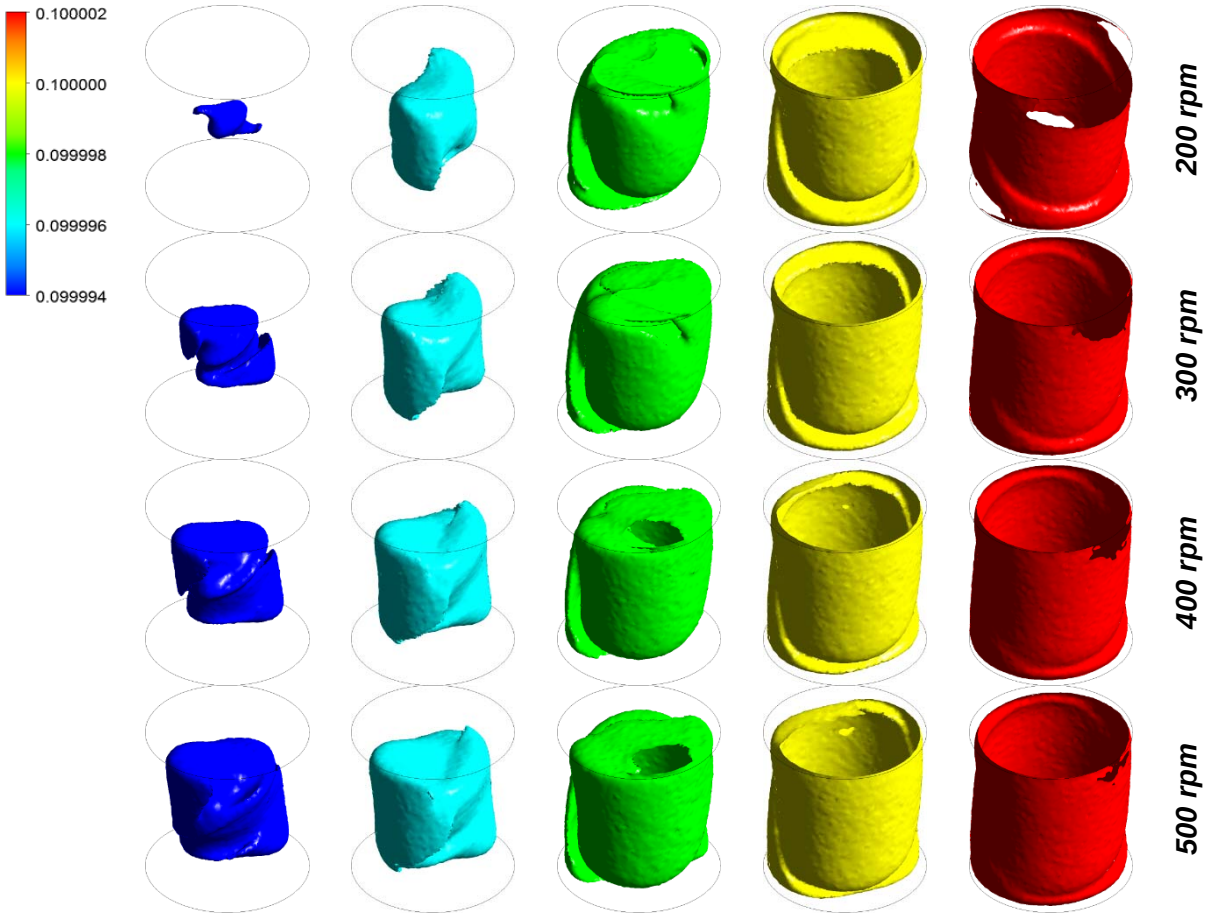

Fig. 6.16. Isosurface of volume fractions of SiC particulates at different equivalent stirrer speeds in glycerine/water system.

6.8 Flow pattern for Gyro casting

The isosurfaces of vorticity coloured by fluid velocity at equivalent stirrer speeds of 200 rpm and 300 rpm are shown in Fig. 6.17 and Fig. 6.18 respectively. The maximum values of vorticity inside the fluid domain at 200 rpm for glycerine/water and water were 147.668 S^{-1} and 497.636 S^{-1} respectively. At 300 rpm, the corresponding values were 267.327 S^{-1} and 750.278 S^{-1}. In water system, the magnitude of vorticity was found rapidly increasing near the walls of the container. The magnitude of vorticity was found very low at the inner fluid region. This was due to the low viscosity of the water which transfers less amount of momentum to the inner part of the fluid region inside the cylinder. The increase in speed of rotation had not influenced much on the magnitude of vorticity inside fluid region. But, the vorticity near the surface was increased as the speed of rotation of the vessel increased. The fluid velocity was also low inside the mixing vessel as compared to the velocity near the walls.

The magnitude of vorticity was found to be increasing in glycerine/water system from the centre of the mixing tank towards the walls of the container. The maximum magnitude was found lower than water system at the same rotational speed of mixing cylinder. As the speed increased, the vorticity magnitude also got increased. The momentum transfer from the wall was higher in the glycerine/water system as compared to the water system due to the higher viscosity of the glycerine/water mixture. The fluid velocity was also found increasing towards the walls of the container.

The isosurfaces of vorticity coloured by swirling strength are shown in Fig. 6.19. The swirling strength determines the swirling frequency of eddies formed by fluid particles at local points. The eddies inside the fluid domain enhances the fluid mixing. The maximum value of swirling strength at equivalent stirrer speed of 200 rpm and 300 rpm were 53.12 S^{-1} and 79.45 S^{-1} respectively for water system. The corresponding values were 35.50 S^{-1} and 55.22 S^{-1} for glycerine/water system. The swirling strength was low in water system as compared to glycerine/water system. The increasing in rotational speed of mixing vessel has little effect in water system. The swirling strength was found to be increasing as the rotational speed of vessel was increased. The mixing was faster in glycerine/water system due to this increase in the swirling strength of eddies.

The streamlines of fluid flow, velocity contour and velocity vector for water system at gyration speed of 87.27 rpm obtained from the steady-state simulation is shown in Fig. 6.20,

6.22 and 6.24 respectively. For Glycerine/water system these are shown in Fig. 6.21, 6.23 and 6.25 respectively. The streamlines were plotted in the entire domain whereas the velocity contour and velocity vectors were plotted in the middle vertical section.

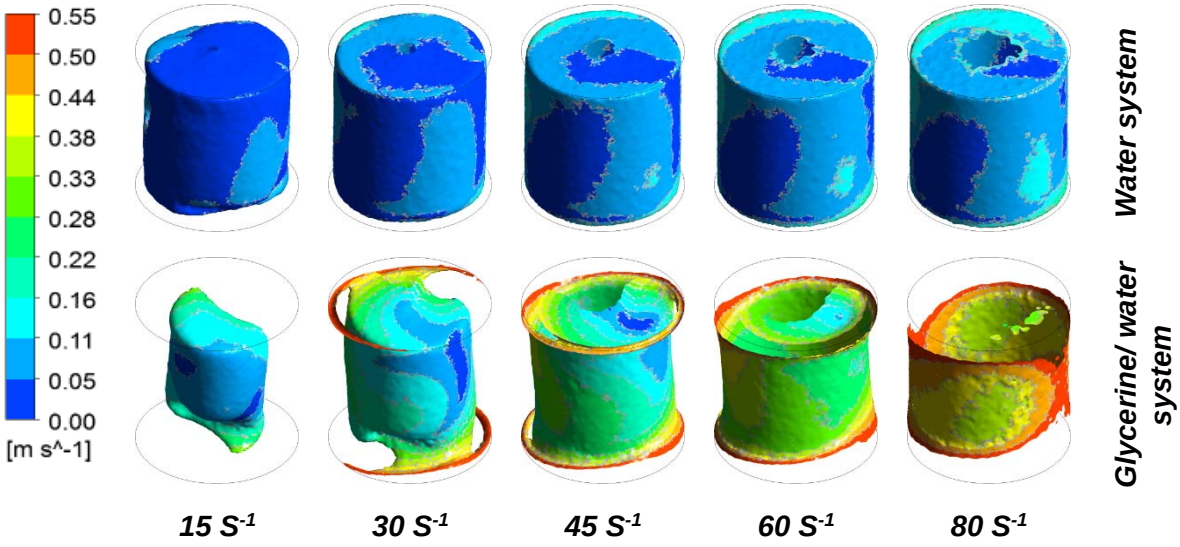

Fig. 6.17. Isosurface of vorticity at an equivalent speed of 200 rpm coloured by velocity

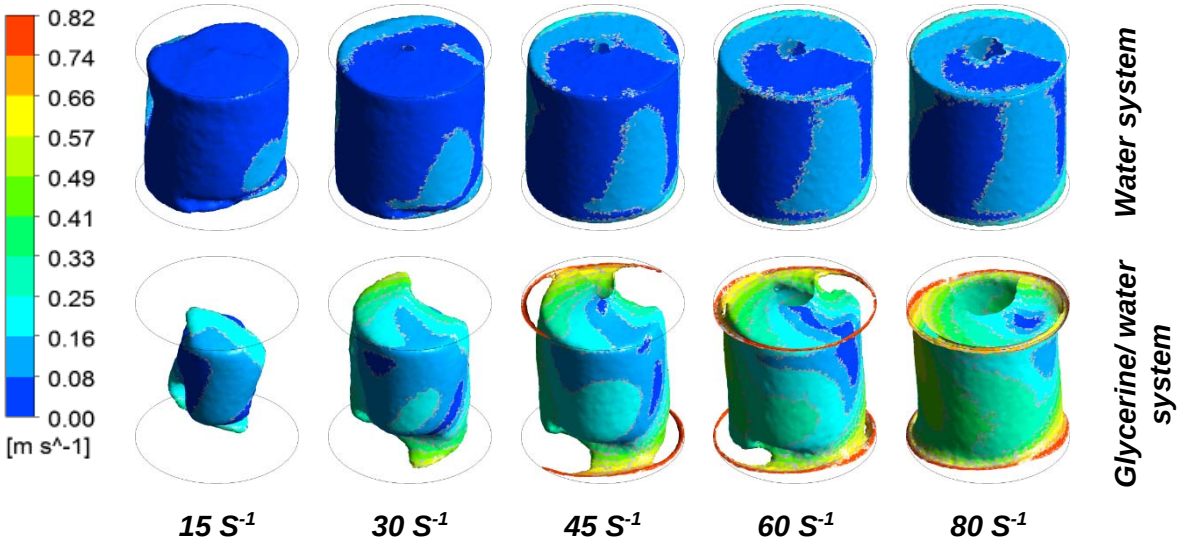

Fig. 6.18 Isosurface of vorticity at an equivalent speed of 300 rpm coloured by velocity

The mixing was found to be vigorous in both systems. The flow path is found circulating near the walls of the mixing tank in the water system. The fluid velocity near the centre of the mixing tank was found to be higher in glycerine/water system than water system. This was due to the higher viscosity of the glycerine/water system which helped to transfer the momentum delivered by the walls of the mixing tank.

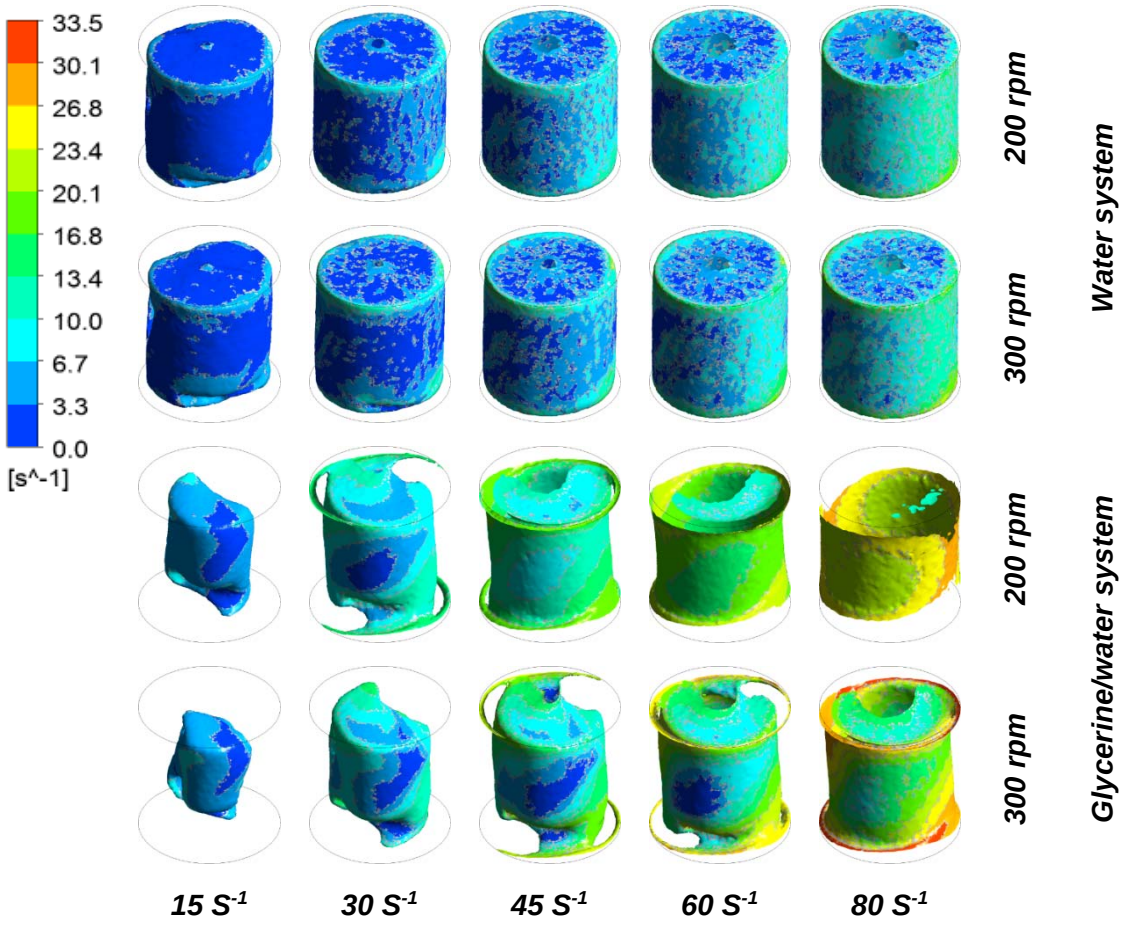

Fig. 6.19.Isosurface of vorticity coloured by swirling strength

The circulation of the flow near the centre of the tank was obtained from velocity vector plot for glycerine/water system. The circulation of fluid flow for the water system was observed near the corners of the mixing tank.

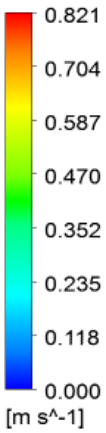

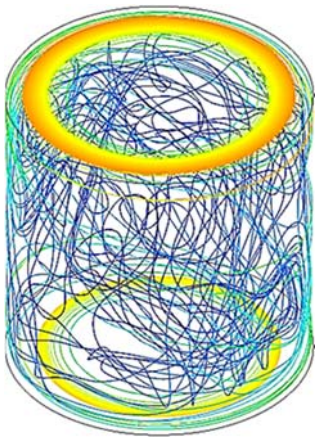

Fig. 6.20. Streamlines of fluid flow for water system

Fig. 6.21. Streamlines of fluid flow for glycerine/water system

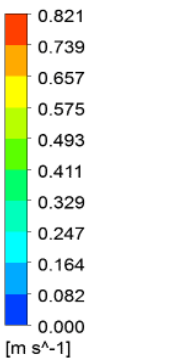

Fig. 6.22. Velocity contour of the water system

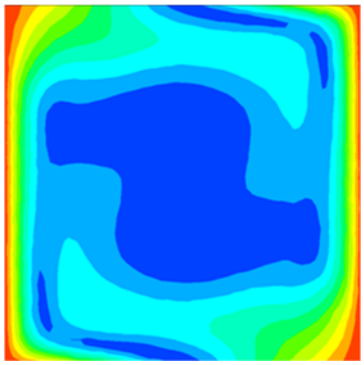

Fig. 6.23.Velocity contour of glycerine/water system

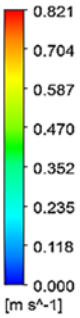

Fig. 6.24. Velocity vector of the water system

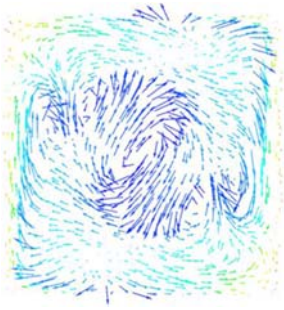

Fig. 6.25. Velocity vector of glycerine/water system

6.9 Summary

The mixing of SiC particulates with liquid and mushy state aluminium was simulated by replacing liquid aluminium with water and mushy state aluminium with glycerine/water mixture. CFD simulation model was designed for the gyro casting using Eulerian k-Ɛ dispersed multi-phase turbulence model. The simulation model for gyro casting was developed by validating the mixing power obtained from CFD simulation with experiment. The characteristic velocity for gyro casting was formulated for comparing the mixing performance with the stir casting method. The simulation for mixing of SiC particulates with liquid aluminium and semi-solid aluminium was carried out in an equivalent viscosity model of water and glycerine/water system. The mixing time in the water system for gyro casting was found to be higher than that of stir casting at higher gyration speeds. The mixing time was found to be very low in Glycerine/water system for gyro casting. The particle distribution in gyro casting was found more uniform than the stir casting for both water and

glycerine/water systems. This was due to the vigorous mixing caused by the two axes rotation of the mixing cylinder.

The proposed gyro casting method can be adopted for getting a more homogeneous suspension of particulates as compared to the existing stir casting method for the production of PMMC. This mixing process can be continued while solidification occurs resulting in avoiding the formation of dendritic growth of microstructure which helps in improving mechanical properties of the cast composite.In such a situation, the breakage of dendritic growth might happen caused by the movement of the molten metal.

CHAPTER 7

CONCLUSIONS

Compositesfind numerous applications in engineering due to its excellent mechanical properties. Composites are produced by reinforcing the base material with either fibersor particulates. This research work was conducted on the broad area of improving the quality of PMMCs. The most widely used production method for PMMC is stir casting, which is a liquid processing having low manufacturing cost. In stir casting, the particulate reinforcement is vigorously stirred inside a cylindrical mixing vessel. The major disadvantage of this process is the difficulty in getting a homogeneous mixture of the particulates. Obtaining a uniform particulate distribution is extremely important in producing good quality composite materials.

The mechanical properties of the cast product are related to the homogeneity of the particulate distribution. Homogeneous mixing of the particulates and matrices are the primary requirement for producing quality PMMCs. This research work was carried out with the specific objectives of improving the mixing quality by making use of gyro mixing and conducting CFD simulations on the mixing and gyro casting. The major results of the research work and their implications are described in the succeeding sections.

7.1 Development of Simulation Model for Gyro casting

A new method of mixing which has a two mutually perpendicular axis of rotation of the mixing vessel with no stirring impellers, known as Gyro casting is proposed in this research work. The CFD simulation model for gyro casting was developed for assessing the mixing performance of the liquid and particulates. The new method was compared with the existing method of stir casting. Characteristic velocity, Reynolds number and power number were derived for this purpose by considering the experimental works reported on planetary mixing devices.

The experiment was conducted in a modified gyro shaker, which is usually employed for mixing highly viscous fluids. The liquid phase was selected as glycerine, which is a highly viscous fluid and the particulate phase as SiC particulates with 30μm size.

The multiphase simulation models selected were Eulerian granular and mixture models for this analysis. The suitability of the VOF model was also observed. The RNG-kε turbulence model was used to capture the flow characteristics of the highly swirling flow

inside the mixing vessel. The computational domain was a cylinder of both diameter and height of 140 mm as in the case of the experiment.

The simulation results were validated by comparing the mixing power required in the experiment and simulation. Two methods namely viscous dissipation and torque methods were used to find out the mixing power from the CFD simulation.The mixture model predicted the mixing power more closely because the particulate flow had followed the fluid flow very closely. The velocity, pressure and volume fraction distribution in the VOF model were almost similar to the mixture model. The slight variation of the power number concerning Reynolds number proved the flow is in the transition region.

The stream lines obtained from CFD simulation indicated that the mixing was vigorous in the entire domain. The fluid velocity and pressure was higher near the walls of the mixing vessel and very low near the centre of the mixing vessel. The contours of volume fraction of the particulate phase showed a faster mixing near the walls than at the centre of the mixing vessel. The contours of velocity and pressure were almost the same in Eulerian k-Ɛ dispersed model, mixture model and VOF model. The contours of volume fraction of the secondary phase obtained from Eulerian k-Ɛ dispersed model had a slight change than that of mixture and VOF models. The variation of pressure and velocity along radial and axial directions were found almost same in all the models.

The two axes rotation of the mixing vessel with liquid and particulates inside the cylinder was modelled in three different multiphase approaches. The effect of flow parameters on the process variables like gyration speed, spin speed, length and diameter of the mixing vessel can be studied using this CFD simulation model.

7.2 CFD simulation of liquid-solid dispersion in a gyro shaker

The results of a comparative study of the traditional method of solid-liquid mixing in a stirred vessel with gyro shaker mixer were conducted for analysing the particle distribution in both the cases. The flow parameters inside the mixing cylinder of the gyro shaker were also observed. Compared to the CFD simulation studies conducted in the stirred vessel reported by Wang et al. (2010) for inspecting the solid particle distribution, an improvement in the solid particle loading resulting in a perfectly homogeneous mixture is observed in the gyro shaker.

The developed CFD simulation model was also used for the numerical simulation for glycerine/water and sand. In gyro shaker mixing, the sand particle concentration was found

to be fluctuating due to the high recirculation flow. As the speed increased, the quality of mixing got increased, as compared to the stirred vessel mixing. At high gyration speeds of the mixing cylinder, the mixing time was found to be shorter.The two axes rotating system for liquid and solid particulates mixing developed was found better than the existing stirred vessel for attaining homogeneity of solid particles distribution.

7.3 Gyro casting simulation

CFD simulation for investigating the mixing performance of gyro casting was also conducting using the CFD simulation model. The liquid phases considered were liquid aluminium and semi-solid aluminium. The simulation was conducted by replacing liquid aluminium with and semi-solid aluminium with glycerol/water mixture. The particulate phase was SiC of 13 μm size with a volume fraction of 10%. The cylindrical mixing domain was a size of 105 mm diameter and 65 mm in height.

The same volume of the computational domain, the same materials and mixing conditions as used by Neher et al. (2007) for simulating stir casting were used for the CFD simulation of gyro casting for comparing the mixing effectiveness with stir casting. Both the diameter and height of the mixing cylinder of the gyro casting was kept as 90mm. Transient and steady-state CFD simulations were conducted in gyro casting for both aluminium and semi-solid aluminium mixing with SiC particulates. The mixing time and particulate distributions at various positions obtained from gyro casting were compared with sir casting.

The particle distribution of the water system was found to be more uniform in gyro casting than stir casting. The mixing time was found lower at lower speed in gyro casting than stir casting. But, at higher speeds, the stir casting showed a lower mixing time than gyro casting.

The particle distribution of glycerol/water system for gyro casting simulation was found to be improvedas compared to the stir casting. The high viscosity of the liquid phase supported the mixing in the gyro casting. The mixing time in this system was found to be very low as compared with the stir casting.

The stream line obtained from the steady-state CFD simulation showed a strong mixing of the liquid phase with the particulates. The particles were observed to be recirculated in the entire domain for achieving perfect mixing. The velocity of fluid flow was found to be higher near the walls than at the centre of the mixing vessel.

In stir casting, the stirring action should be stopped before the solidification starts because of the mechanical stirrer which is immersed in the molten liquid metal. The mixing near the stirrer is also a drawback in semi-solid mixing process due to its high viscosity. The advantage of the gyro casting is that it can be applied during the entire solidification process. This mixing process that continued while solidification occurs, resulting in avoiding the formation of dendritic growth of microstructure, which helps in improving mechanical properties of the cast composite.

7.4 Future works

The development of a new casting method for producing PMMC was in this research work. The CFD simulation model for two axes mixing device was developed by validating with mixing power obtained from the experiment. The gyro casting simulation was then carried out for studying the mixing performance in gyro casting and compared with stir casting. The design and construction of an equipment for performing the gyro casting for the casting of PMMC is not carried out as part of this work.

The optimization of process parameters like spin speed, gyration speed, mixing time and length to diameter ratio of mixing vessel are not carried out in this work. The usual volume fraction of the secondary particulate phase is also limited to 30% in stir casting due to the inefficiency of mixing. The casting with higher particulate loading can also be examined in gyro casting. The mixing performance can also be checked by introducing baffles along the walls of the container as usually done in stirred vessels.

REFERENCES

1. Abhishek, M.S., Choudhari, S. & Muller, F. 2012. Observations of solid-liquid systems in anchor agitated vessels. *Chemical Engineering Research and Design*, Vol. 20: 750-756.
2. Aigbodion, V.S. 2014. Thermal ageing on the microstructure and mechanical properties of Al-Cu-Mg alloy/bagasse ash particulate composites. *Journal of King Saud University – Engineering Sciences*, Vol. 26:144-151.
3. Alaneme, K.K., Akintunde, I.B., Olubambi, P.A.&Adewale., T.M. 2013. Fabrication characteristics and mechanical behavior of rice husk ash – Alumina reinforced Al-Mg-Si alloy matrix hybrid composites. *Journal of Materials Research and Technology*, Vol. 2:.60-67.
4. Aldas, K.& Mat, M.D. 2005. Experimental and theoretical analysis of particle distribution in particulate metal matrix composite. *Journal of Materials Processing Technology*, Vol. 160: 289-295.
5. Alfaro-Ayala, J.A., Ayala-Ramierz, V., Gallegos-Munoz & Uribe-Ramirez, A.R. 2015. Optimal location of axial impellers in a stirred tank applying evolutionary programing and CFD. *Chemical Engineering Research and Design*, Vol. 100: 203-211.
6. Ali, M.S.M., Doolan, C.J. & Wheatley, V. 2009. Grid convergence study for a two-dimensional simulation of flow around a square cylinder at a low Reynolds number. *Seventh International Conference on CFD in the Minerals and Process Industries*, CSIRO, Melbourne, Australia, 9-11 December 2009.
7. Alliet-Gaubert, M., Sardeing, R., Xuereb, C., Hobbes, P., Letellier, B. &Swaels, P. 2006. CFD analysis of industrial multi-staged stirred vessels, *Chemical Engineering and Processing*, Vol. 45: 415-421.
8. Almadhoni., K. & Khan., S. 2015. Review of Effective Parameters of Stir Casting Process on Metallurgical Properties of Ceramics Particulate Al Composites. *IOSR Journal of Mechanical and Civil Engineering*, Vol. 12: 22-40.
9. Almohammadi, K.M., Ingham, D.B., Ma, L. &Pourkashan, M. 2013. Computational fluid dynamics (CFD) mesh independency techniques for a straight blade vertical axis wind turbine. *Energy*, Vol. 58: 483-493.
10. Amirkhanlou, S., Rezaei, M.R., Niroumand, B. &Toroghinejad, M.R. 2011. High-strength and highly-uniform composites produced by compocasting and cold rolling process. *Materials and Design*, Vol.32: 2085-2090.
11. Andre, C., Demeyre, J.F., Gatumel, C., Berthiaux, H. &Delaplace, G. 2012. Dimensional analysis of a planetary mixer for homogenizing of free flowing powders: Mixing time and Power consumption. *Chemical EngineeringJournal*, :198-199,371-378.

12. Andre, C., Demeyre, J.F., Gatumel, C., Berthiaux, H. &Delaplace, G. 2014. Derivation of dimensionless relationships for the agitation of powders of different flow behaviours in a planetary mixer. *Powder Technology*, Vol. 256: 33–38.

13. Auger, F., Delaplace, G., Bouvier, L., Redl, A. & Andre, C. 2013. Hydrodynamics of planetary mixer used for dough process: speeds ratio on the power dissipated for Newtonian fluids. *Journal of Food Engineering*, Vol. 118: 350-357.

14. Bai, L., Zheng, Q.J. & Yu, A.B. 2017. FEM simulation of particle flow and convective mixing in a cylindrical bladed mixer. *Powder Technology*, Vol. 313: 175-183.

15. Balaji, V., Sateesh, N. &Hussain.M.M. 2015. Manufacture of Aluminium Metal Matrix Composite (Al7075-SiC) by Stir Casting Technique. Materials Today: Proceedings, Vol. 2: 3403-3408.

16. Barman, N., Kumar, P. & Dutta, P. 2009. Studies on transport phenomena during solidification of an aluminium alloy in the presence of linear electromagnetic stirring. *Journal of Materials Processing Technology*, Vol. 209: 5912-5923.

17. Bao, Y., Lu, Y., Cai, Z.& Gao, Z. 2018. Effects of rotational speed and fill level on particle mixing in a stirred tank with different impellers. *Chinese Journal of Chemical Engineering*, Vol. 26: 1383-1391.

18. Beffort, O., Long, S., Cayron, C., Kuebler, J. &Buffat, P. 2007. Alloying effect on microstructure and mechanical properties of high volume fraction SiC-particle reinforced Al-MMCs made by squeeze casting infiltration. *Composites Science and Technology*, Vol.67: 737-745.

19. Behera, R., Mohanta, N.R. &Sutradhar, G. 2012. Distribution of SiC particulates in stir cast Aluminium alloy Metal matrix composites and its effect on mechanical properties. *International Journal of Emerging trends in Engineering and Development,* Vol. 1: 194-205.

20. Bodunrin, M.O., Alaneme, K.K.&Chown, L.H. 2015. Aluminium matrix hybrid composites: a review of reinforcement philosophies; mechanical, corrosion and tribological characteristics. *Journal of Materials Research and Technology*, Vol.4: 434-445.

21. Busciglio, A., Montante, G., Kracik, T., Moucha, T.&Paglianti, A. 2017. Rotary sloshing induced by impeller action in unbaffled stirred vessels. *Chemical Engineering Journal*, Vol. 317: 433-443.

22. Canakci, A. &Varol, T. 2014. Microstructure and properties of AA7075/Al-SiC composites fabricated using powder metallurgy and hot pressing. *Powder Technology*, Vol.268: 72-79.

23. Celik, I.B. 2008. Procedure for estimation and Reporting of Uncertainty Due to Discretization in CFD Applications. *Journal of Fluids Engineering*, Vol.130, 78001-78005.

24. Cokljat, D., Slack, M., Vasquez, S.A., Bakker, A. &Montante, G. 2006. Reynolds-Stress Model for Eulerian multiphase. *Progress in Computational Fluid Dynamics*, Vol. 6: 168-178.

25. Coroneo, M., Montante, G., Paglianti, A. &Magelli, F. 2011. CFD Prediction of fluid flow and mixing in stirred tanks: Numerical issues about the RANS simulation. *Computers and Chemical Engineering*, Vol. 35: 1959-1968.

26. Coughtrie, A.R., Borman, D.J. & Sleigh, P.A. 2013. Effects of turbulence modelling on prediction of flow characteristics in a bench-scale anaerobic gas-lift digester. *Bioresource Technology*, Vol. 138: 297-306.

27. Crow, C., Sommerfield, M.& Tsuji, Y.T. 1998. Multiphase Flows with Droplets and Particles. *CRC press, New York.*

28. Deglon, D.A. & Meyer, C.J. 2006. CFD modelling of stirred tanks: Numerical considerations. *Minerals Engineering*, Vol. 19: 1059-1068.

29. Delaplace, G., Thakur, R.K., Bouvier, L., Andre, C. & Torrez, C. 2007. Dimensional analysis for planetary mixer: Mixing time and Reynolds numbers. *Chemical Engineering Science, Vol.* 62: 1442- 1447.

30. El-Khair, M.T.A. &Aal, A.A. 2007. Erosion-corrosion and surface protection of A356 Al/ZrO_2 composite produced by vortex and squeeze casting. *Materials Science and Engineering A*, Vol. 454: 156-163.

31. Ezatpour, H.R., Sajjadi, S.A., Sabzevar, M.H. & Huang, Y. 2014. Investigation of microstructure and mechanical properties of Al6061-nanocomposite fabricated by stir casting. *Materials and Design*, Vol.55: 921-928.

32. Fletcher, D.F. & Brown, G.J. 2009. Numerical simulation of solid suspension via mechanical agitation: effect of the modelling approach, turbulence model and hindered settling drag law. *International Journal of Computational Fluid Dynamics*, Vol. 23: 173-187.

33. Ghauri, K.M., Ahmad, A., Ahmad, R., Din, K.M.& Chaudhary, J.A. 2013. Synthesis and Characterization of Al/SiC Composite Made by Stir Casting Method. *Pakiastan Journal of Engineering and Applied Science,* Vol. 12: 102-110.

34. Gopalakrishnan,S.&Murugan, N. 2012. Production and wear characterisation of AA 6061 matrix titanium carbide particulate reinforced composite by enhanced stir casting method, Composites Part B: Engineering, Vol 43: 302-308.

35. Gu, D., Liu, Z., Xu, C., Li, J., Tao, C.& Wang, Y. 2017. Solid-liquid mixing performance in a stirred tank with a double punched rigid-flexible impeller coupled with a chaotic motor. *Chemical Engineering & Processing: Process Intensification*, Vol. 118: 37-46.

36. Guillaume, D., Philippe, C., Jose, C. &Fabrice, D. 2012. Influence of whip speed ratios on the inclusion of air into a bakery foam produced with a planetary mixer device. *Journal of Food Engineering*, Vol. 108: 532-540.

37. Haavisto, S., Syrjanen, J., Koponen, A. &Manninen, M. 2009. UDV measurement and CFD simulation of two-phase flow in a stirred vessel. *Progress in Computational Fluid Dynamics*, Vol. 9: 375-382.

38. Hashim, J., Looney, L. & Hashmi, M.S.J. 1999. Metal matrix composite: production by the stir casing method.*Journal of Materials Processing Technology,* Vol. 92: 1-7.

39. Hashim, J., Looney, L. & Hashmi, M.S.J. 2002. Particle distribution in cast metal matrix composites – Part II. *Journal of Materials Processing Technology,*Vol. 123: 258-263.

40. Hreiz, R., C. Gentric& N. Midoux 2011. Numerical investigation of swirling flow in cylindrical cyclones. Chemical Engineering Research and Design, Vol.89: 2521-2539.

41. Hu, J., Wu, G., Zhang, Q. & Gou, H. 2014. Mechanical properties and damping capacity of SiCp/TiNif/Al composites with different volume fraction of SiC particle. *Composites: Part B*, Vol.66: 400-406.

42. Huang, A. & H. Kuo 2014. Developments in the tools for the investigation of mixing in particulate systems – A review. Advanced Powder Technology , Vol.25: 163 – 173.

43. Jahoda, M., Tomaskova, L. &Mostek, M. 2009. CFD prediction of liquid homogenization in a gas-liquid stirred tank. *Chemical Engineering Research and Design*, Vol. 87: 460-467.

44. Javed, K. H., T. Mahmud & J. M. Zhu 2006. Numerical simulation of turbulent batch mixing in a vessel agitated by a Rushton turbine. Chemical Engineering and Processing, Vol. 45: 99-112.

45. Kandpal, B.C., Kumar, J. &Sing, H. 2017. Fabrication and characterization of Al2O3/aluminium alloy 6061 composites fabricated by stir casting. *Materials Today: Proceedings*, Vol. 4: 2783-2792.

46. Kasat, G.R., Khopkar, A.R., Ranade, V.V &Pandit, A.B. 2008.CFD simulation of liquid-phase mixing in solid–liquid stirred reactor, Chemical Engineering Science, Vol 63: 3877-3885

47. Kaushal, D.R., Thinglas, T., Tomita, Y., Kuchii, S. & Tsukamoto H.2012. CFD modeling for pipeline flow of fine particles at high concentration. *International Journal of Multiphase Flow,* Vol. 43: 250-254.

48. Khorshidi, R., Raouf, A.H. &Emamy, M. 2011. The study of Li effect on the microstructure and tensile proportion of cast Al-Mg_2Si metal matrix composite. *Journal of Alloys and Compounds*, Vol. 509: 9026-9033.

49. Khosravi, K. &Akhlaghi, F. 2015. Comparison of microstructure and wear resistance of A356-SiC_P composites processed via compocasting and vibrating cooling slope. *Transactions of Nonferrous Metals Society of China,* Vol. 25: 2490-2498.

50. Khopkar, A.R., Rammohan, A.R., Ranade, V.V. &Dudukovic, M.P. 2005. Gas-liquid flow generated by a Rushton turbine in stirred vessel: CARPT/CT measurements and CFD simulations. *Chemical Engineering Science*, Vol. 60: 2215-2229.

51. Khopkar, A.R., Kasat, G.R., Pandit, A.B. &Ranade, V.V. 2006. CFD simulation of mixing in tall gas-liquid stirred vessel: Role of local flow patterns. *Chemical Engineering Science*, Vol. 61: 2921-2929.

52. Kok, M. 2005. Production and mechanical properties of Al_2O_3 particle-reinforced 2024 aluminium alloy composites.*Journal of Materials Processing Technology*, Vol. 161: 381-387.

53. Kumar, A., Kumar, S. &Mukhopadhyay. 2018. Introduction to magnesium alloy processing technology and development of low-cost stir casting process for magnesium alloy and its composites. *Journal of Magnesium and Alloys*, Vol. 6: 245-254.

54. Kumar, A., Lal, S. & Kumar, S. 2013. Fabrication and Characterization of A359/Al_2O_3 metal matrix composite using electromagnetic stir casting method. *Journal of Materials Research and Technology*, Vol.2: 250-254.

55. Kumar, M.V.S.P., Babu, M.V.S. &Ramana, V.S.N.V. 2015. Simulation of Stir Casting Process Using Computational Fluid Dynamics. *International Journal of Engineering Research and Applications*, Vol. 5: 132-135.

56. Lashgari, H.R., Sufizadeh, A.R. &Emamy, M. 2010. The effect of strontium on the microstructure and wear properties of A356-10%B_4C cast composites. *Materials and Design*, Vol. 31: 2187-2195.

57. Lassaigne, M., Blais, B., Fradette, L.& Bertrand, F. 2016. Experimental investigation of the mixing of viscous liquids and non-dilute concentrations of particles in a stirred tank. *ChemicalEngineering Research and Design*, Vol. 108: 55-68.

58. Li, Y., Li, Q., Li, D., Liu, W. & Shu, G. 2016. Fabrication and characterization of stir casting AA6061-31%B_4C composite. *Trans.Nonferrous Metals Society of China*, Vol. 26: 2304-2312.

59. Lina, G., Lin, G., Hong-wei, Z. & Lu-jun, H. 2011. Effects of stirring parameters on microstructure and tensile properties of (ABOw+SiC)/6061Al composites fabricated by semi-solid stirring technique. *Transactions of Nonferrous Metals Society of China,* Vol. 21: 274-279.

60. Liu, D., Hu, P. & Min, G. (2015). Interfacial reaction in cast WC particulate reinforced titanium metal matrix composites coating produced by laser processing.*Optics& Laser Technology*, Vol. 69: 180-186.

61. Longest, P.W.&Vinchurkar, S. 2007. Effects on mesh style and grid convergence on particle deposition in bifurcating airway models with comparisons to experimental data. *Medical Engineering & Physics*, Vol. 29: 50-366.

62. Mattei, G. &Vozzi, G. 2016. CFD modelling of a mixing chamber for the realization of functionally graded scaffolds.*Computers and Chemical Engineering*, Vol. 84: 43-48.

63. Meng-ou, T., Jun, X., Zhi-feng, Z. & Yue-long, B. 2010. New method of direct chill casting of Al-6Si-3Cu-Mg semisolid billet by annulus electromagnetic stirring. *Trans. Nonferrous Met. Soc. China*, Vol.20: 1591-1596.

64. Micale, G., Grisafi, F., Rizzuti, L. &Brucato, A. 2004). CFD simulation of particle suspension height in stirred vessels. *Chemical Engineering Research and Design*, Vol. 82: 1204-1213.

65. Mishra, P., &Ein-Mozaffari, F. 2017. Using computational fluid dynamics to analyse the performance of the Maxbled impeller in solid-liquid mixing operations. *International Journal of Multiphase Flow*, Vol. 91: 194-207.

66. Meng, Z., Liu, M., Xie, J., Wang, W. & Lu, C. 2018. Comparative study on the hydrodynamics and mixing characteristics of a new-type particle mixer. *Powder Technology*, Vol. 332: 90-105.

67. Moghari, R.M., Akbarinia, A., hariat, M., Talebi, F.&Laur, R.2011. Two phase mixed convection Al_2O_3-water nanofluid flow in an annulus. *International Journal of Multiphase flow*, Vol. 37: 585-595.

68. Montante, G. &Magelli, F. 2005. Modelling of solids distribution in stirred tanks: analysis of simulation strategies and comparison with experimental data. *International Journal of Computational Fluid Dynamics,*Vol. 19: 253-262.

69. Murthy, I.N., Rao, D.V. & Rao, J.B. 2012. Microstructure and mechanical properties of aluminium-fly ash nano composite made by ultrasonic method. *Materials and Design*, Vol. 35: 55-65.

70. Naher, S., Brabazon, D. & Looney, L. 2007. Computational and experimental analysis of particulate distribution during Al-SiC MMC fabrication. *Composites. Part A: applied science and manufacturing,* Vol. 38: 719-729.

71. Nino-Lopez, L.C. &Gelves-Zambrano, G.R. 2015. Simulating gas-liquid mass transfer in a spin filter bioreactor. *RevistaFacultad de Ingenieria Universidad de Antioquia*, Vol. 75: 163-174.

72. Nouri, J.M. & Whitelaw, J.H.1992. Particle velocity characteristics of dilute to moderately dense suspensions flows in stirred reactors. *International Journal of Multiphase Flow*, Vol. 18: 21-33.

73. Oumer, A.N. &Mamat.O. 2014. Numerical modelling of non-isothermal flow of fibre suspensions: prediction of fibre orientation in three-dimensional cavities. *International Journal of Computational Science and Engineering*, Vol. 9: 247-256.

74. Panneerselvam, R., Savithri, S. &Surender, G.D. 2008. CFD modelling of gas-liquid-solid mechanically agitated contactor. *Chemical Engineering Research and Design*, Vol. 86: 1331-1344.

75. Prabu, S.B., Karunamoorthy, L., Kathiresan, S. & Mohan, B. 2006. Influence of stirring speed and stirring time on distribution of particulates in cast metal matrix composite. *Journal of Materials Processing Technology*, Vol.171: 268-273.

76. Prabhu, T.R., Varma, V.K. &Vedantam, S. 2014. Effect of SiC volume fraction and size on dry sliding wear of Fe/SiC/graphite hybrid composites for high sliding speed applications. *Wear*, Vol. 309: 1-10.

77. Ramnath, B.V., Elanchezhian, C., Jaivignesh, M., Rajesh, S. &Parswajinan, C. 2014). Evaluation of Mechanical properties of aluminium alloy-alumina-boron carbide metal matrix composites. *Materials and Design*, Vol. 58: 332-338.

78. Ramesha, D.K., Vidyasagar, H.N., PremKumar.G., Nataraj, B.R. & Mahesh Kumar.N. 2012. CFD simulation of gas-solid-liquid fluidised bed reactor. *International Journal of Computational Science and Engineering*, Vol. 7: 162-174.

79. Rao, D.A. &Sivashanmugam, P. 2010. Experimental and CFD simulation studies on power consumption in mixing using energy saving turbine agitator. *Journal of Industrial and Engineering Chemistry,* Vol. 16: 157-161.

80. Reihani, S.M.S. 2006. Processing of squeeze cast Al6061-30vol% SiC composites and their characterization. *Materials and Design*, Vol.27: 216-222.

81. Roache, P.J. 1994. Perspective: A method for uniform reporting of grid refinement studies. *Journal of Fluids Engineering*. Vol. 116(3): 405-441.

82. Roudsari, S.F., Turcotte, G., Dhib, R. &Ein-Mozaffari, F. 2012. CFD modeling of the mixing of water in oil emulsions. *Computers and Chemical Engineering*, Vol. 45: 124-136.

83. Sahin, Y. &Acilar, M. 2003. Production and properties of SiCp-reinforced aluminium alloy composites. *Composites: Part A*, Vol.34: 709-718.

84. Sajjadi, S.A., Ezatpour, H.R. &Parizi, M.T. 2012. Comparison of microstructure and mechanical properties of A356 aluminium alloy/Al_2O_3 composite fabricated by stir and compo-casting process. *Materials and Design*, Vol.34: 106-111.

85. Sharma, P., Sharma, S. &Khanduja, D. 2015. A study on microstructure of aluminium matrix composites. *Journal of Asian Ceramic Societies,* Vol. 3: 240-244.

86. Sharma, P., Sharma, S. &Khanduja, D. 2015. Production and some properties of Si_3N_4 reinforced aluminium alloy composites. *Journal of Asian Ceramic Societies,* Vol. 3: 352-359.

87. Shekhar, S, M. &Jayanti, S. 2002. CFD study of power and mixing time for paddle mixing in unbaffled vessels. *Trans. IChem E, Part A*, Vol. 80: 482-498.

88. Singh, H., Fletcher., D.F. &Nijdam, J.J. 2011. An assessment of different turbulence models for predicting flow in a baffled tank stirred with a Rushton turbine. *Chemical EngineeringScience*, Vol. 66: 5976-5988.

89. Srilatha, C., Mundada, T.P. &Patwardhan, A.W. 2010. Scale-up of pump-mix mixers using CFD. *Chemical Engineering Research and Design*, Vol. 88: 10-22.

90. Su, H., Gao, W., Zhang, H., Liu, H., Lu, J. & Lu, Z. 2010. Optimization of Stirring Parameters Through Numerical Simulation for the Preparation of Aluminum Matrix Composite by Stir Casting Process. *Journal of Manufacturing Science and Engineering*, Vol. 32: 1-7.

91. Taghavi, M., Zadghaffari, R., Moghaddas, J. &Moghaddas, Y. 2011. Experimental and CFD investigation of power consumption in a dual Ruston turbine stirred tank. *Chemical Engineering Research and Design,* Vol.89: 280-290.

92. Takahashi, K. &Motoda, M. 2009. Chaotic mixing created by object inserted in a vessel agitated by an impeller. *Chemical Engineering Research and Design*, Vol. 87: 386-390.

93. Tamburini, A., Cipollina, A., Brucato, A. &Ciofalo, M. 2012. CFD simulations of dense solid-liquid suspensions in baffled stirred tanks: Prediction of the minimum impeller speed for complete suspension. *Chemical Engineering Journal*, Vol. 193: 234-255.

94. Tennyson, P.G., Kumar, P., Lakshmi, H., Phanikumar, G. & Dutta, P. 2010. Experimental studies and phase field modeling of microstructure evolution during solidification with electromagnetic stirring. *Trans. Nonferrous Met. Soc. China*, Vol.20: 774-780.

95. Torre, J., Fletcher, D.F., Lasuye, T. &Xuereb, C. 2007. Single and multiphase CFD approaches for modelling partially baffled stirred vessels: Comparison of experimental data with numerical predictions. *Chemical Engineering Science*, Vo. 62: 6246-6262.

96. Varela, S., Martinez, M., Delgado, J.A., Godard, C., Curulla-Ferre, D., Pallares, J. &Vernet, A. 2018. Numerical and experimental modelization of the two-phase mixing in a small scale stirred vessel. *Journal of industrial and Engineering Chemistry*, Vol. 60: 286-296.

97. Vikash., Deshawar, D.& Kumar, V. 2017. Hydrodynamics and mixing characterization in a novel high shear mixer. *Chemical Engineering & Processing: Process Intensification*, Vol. 120: 57-67.

98. Volk, A., Ghia, U. & Stoltz, C. 2017. Effect of grid type and refinement method on CFD-DEM solution trend with grid size. *Powder Technology*, Vol. 311: 137-146.

99. Vrabel, P., Lans, R.G.J.M., Luyben, K.C.A.M., Boon, L. &Nienow, A.W. 2000. Mixing in large-scale vessels stirred with multiple radial or radial and axial up-pumping impellers: modelling and measurements. *Chemical Engineering Science*, Vol. 55: 5881-5896

100. Wang, L., Zhang, Y., Li, X. & Zhang, Y. 2010. Experimental investigation and CFD simulation of liquid-solid-solid dispersion in a stirred reactor. *Chemical Engineering Science,* Vol. 65: 5559-5572.

101. Wang, X.J., Wang, N.Z., Wang, L.Y., Hu, X.S., Wu, K., Wang, Y.Q. & Huang, Y.D. 2014. Processing, Microstructure and mechanical properties of Micro-SiC particle reinforced magnesium matrix composites fabricated by stir casting assisted by ultrasonic treatment processing. *Materials and Design*, Vol.57: 638-645.

102. Wu, H., Shu, S., Yang.N., Lian.G., Zhu.S. & Liu, M. 2014. Modelling of power characteristics for multistage rotor-stator mixers of shear-thinning fluids. *Chemical Engineering Science*, Vol. 117: 173-182.

103. Wu, B. 2010. CFD analysis of mixing in large aerated lagoons. *Engineering Applications of Computational Fluid Mechanics*, Vol. 4: 127-138.

104. Wu, J., Wang, S., Nguyen, B., Lane, G., Graham, L., Short, G. &Ruster, J. 2015. Improved viscous slurry agitation for mineral processing. *Minerals Engineering*, Vol. 78: 21-31.

105. Xie, L. & Luo, Z. 2018. Modeling and simulation of the influences of particle-particle interactions on dense solid-liquid suspensions in stirred vessels. *Chemical Engineering Science*, Vol. 176: 439-453.

106. Yang, F.L., Zhou, S.J., Zhang, C.X., Evans, G.M. & Wang, G.C. 2013. Study of the turbulent flow in an unbaffled stirred tank by detached eddy simulation. *Chemical EngineeringCommunications*, Vol. 200: 1347-1365.

107. Yashpal., Sumankant., Jawalkar, C.S., Verma, A.S. & Suri, N.M. 2017. Fabrication of Aluminium Metal Matrix Composite with Particulate Reinforcement: A Review. *Materials Today: Proceedings*, Vol. 4: 2927-2936.

108. Yavuz, N. & Sandeep, K.P. 2018. Investigation of impeller modification and eccentricity for non-Newtonian fluid mixing in stirred vessels. *Chemical Engineering Communications*, DOI: 10.1080/00986445.2018.1488690.

109. Yigezu, B.S., Mahapatra, M.M. &Jha, P.K 2013. Influence of reinforcement type on microstructure, hardness, and tensile properties of an aluminium alloy metal matrix composite.*Journal of Minerals and Materials Characterization and Engineering*, Vol. 1: 124-130.

110. Youssef, Y.M., Dashwood, R.J. & Lee, P.D. 2005. Effect of clustering on particle pushing and solidification behavior in TiB_2 reinforced aluminium PMMCs. *Composites Part A: applied science and manufacturing*, Vol. 36: 747-763.

111. Yu., L., Ma, J., Frear, C., Zhao, Q., Dillon, R., Li, X. & Chen, S. 2013. Multiphase modeling of settling and suspension in anaerobic digester.*Applied Energy*, Vol. 111: 28-39.

112. Zadghaffari, R., Mohghaddas, J.S. &Revstedt, J. 2010. Large-eddy simulation of turbulent flow in a stirred tank driven by a Rushton Turbine. *Computers& Fluids*, Vol. 29: 1183-1190.

113. Zamiri, A. & Chung, J.T. 2018. Numerical evaluation of turbulent flow structures in a stirred tank with a Rushton turbine based on scale-adaptive simulation. *Computers & Fluids*, Vol. 170: 236-248.

114. Zhang, T., Wang, Y., Zhou, Y. & Song, G. 2010. High temperature electrical resistivities of ZrC particle-reinforced tungsten-matrix composites.*International Journal of Refractory Metals & Hard Materials*, Vol. 28: 498-502.

115. Zhang, X.N., Geng, L. & Wang, G.S. 2006. Fabrication of aluminium based hybrid composite reinforced with SiC whiskers and SiC nanoparticles by squeeze casting. *Journal of Materials Processing Technology*, Vol.176: 146-151.

116. Zhao, H., Zhang, Z., Zhang, T., Liu, Y., Gu, S. & Zhang, G. 2014. Experimental and CFD studies of solid-liquid slurry tank stirred with an improved Intermig impeller. *Trans. Nonferrous Met. Soc. China*, Vol. 24: 2650-2659.

117. Zhu, H., Nienow, A.W., Bujalski, W. & Simmons, M.J.H. 2009. Mixing studies in a model aerated bioreactor equipped with an up- or a down-pumping 'Elephant Ear' agitator: Power, hold-up and aerated flow field measurements. *Chemical Engineering Research and Design*, Vol. 87: 307-317.

LIST OF PUBLICATIONS

1. “Computational Fluid Dynamics Simulation on Particulate Distribution in Gyro Casting for the Manufacture of Al/SiC Particulate Metal Matrix Composite” *Journal of Applied Fluid Mechanics,* Vol. 12, No.5, pp. 1585-1597. Online Scientific Journal System, indexed in Science Citation Index Expanded, ISI (Thomson Reuters) IF (2017) = 1.09. DOI:10.29252/jafm.12.05.29637.
2. “Experimental investigation and CFD simulation of power consumption for mixing in Gyro Shaker” *International Journal of Computational Science and Engineering*, the journal paper listed in the forthcoming articles. Inderscience publishers, Indexed in Scopus.